UCLouvain

FACULTE DES SCIENCES

Leptogenesis across the electroweak scale

Mémoire présenté en vue de l'obtention du grade académique de

Master [120] en sciences physiques, finalité approfondie.

UCLouvain, Faculté des Sciences, École de physique

Yannis Georis

Promoteur · rice: Prof. Marco Drewes
Lecteur · rice: Prof. Celine Degrande
Lecteur · rice: Prof. Fabio Maltoni

Année académique
2020-2021

Acknowledgements

This master thesis could obviously not have been conducted alone and I would like to take advantage of these few lines to warmly thank all the people who have made this work possible.

First and foremost, I would like to thank my supervisor, Prof. Marco Drewes for introducing me to this fascinating topic of leptogenesis. His availability, guidance and patience to answer my endless list of questions were really precious throughout the year. This work would not have been possible without Dr. Juraj Klarić, our close collaborator throughout the thesis. His expertise on the numerical simulations was in particular invaluable. I also wish to express all my gratitude to Prof. Claudia Hagedorn for useful discussions throughout this last semester and to Prof. Degrande and Maltoni for agreeing to take the time to read this master thesis and assess it.

UCLouvain have been my second home for a few years now and I am really grateful to all the staff and people I have met there for these mind opening five years. I would like to express a special thank to some of my colleagues at CP3 for our short collaboration. Loïc, Quentin, Valentin, I really appreciated our discussions to dissect Le Bellac's book. I am in addition particularly grateful to Benoit, Joyce and Quentin for useful comments on the draft of this master thesis.

Finally, I wanted to express all my gratitude to my parents and brothers for their support during all my studies and especially during this very particular year.

Contents

Introduction

The construction of the Standard Model of particle physics (SM) is undoubtedly one of the greatest successes of physics during the past century. Together with the theory of General Relativity, it is able to account for most particle physics data and cosmology observations covering an incredible range of phenomena, from the interactions of subatomic particles to the expansion of our observable universe. It is however now known that the SM is not flawless and cannot explain several phenomena such as

- The origin of the neutrino masses.
- The exact amount of asymmetry between matter and antimatter (baryogenesis).
- The origin of Dark Matter.

The Standard Model thus needs to be extended to account for these. Heavy neutrinos are a potential elegant solution to all these three problems. They can explain the non-zero neutrino masses through the type-I seesaw mechanism [1], can generate an asymmetry between matter and antimatter through their decay [2] or oscillations [3] and can also be a Dark Matter candidate [4]. They can even solve those three problems simultaneously within the Neutrino Minimal Standard Model (νMSM) [5].

However, these heavy neutrinos have not been detected at present and are still actively searched at various experiments including NA62 [6], Atlas [7], CMS [8–10], T2K [11]. In the near future, many new experiments such as SHiP [12], DUNE [13] or MATHUSLA [14] will be able to strengthen these searches. There is therefore a need for theoretical predictions to provide experiments with guidelines on "where" to look for these heavy neutrinos: What are their masses and couplings to the Standard Model particles, ... In this master thesis, we solely focus on heavy neutrinos that can simultaneously solve the neutrino masses problem and generate a sufficient amount of matter-antimatter asymmetry. Leptogenesis is a category of models within which the baryon asymmetry is first created as a lepton asymmetry before being transferred into the baryon sector through the so-called sphaleron process [15]. Early leptogenesis models [16], relying on a hierarchical heavy neutrinos mass spectrum and lepton asymmetries produced during heavy neutrino decays, required large heavy neutrino masses, above 10^9 GeV, to work. While these models are particularly attractive from a theoretical viewpoint as the heavy neutrinos can be naturally embedded in Grand Unified Theories (GUT), such as SO(10) [17] or left-right symmetric models [18], such heavy neutrinos cannot be produced on-shell in current or near-future experiments which makes the testability of the heavy neutrino hypothesis difficult. During the last 20 years, several scenarios where the mass of these heavy neutrino can be lowered have been developed [3, 19].

Resonant leptogenesis and leptogenesis from neutrino oscillations are two of these low-scale models. In resonant leptogenesis, the asymmetries are still produced during the decays of heavy neutrinos but are typically enhanced by degeneracies in the heavy neutrino mass spectrum. On the other hand, leptogenesis from neutrino oscillations relies on a production of asymmetries during the approach of these heavy neutrinos to equilibrium by their oscillations. These two

regimes would allow for heavy neutrino masses at or below the TeV scale, accessible to present-day experiments. The last decade have seen an increasing interest in the precision computation of the baryon asymmetry within these two scenarios, ultimately leading to the development of a set of quantum kinetic equations (QKEs), see *e.g.* [20], governing the time evolution of number densities and correlations between heavy neutrinos.

The main challenge is to study in a comprehensive manner the parameter space of these new models using these QKEs. Adding right-handed neutrinos typically comes along with $7n-3$ new parameters, n being the number of added heavy neutrino flavours, from which only five are constrained by experiments. Not all choices of these parameters give rise to successful baryogenesis and one needs to study the region compatible with the neutrino masses and baryogenesis. Such comprehensive study of the parameter space across the entire range of experimentally accessible heavy neutrino masses has already been performed for the minimal scenario $n = 2$ [21] but was still lacking when $n = 3$, a gap filled by the present work [22]. Guided by the experimental testability of the model, this master thesis aims at studying the range of overall coupling strength of the heavy neutrinos to their SM counterparts for which $n = 3$ leptogenesis is feasible. We performed this study across the entire mass range that will be accessible at high-energy experiments in the near-future. In this work, we restricted ourselves to the case where heavy neutrinos are approximately mass degenerate, where we expect the heavy neutrino coupling strength to be the largest.

This thesis is split into three main parts. In **chapter 1**, we introduce the main concepts necessary for our problem. After a quick historical introduction to neutrinos and neutrino oscillations, we describe the type-I seesaw mechanism. We then discuss how an asymmetry between matter and antimatter can be created starting from a symmetric universe, a process called baryogenesis. We finish by a rapid review of standard thermal leptogenesis, a specific baryogenesis model, and the reasons to go beyond it. In **chapter 2**, we start by describing resonant leptogenesis and leptogenesis from neutrino oscillations. We then discuss the set of quantum kinetic equations governing the time evolution of the heavy neutrinos for these two regimes. We finish by a short review of early studies of the viability of these scenarios. **Chapter 3** is devoted to the resolution of our research question. We first detail how the numerical scan was performed and analyse its outcomes. We finish by a quick review of further improvements that could be realised during future works. Lastly, two **appendices** deriving the form of the susceptibility matrix and the set of quantum kinetic equations used for this work, but limited to the relativistic regime, are available at the end of this thesis.

Throughout this thesis, we will assume that the reader has prior knowledge of quantum field theory, of the Standard Model and its construction and knows some basics of cosmology. It is also worth noting we will always work in the system of natural units where $\hbar = c = 1$ and we will express temperature T directly in eV instead of degrees Kelvin and therefore never write explicitly the factor k_B. We will also use the convention that time flows from left to the right in all the Feynman diagrams presented. Finally, we will also work with the convention that repeated indices are summed over, *i.e.* $A_i \cdot B_i \equiv \sum_i A_i \cdot B_i$, and that $\gamma^i p_i \equiv \not{p}$, where γ^i is a γ-matrix, as is usual.

This master thesis is based on the following publication:

• M. Drewes, Y. Georis, and J. Klarić, "Mapping the viable parameter space for testable leptogenesis," 6 2021, ARXIV:2106.16226

Chapter 1

General background

In this chapter, we review the necessary background to understand the core of the project. We first begin by a quick historical overview of the neutrino discovery. We then review how the introduction of new heavy particles can give neutrinos a non-zero mass. The second part of this chapter is dedicated to the origin of the matter-antimatter asymmetry. We first detail the necessary conditions to get an asymmetry and mention some of the main mechanisms that can be responsible for this asymmetry. We end this chapter with a description of standard thermal leptogenesis, where heavy neutrinos play a central role, and the main motivations to refine this model.

1.1 Historical overview of the neutrino and neutrino oscillations discoveries

Neutrinos lie among the most intriguing particles ever discovered. The first hint of their existence is to be found in the study of the energy spectrum of the electrons emitted during the so-called β decay. Discovered at the end of the 19^{th} century, β decay consists in the transmutation of a nucleus into another one associated with the simultaneous emission of an electron and an antineutrino. At first, only the electrons were detected which led physicists to think of β decay as a 2-body decay. If this was the case, the energy of the emitted electron would have been completely determined by the 4-momentum conservation rules. However, this was not the case as shown in the following Figure 1.1.

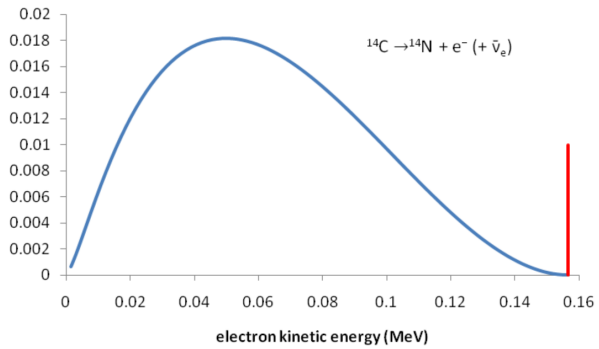

Figure 1.1: Energy spectrum of the emitted electron in a carbon to nitrogen transmutation. The blue line corresponds to what has been measured while the red line corresponds to the expected spectrum in the case of a 2-body decay. Taken from [23].

Several explanations had been proposed for this unexpected feature. N. Bohr, for instance, proposed that the energy conservation law could be valid only in a statistical sense. However,

W. Pauli showed in 1930 that the given spectrum is also consistent with a 3-body decay if we assume the additional particle to be very light [24]. This new particle had also to interact very feebly with matter, since it had not been detected at that time, and be neutral to respect the conservation of charge. Neutrinos were subsequently discovered in 1956 by F. Reines and C. Cowan [25] using the huge neutrinos fluxes produced in nuclear power plant to compensate for their extremely low cross-section. Soon after, it was realised that, exactly as for the charged leptons, there in fact exist three different types of neutrinos corresponding to each of the lepton flavours. In addition to the already discovered electron neutrino ν_e, the muon and tau neutrino, written ν_μ and ν_τ, were discovered in 1962 and 2000 respectively [26,27], this time using particle accelerators.

However, not all the neutrinos are artificially produced, either in nuclear power plant facilities or in particle accelerators. Main sources for the Earth neutrino flux also include cosmic rays and the sun. In parallel to these study of neutrino properties using artificial sources, R. Davis and J. Bahcall developed in the late 1960s the Homestake experiment devoted to the measurement of the neutrino flux emitted by the sun. Indeed, stars mainly produce energy via some nuclear fusion reactions such as

$$p + p \to D + e^+ + \nu_e.$$

This means that neutrinos are almost exclusively produced as electron neutrinos. The results published in 1978 [28] showed that the measured flux was approximately $\frac{1}{3}$ of what was theoretically expected. The key point to understand this discrepancy is the observation that the detector used was only sensitive to electron neutrinos. The solution to this problem, later confirmed by the SNO experiment [29], was not to question the existing solar models but to assume that oscillations between different flavours of neutrinos occurred during their journey to the earth. However, as we shall see in section 1.2.2, this peculiar behaviour is only possible if neutrinos have different masses. This experiment therefore proved that at least one neutrino has a non-zero mass. Further studies have since shown that at least two of the three neutrino species have a non-zero mass and the mass splittings are given by[1] [30]

$$\Delta m^2_{12} \equiv m^2_2 - m^2_1 \simeq 7.4 \cdot 10^{-5}\text{eV}^2, \quad \Delta m^2_{23} \equiv m^2_3 - m^2_2 \simeq 2.5 \cdot 10^{-3}\text{eV}^2 \text{ (N.O.)}. \tag{1.1}$$

See Table 1.1 in next section for the exact estimates of these mass splittings at a confidence level of 1σ. For historical reasons, Δm^2_{12} and Δm^2_{23} are also called the solar and atmospheric mass splittings. The discovery of neutrino oscillations is still for now the only well-established laboratory evidence of physics beyond the Standard Model[2]. However, there is experimentally still a lot to unravel. In particular, the question of whether or not the lightest of the three neutrinos have a non-zero mass is still unsolved and an active research topic. For now, only an upper limit

$$m_{\text{lightest}} < 0.037 \text{ eV (N.O.) or } m_{\text{lightest}} < 0.042 \text{ eV (I.O.) (95\% CL)} \tag{1.2}$$

on the mass of the lightest neutrino and upper and lower bounds on the sum of the three neutrinos masses

$$\begin{aligned} 0.058 \text{ eV} < \sum_\nu m_\nu < 0.139 \text{ eV (N.O.) or} \\ 0.098 \text{ eV} < \sum_\nu m_\nu < 0.174 \text{ eV (I.O.) (95\% CL)} \end{aligned} \tag{1.3}$$

[1] N.O. and I.O. refer to normal and inverted ordering of the neutrino masses as will be explained right after.

[2] This could change in the next few years if for instance the deviation of the muon anomalous magnetic moment from the SM prediction [31] or the B meson anomalies [32] are confirmed.

can be derived from cosmological observations [33]. A second important question mark regards the hierarchy of the neutrino masses. Experiments have not yet been able to determine the sign of $m_3^2 - m_2^2$. Two scenarios are therefore allowed, respectively called *normal* ($m_1 < m_2 < m_3$) and *inverted* ($m_3 < m_1 < m_2$) ordering. Currently, normal ordering seems to be experimentally favoured [30] but not yet at the required level of confidence.

1.2 The type-I seesaw mechanism

The non-zero neutrino masses raise a lot of questions also on theoretical ground. While we have detailed some of the experimental evidences pointing towards a non-zero neutrino mass, theoretical explanations for the origin of the neutrino masses and how it can induce oscillations between neutrino flavours are still to be given. This is the goal of the present section.

Chirality is an intrinsic properties of particles depending on how they transform under Lorentz transformation. There are two possible chiralities: left-handed and right-handed. Whether a particle is left- or right-handed has strong physical implications since only left-handed particles feel the weak interaction within the Standard Model. As can be seen from Figure 1.2, all the Standard Model particles have been found as both right- and left-handed. The only known exceptions are the neutrinos which have solely been discovered in their left-handed version.

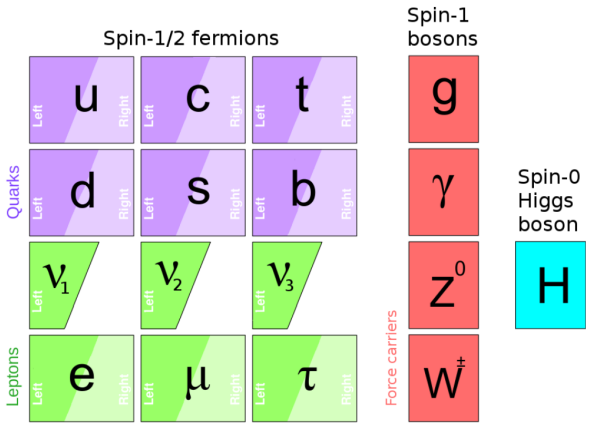

Figure 1.2: Particle content of the Standard Model. Taken from [34].

This is problematic as all the fermions within the Standard Model get their mass through a Yukawa interaction of the form

$$Y(\bar{\psi}_L \cdot \phi)\psi_R + \text{hermitian conjugate (h.c.)} \tag{1.4}$$

After the electroweak symmetry breaking, the Higgs field ϕ takes the expectation value $\begin{pmatrix} 0 \\ v \end{pmatrix}$, $v \simeq 174$ GeV being the expectation value at zero temperature of the Higgs field, and (1.4) takes the form of a mass term. For the SM, the symmetry breaking has been estimated to happen approximately at $T_{\text{ew}} \simeq 160$ GeV [35], referred as the electroweak scale. This is the celebrated *Brout-Englert-Higgs mechanism* [36, 37].

The simplest way to give a mass to neutrinos is then to extend the Standard Model with right-handed neutrinos and couple them to the Higgs boson and left-handed neutrinos as in

(1.4), a solution called the *type-I seesaw mechanism*. This is far from being the only way to make the neutrinos massive. Other solutions include the type-II [38] and type-III [39] seesaw mechanisms where the right-handed neutrinos are replaced by SU(2) scalar and fermionic triplets respectively. One can also choose to introduce more than one new field [40] to generate neutrino masses or to induce these at the loop level [41]. A common feature to all these models is the introduction of yet undiscovered new heavy particles coupled to the left-handed neutrinos.

In the rest of this thesis, we only consider the type-I seesaw model. As already said, it consists of adding an arbitrary number[3] n of right-handed neutrinos generations coupled to the left-handed neutrinos. Their masses and interactions are described by the Lagrangian

$$\mathcal{L}_{\text{int}} = F_{ai}(\bar{\ell}_a\tilde{\phi})\nu_{Ri} + \frac{1}{2}\bar{\nu}^c_{Ri}(M_M)_{ij}\nu_{Rj} + \text{h.c.} \tag{1.5}$$

before the electroweak symmetry breaking. $\tilde{\phi} = i\sigma_2\phi^* = \begin{pmatrix} 0 & 1 \\ -1 & 0 \end{pmatrix}\phi^*$. F is generically a $3 \times n$ matrix of complex Yukawa couplings, ℓ is the usual lepton doublet and a, i, j are the flavour indices. After the symmetry breaking, this part of the Lagrangian becomes

$$\frac{1}{2}\big(\bar{\nu}_{La}(M_D)_{ai}\nu_{Ri}\big) + \bar{\nu}^c_{Ri}(M_M)_{ij}\nu_{Rj} + \text{h.c.} \tag{1.6}$$

The mass term therefore consists of a Dirac mass $M_D = v \cdot F$ coming from the standard Higgs mechanism. However, if the neutrino masses solely originates from the Brout-Englert-Higgs mechanism, the smallness of the neutrino masses would imply incredibly small Yukawa couplings $|F| \sim \frac{m_\nu}{v} = \mathcal{O}(10^{-13})$. Such a small number is usually seen as "unnatural" by theorists. For comparison, the Yukawa coupling of the lightest known charged fermion, the electron, is $\mathcal{O}(10^{-6})$. There is therefore no reason not to add a second term, a Majorana mass M_M. This peculiar term is forbidden for every other particles since the fields $\bar{\psi}^c_R$ and ψ_R have the same quantum numbers which implies that this term is not gauge invariant except for gauge singlets like the right-handed neutrinos.

We can rewrite the mass term (1.6) in a block-matrix form

$$\frac{1}{2}\begin{pmatrix}\bar{\nu}_L & \bar{\nu}^c_R\end{pmatrix}\begin{pmatrix} 0 & M_D \\ M_D^t & M_M \end{pmatrix}\begin{pmatrix}\nu^c_L \\ \nu_R\end{pmatrix} + \text{h.c.} \tag{1.7}$$

making use of the relations[4] $\bar{\nu}^c_R M_D^t \nu^c_L = \bar{\nu}_R M_D \nu_L$. Flavour indices are implicit in this formulation as spinors of different flavours were concatenated into a unique one. (1.7) is expressed in terms of the interaction eigenstates ν_L, ν_R. The physical masses of the particles are given by the eigenvalues of this matrix. Before performing the diagonalisation in the most general case, let us first study the one-flavour scenario. In this case, the mass matrix can be written

$$\begin{pmatrix} 0 & m \\ m & M \end{pmatrix}$$

where $m, M > 0$ are real numbers. The eigenvalues of this matrix can be easily found

$$\lambda_\pm = \frac{1}{2}(M \pm \sqrt{M^2 + 4m^2}) \underset{m \ll M}{\longrightarrow} \begin{cases} \lambda_- \simeq -\frac{m^2}{M} \\ \lambda_+ \simeq M \end{cases} .$$

[3] Since right-handed neutrinos are gauge singlets, there is no constraint on their number of generations from anomaly cancellations.

[4] We remind the reader that $\psi^c = -i\gamma^2\psi^*$ by definition of the charge conjugation operator.

The limit where the Majorana mass is way larger than the Dirac mass $M \gg m$ is usually referred as the seesaw limit. One can now understand the denomination "seesaw" for the model: The light neutrino mass decreases as the mass of the heavy one increases. This may therefore explain why the SM neutrinos are so light compared to the rest of the particles. A typical Dirac mass around the electroweak scale $M_D \sim \mathcal{O}(100 \text{ GeV})$, induced by "natural" Yukawa couplings $F \sim \mathcal{O}(1)$, combined with a Majorana mass at the GUT scale $M_M \sim \mathcal{O}(10^{14} \text{ GeV})$ would be enough to account for the 6 orders of magnitude of difference between the upper limit (1.3) and the electron mass without requiring artificially small couplings.

Let us now go back to the general case. As the mass matrix is a square, complex and symmetric matrix, it admits a Takagi factorisation, meaning there exists U unitary such that

$$U^\dagger M U^* = \begin{pmatrix} m_\nu & 0 \\ 0 & m_N \end{pmatrix} \tag{1.8}$$

where m_ν and m_N are the diagonalised mass matrices of respectively the light and heavy neutrinos. U can be parameterised as

$$U = \begin{pmatrix} \cos(\theta) & \sin(\theta) \\ -\sin(\theta^\dagger) & \cos(\theta^\dagger) \end{pmatrix} \begin{pmatrix} U_\nu & 0 \\ 0 & U_N^* \end{pmatrix}. \tag{1.9}$$

θ is a mixing matrix and the functions sin and cos are as usual generalised to matrices using the Taylor series

$$\sin(\theta) = \sum_{k=0}^{+\infty} \frac{(-\theta\theta^\dagger)^k \theta}{(2k+1)!} \text{ and } \cos(\theta) = \sum_{k=0}^{+\infty} \frac{(-\theta\theta^\dagger)^k}{(2k)!}.$$

θ will transform the mass matrix of equation (1.7) into a semi-diagonalised version $\begin{pmatrix} M_\nu & 0 \\ 0 & M_N \end{pmatrix}$ similarly to the one-flavour scenario. Physically, θ encode how strong the mixing between left- and right-handed neutrinos is. In the seesaw limit, it is given by $\theta \simeq M_D \cdot M_M^{-1}$. But since M_ν, M_N are matrices and not numbers, additional matrices U_ν, U_N are also necessary to diagonalise these and obtain (1.8). U_ν is usually known as the *PMNS matrix* and is most commonly parameterised as [42]

$$\begin{pmatrix} c_{12}c_{13} & s_{12}c_{13} & s_{13}e^{-i\delta} \\ -s_{12}c_{23} - c_{12}s_{23}s_{13}e^{i\delta} & c_{12}c_{23} - s_{12}s_{23}s_{13}e^{i\delta} & s_{23}c_{13} \\ s_{12}s_{23} - c_{12}c_{23}s_{13}e^{i\delta} & -c_{12}c_{23} - s_{12}c_{23}s_{13}e^{i\delta} & c_{23}c_{13} \end{pmatrix} \cdot \begin{pmatrix} 1 & 0 & 0 \\ 0 & e^{i\frac{\alpha_1}{2}} & 0 \\ 0 & 0 & e^{i\frac{\alpha_2}{2}} \end{pmatrix}$$

where $s_{ij} = \sin(\Theta_{ij})$ and $c_{ij} = \cos(\Theta_{ij})$, Θ_{ij} being the PMNS mixings angles. The phase δ is usually called the Dirac phase. This parameterisation is similar to the one used for the CKM matrix, the only difference being the presence of two additional complex phases, called the Majorana phases, α_1 and α_2. These arise due to the impossibility to redefine the right-handed neutrino phases. The Majorana mass term is indeed not invariant under the transformation $\nu_R \to e^{i\alpha}\nu_R$

$$\bar{\nu}^c_{Ri}(M_M)_{ij}\nu_{Rj} \to e^{2i\alpha}\bar{\nu}^c_{Ri}(M_M)_{ij}\nu_{Rj}.$$

As we will see in section 1.3, complex phases can induce a matter-antimatter asymmetry, hence the importance of Majorana and Dirac phases. However, these three complex phases have not yet been measured and one cannot for now exclude that all three are zero, even though latest measurements point towards a non-zero Dirac phase. Best fit values as of June 2020 [30] at the

Parameter	Normal ordering	Inverted ordering
Θ_{12} (°)	$33.44^{+0.78}_{-0.75}$	$33.45^{+0.78}_{-0.75}$
Θ_{23} (°)	$49.0^{+1.1}_{-1.4}$	$49.3^{+1.0}_{-1.2}$
Θ_{13} (°)	$8.57^{+0.13}_{-0.12}$	$8.61^{+0.12}_{-0.12}$
δ (°)	195^{+51}_{-25}	286^{+27}_{-32}
Δm^2_{12} ($\cdot 10^{-5}$eV^2)	$7.42^{+0.21}_{-0.20}$	$7.42^{+0.21}_{-0.20}$
Δm^2_{k3} ($\cdot 10^{-3}$eV^2)	$2.514^{+0.028}_{-0.027}$ $(k=2)$	$-2.497^{+0.028}_{-0.028}$ $(k=1)$

Table 1.1: Latest estimates at the 1σ confidence limit for the PMNS angles, Dirac phase and mass splittings published by the ν-fit collaboration [30].

1σ confidence limit for the Dirac phase and PMNS angles for both normal and inverted ordering are summarised in Table 1.1.

Back to our problem, one can then deduce the (non-diagonalised) mass matrices for light and heavy neutrinos, in the seesaw limit where $|\theta_{ij}| \ll 1$ for each $i \in \{1,2,3\},\ j \in \{1,\dots,n\}$, by performing a Taylor expansion in θ

$$M_\nu \simeq -\theta M_M \theta^t \tag{1.10a}$$

$$M_N \simeq M_M + \frac{1}{2}\cdot(\theta^\dagger\theta M_M + M_M^t\theta^t\theta^*). \tag{1.10b}$$

We limited ourselves to the second order in θ, meaning that $\cos(\theta) = 1 - \frac{\theta\theta^\dagger}{2}$ and $\sin(\theta) = \theta$ in this approximation. The seesaw relation (1.10a) allows us to constrain the minimal number of right-handed neutrinos needed to explain neutrino oscillations experiments. Indeed, we know from (1.1) that at least two ordinary neutrinos are massive. Moreover, θ is a $3 \times n$ matrix and $M_\nu \simeq -\theta M_M \theta^t$ will thus have at most n non-zero eigenvalues. This forces the presence of at least two right-handed neutrinos.

Finally, we can also deduce the low-energy mass eigenstates, at tree level, in terms of the interaction eigenstates. The light neutrinos of mass m_ν are defined by

$$\nu_a = \left[V_\nu^\dagger \nu_L + V_\nu^t \nu_L^c - U_\nu^\dagger \theta \nu_R^c - U_\nu^t \theta^* \nu_R\right]_a \tag{1.11}$$

while the heavy neutrinos of mass M_M are defined by

$$N_i = \left[V_N^\dagger \nu_R + V_N^t \nu_R^c - \theta^t U_N^\dagger \nu_L^c - \theta^\dagger U_N^t \nu_L\right]_i. \tag{1.12}$$

We have defined $V_\nu = (1 - \frac{1}{2}\theta\theta^\dagger)U_\nu$ and $V_N = (1 - \frac{1}{2}\theta^t\theta^*)U_N$. These new heavy particles N_i are sometimes also called heavy neutral leptons (HNLs). As they do only interact through their mixing with left-handed neutrinos in minimal scenarios, these HNLs are sometimes referred as *sterile neutrinos* in opposition to the *active* (SM) neutrinos. This definition of heavy neutrinos can be extended to the symmetric phase where we instead consider eigenstates of the Majorana mass M_M as heavy neutrinos.

For $M_M = 0$, relations (1.11) and (1.12) are not valid and neutrinos are usual Dirac particles. However, if $M_M \neq 0$, then the light and heavy mass eigenstates ν_a, N_i are Majorana spinors since they verify the relation $\psi^c = \psi$ as can be seen from (1.11) and (1.12). Note that this relation holds at every order in the θ-expansion. The exact nature of the neutrino is still an open question for the moment and several experiments (see *e.g.* GERDA [43], EXO-200 [44], KamLAND-Zen [45]) are currently trying to unravel this problem. One way to decide would be to observe a neutrinoless double beta decay. If the neutrinos are Majorana particles, then they are their own antiparticles and can annihilate each other. One could hope to detect such annihilation in nuclei decay. If the simple beta decay is kinematically disfavoured, nuclei will mostly decay while emitting two electrons and neutrinos. The emitted neutrinos could then annihilate each other and we would observe an absence of missing energy in the electrons spectra. The exact Feynman diagram of the process is shown in Figure 1.3.

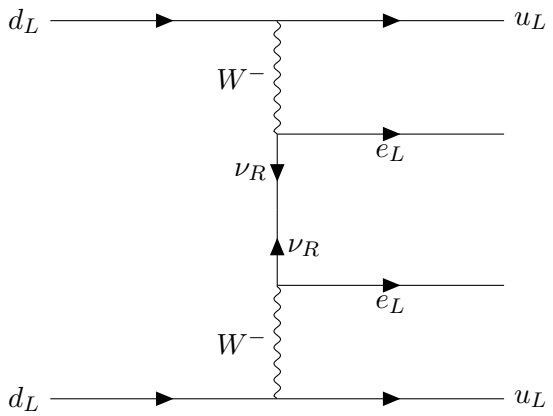

Figure 1.3: Standard example of neutrinoless double beta decay.

Even though it provides an explanation for the origin of light neutrino masses, the seesaw mechanism however does not precise the order of magnitude of M_M itself since light neutrino masses are only sensitive to a combination of the Yukawa coupling F and the Majorana mass. For a review of the different possible scales and their motivations, we refer the reader to [46]. One can still deduce an upper bound on the scale of the Majorana mass

$$M_M \lesssim 10^{15} \text{ GeV},$$

imposing unitarity on $\nu + \nu \to W + W$-type processes as has been done in [47]. Using this freedom, one usually divides seesaw models in two main categories. Models where the Majorana mass M_M is way above the electroweak scale are called *high-scale seesaw* models. These are appealing from a theoretical point of view as they can be naturally embedded in some Grand Unification theories [48] and can directly explain the smallness of the neutrino masses by the smallness of the ratio vM_M^{-1}. On the contrary, *low-scale seesaw* models assume that M_M lies at or below the TeV scale. These are particularly interesting from an experimental point of view as the smallness of the HNL mass makes the detection of the HNLs in high-energy experiments conceivable. However, the ratio vM_M^{-1} is not small anymore in low-scale seesaw models and cannot explain the smallness of light neutrino masses by its own. If we want the Yukawa couplings F not to be small and have a chance to detect these HNLs, cancellations in the matrix product $FM_M^{-1}F^t$ are needed. This can be achieved via a new symmetry, detailed in section 2.3.

As mentioned in the introduction, heavy neutrinos are well motivated particles that can solve

several shortcomings of the Standard Model, not only the neutrino mass problem. They can also produce a sufficient amount of baryon asymmetry through leptogenesis, which we will talk about in section 1.4, and are also potential Dark Matter candidates [4]. They can even solve those three problems simultaneously within the Neutrino Minimal Standard Model [5]. Heavy neutrinos are also quite well motivated from a theoretical point of view as they quite naturally appear in several gauge extensions of the Standard Model such as the left-right symmetric models [18, 49], SO(10) [17] or SU(5) [50].

1.2.1 The Casas-Ibarra parametrisation

Adding right-handed neutrinos to the Standard Model Lagrangian means that we have to keep track of more parameters. In fact, one can deduce from Lagrangian (1.6) that $7n-3$ new parameters are needed when adding n generations of right-handed neutrinos. Indeed, it is always possible to place ourselves in a basis where M_M is diagonal which means that one have to keep track of n real Majorana masses. Moreover, in this basis, M_D is *a priori* a complex $3\times n$ matrix which implies that $6n$ new parameters will be needed. However, we can always redefine the phase of the left-handed neutrinos $\nu_L \to e^{i\alpha}\nu_L$ to get rid of three additional phases. The total number of free parameters is therefore

$$n + 6n - 3 = 7n - 3$$

as expected. Five of these new parameters are constrained by experiments (the two light neutrinos mass splittings Δm^2_{12} and Δm^2_{k3} and the three PMNS angles Θ_{ij}, see Table 1.1). In general, Lagrangian (1.5) can be expressed in various different basis. A choice which will reveal to be particularly useful is the so-called *Casas-Ibarra parametrisation* [51]. Let us work in the basis where

- ⋆ The Yukawa matrix h_{ab}, coupling charged leptons e_b to left-handed neutrinos $\nu_{L,a}$ via the Yukawa interaction $h_{ab}(\bar{\nu}_{L,a}\cdot\phi)e_b$, is diagonal and real.
- ⋆ The Majorana mass matrix is diagonal and real.

Using the same notations as in the previous section, let us denote U_ν the PMNS matrix diagonalising M_ν. Then, the Casas-Ibarra parametrisation consists of expressing the Yukawa coupling matrix F in terms of a complex orthogonal matrix $\mathcal{R}$

$$F = \frac{i}{v} U_\nu m_\nu^{\frac{1}{2}} \mathcal{R} M_M^{\frac{1}{2}}. \tag{1.13}$$

This parametrisation of the Yukawa coupling matrix F is particularly useful as it ensures consistency with neutrino oscillations data: $M_\nu \simeq -\theta M_M \theta^t$ is automatically verified. In this parametrisation, the $7n-3$ parameters respectively are the three eigenvalues of $h\cdot h^\dagger$, the n of M_M and the three of M_ν in addition to the $6n-12$ independent[5] from $\mathcal{R}$. In the $n=2$ and normal ordering case for instance, $\mathcal{R}$ can be parametrised by a single complex parameter w

$$\mathcal{R} = \begin{pmatrix} 0 & 0 \\ \cos w & \sin w \\ -\xi \sin w & \xi \cos w \end{pmatrix} \tag{1.14}$$

[5]This number of free parameters is only valid for $n \geq 3$. $\mathcal{R}$ is a $3\times n$ which has *a priori* $6n$ free parameters to which we have to subtract 12 already fixed by the relation $\mathcal{R}\mathcal{R}^t = \mathbb{1}$. In the $n=2$ case, $\mathcal{R}$ is made of only two real parameters.

and the overall coupling strength of the HNLs can be expressed as [52]

$$U^2 = \sum_{i,a} |(\theta U_N^*)_{ai}|^2 = \frac{M_2 - M_1}{2M_2M_1}(m_2 - m_3)\cos(2\mathrm{Re}w) + \frac{M_1 + M_2}{2M_1M_2}(m_2 + m_3)\cosh(2\mathrm{Im}w) \quad (1.15)$$

where M_1, M_2 is the mass of both HNLs and m_2, m_3 the mass of the light neutrinos ν_2, ν_3. ξ is a constant equal to ± 1 taking into account the sign of the determinant of the orthogonal matrix $\mathcal{R}$. One can however observe from (1.15) that the transformation

$$\xi \to -\xi,\ M_2 - M_1 \to M_1 - M_2,\ \mathrm{Im}(w) \to -\mathrm{Im}(w) \text{ and } \mathrm{Re}(w) \to \pi - \mathrm{Re}(w) \quad (1.16)$$

is equivalent to swapping the heavy neutrinos $N_1 \longleftrightarrow N_2$

$$\mathcal{R} \longrightarrow \begin{pmatrix} 0 & 0 \\ -\cos w & \sin w \\ \xi \sin w & \xi \cos w \end{pmatrix}$$

and has therefore no physical consequences[6]. Therefore, we can set $\xi = 1$. Relation (1.15) also highlights the fact that, since $\cos(2\mathrm{Re}(w))$ is bounded by 1, the largest value of the overall coupling strength U^2 are reached when $\mathrm{Im}(w)$ is large. In the case where $n = 3$ which will be of primal interest for the rest of this thesis, $\mathcal{R}$ can be expressed using three complex Euler angles w_{ij} as

$$\mathcal{R} = \mathcal{R}^{(12)}\mathcal{R}^{(23)}\mathcal{R}^{(13)}$$

where

$$\mathcal{R}^{(ij)}_{(ii)} = \mathcal{R}^{(ij)}_{jj} = \cos(w_{ij}),\quad \mathcal{R}^{(ij)}_{ij} = \mathcal{R}^{(ij)}_{ji} = \sin(w_{ij}) \text{ and } \mathcal{R}^{(ij)}_{kk,\ k\neq i,j} = 1.$$

1.2.2 Neutrino oscillations

The last important point of this introduction to the type-I seesaw mechanism is how the fact that SM neutrinos are massive can induce the oscillations between the different neutrino flavours that have been observed by the Homestake experiment. Neutrinos are usually produced through the weak interaction. As discussed in section 1.1, they are for instance produced in the sun through the fusion of two protons into deuterium. Therefore, neutrinos are mainly produced as weak interaction eigenstates ν_{La}. However, the light neutrinos mass matrix (1.10a) is not necessarily diagonal in the interaction basis and will induce transitions between different flavours of neutrinos thanks to the term $\bar{\nu}_{La}(M_\nu)_{ab}\nu_{Lb}$ in the Lagrangian. For the purpose of this rapid explanation, we neglect all the $\mathcal{O}(\theta)$ corrections within the definition of the neutrinos mass eigenstates.

One can also understand this feature in a more physically meaningful way using simple quantum mechanics. We will simplify the problem and suppose that only two generations of neutrinos exist. Let us further assume that flavour eigenstates $\nu_e,\ \nu_\mu$ and mass eigenstates $\nu_1,\ \nu_2$ are related by the a unitary transformation

$$\begin{pmatrix} \nu_e \\ \nu_\mu \end{pmatrix} = \begin{pmatrix} \cos\theta & \sin\theta \\ -\sin\theta & \cos\theta \end{pmatrix} \cdot \begin{pmatrix} \nu_1 \\ \nu_2 \end{pmatrix}.$$

[6] This observation can be derived more rigorously applying the transformation (1.16) to the definition of the $\mathcal{R}$-matrix (1.14).

This relation is very similar to (1.12) in the seesaw limit. Initially, neutrinos are produced in flavour eigenstates. However, the time evolution operator e^{iHt}, where H denotes the Hamiltonian and t the time, is diagonal in the mass basis, and the states evolves as

$$\nu_1(t) = e^{iE_1 t}\nu_1(0) \text{ and } \nu_2(t) = e^{iE_2 t}\nu_2(0).$$

$E_a = \sqrt{p^2 + m_a^2}$ is the energy of the produced neutrinos and m_a the mass of the mass eigenstate ν_a. When $m_1 \neq m_2$, the two different components of the flavour eigenstates will evolve differently and this will allow for transitions $\nu_e \to \nu_\mu$. Indeed, an initial electron neutrino will evolve as

$$\nu(t) = (\nu_1 \cos\theta + \nu_2 \; e^{i(E_2 - E_1)t} \sin\theta) \cdot e^{iE_1 t}$$

$$= \nu_e \cdot (\cos^2\theta e^{iE_1 t} + \sin^2\theta e^{iE_2 t}) + \nu_\mu \sin\theta\cos\theta \cdot (e^{iE_1 t} - e^{iE_2 t}).$$

It clearly shows that the initial electron neutrino wavefunction becomes a mixture of electron and muon neutrino as it evolves. Moreover, this also shows that the transition probability depends on the energy via the difference $E_2 - E_1$ only. In absence of mass splittings, no oscillations can therefore take place. The story is actually more complicated if we try to explain the solar neutrino anomaly since we have to take into account the propagation of these neutrinos in matter and not in vacuum anymore. A more detailed introduction to this problem can be found in [53] for the interested reader.

1.3 Baryogenesis in a nutshell

One of the great mystery of modern physics is the reason behind the overabundance of matter with respect to antimatter. It has now been known for almost a century, since the discovery of the positron by Carl D. Anderson in 1932, that a second category of particles must exist in addition to the "ordinary" — at that time, only the proton, neutron and the electron were known — particles. These are known as antiparticles and possess the peculiar property to have the same mass as their standard "partners" but opposite quantum numbers. Paul Dirac had in fact already predicted them four years earlier studying the solutions of its own equation, the Dirac equation, but this idea was not yet widely accepted before Anderson's discovery. Following this discovery, the observation that most of the matter that surrounds us is only made of particles raised the question:

How do we explain the seeming absence of antiparticles in the observable universe ?

More precisely, the difference between the comoving number density of baryons[7] n_b and antibaryons $n_{\bar{b}}$ normalised by the entropy density s of the universe has been measured [54] to be

$$Y_B = \frac{n_b - n_{\bar{b}}}{s} \simeq 8.6 \cdot 10^{-11}. \tag{1.17}$$

The matter-antimatter asymmetry is experimentally much less constrained in the lepton[8] sector. It is expected from a generic universe that it would produce an equal amount of matter and antimatter as initial condition. There must therefore exist a mechanism generating this imbalance between baryons and antibaryons. This physical process, whatever its precise form, is called *baryogenesis*.

[7] Baryons are strictly speaking particles made of three quarks. In cosmology however, the term is used to refer to any particle made of quarks.

[8] We remind the reader that a lepton is a spin $\frac{1}{2}$ particle which do not interact strongly.

This question is deeply linked to another one, just as fundamental, the symmetry of all microphysical processes under time reversal. The equations governing the dynamics of these fundamental processes is expected to be symmetric under time reversal $t \to -t$. Quantum electrodynamics (QED) was actually even shown to be exactly symmetric under three discrete symmetries: charge conjugation (C), parity (P) and time reversal (T). Moreover, the so-called CPT theorem [55, 56] ensured that every physically realistic theory should at least preserve the products of the three. Physicists therefore initially thought that these three symmetries were always preserved by nature.

However, a series of experiments in the 1950s and 1960s proved that each of them could be broken while the product of the three was still preserved. The experiment of Fitch and Cronin in 1964 [57] was particularly decisive in that it showed for the first time that the CP symmetry and, thanks to the CPT theorem, also the T symmetry were both broken at a microscopic level. Since a positron can essentially be seen as an electron going backwards in time, this asymmetry has the particular consequence that it makes possible to overproduce particles compared to antiparticles and therefore confirmed that producing a sizeable matter-antimatter asymmetry starting from a symmetric universe was at least conceivable. However, this was not the sole condition necessary to the production of a baryon asymmetry (BAU) as has been found out by A. Sakharov [58] in 1966 with its celebrated three conditions.

1. There must exist C- and CP-violating processes as already detailed. CP-violation is needed in order to have processes that produce in average more baryons than antibaryons whereas C-symmetry breaking is necessary to prevent processes producing more baryons than antibaryons of being compensated by "symmetric" processes producing more antibaryons than baryons.

2. There must also exist processes violating the baryon number. Baryon number is defined as $B = \frac{1}{3}(n_q - n_{\bar{q}})$ where n_q (resp. $n_{\bar{q}}$) is the number of quarks (resp. antiquarks) constituting the concerned particle. Since, as already stated, $B = 0$ initially, there must clearly exist some processes that must violate B-conservation in order to get an asymmetry.

3. Thermal equilibrium has to be broken at some stage of the universe history. Indeed, at chemical equilibrium, a process producing an excess of baryons takes place at the same rate than the reverse process which produces an excess of antibaryons.

It turns out that these three conditions are all satisfied within the Standard Model. The fact that weak interaction treats differently left-handed and right-handed particles implies that C is violated and CP-violation arises due to the complex phase within the quark mixing matrix, the CKM matrix V. An example of C-violating process is the decay $\pi^+ \to \mu^+\nu_\mu$ [59] while the decay of neutral kaon is an example of CP-violating process [57]. In the rest of this master thesis, we will see that such processes can also possibly arise in the neutrino sector, if extended with respect to the SM, and prove to be crucial for the generation of the baryon asymmetry. The amount of CP-violation coming from the quark sector is usually parametrised using the Jarkslog invariant

$$J = \mathrm{Im}\big(V_{11}V_{22}V_{12}^*V_{21}^*\big) \simeq 3 \cdot 10^{-5}.$$

The baryon number is also violated within the Standard Model by the sphaleron process. Let us define the baryon number as above. By analogy, the lepton number L as being $+1$

for all leptons, 0 for the baryons and -1 for the antileptons. Moreover, the global symmetry transformation

$$b \to e^{\frac{i\alpha}{3}} b, \quad l \to l, \quad \alpha \in \mathbb{R},$$

where b is a baryonic field and l a leptonic one, can be associated to the baryon number. One can define an equivalent transformation for the lepton number. However, these symmetries are anomalous as can be seen from

$$\partial_\mu J_B^\mu = \partial_\mu J_L^\mu = \frac{3g^2}{32\pi^2} \epsilon^{\mu\nu\alpha\beta} G_{\mu\nu} G_{\alpha\beta} \tag{1.18}$$

where g is the weak interaction coupling constant, J_B^μ, J_L^μ are the associated baryonic and leptonic currents and $G_{\mu\nu}$ is the SU(2) field strength tensor. Relation (1.18) has two strong consequences. First of all, it implies that $B - L$ is conserved since $\partial_\mu (J_B^\mu - J_L^\mu) = 0$. Second, it implies the existence of a non-perturbative process which violates the baryon number conservation. Indeed, the $SU(2)$ gauge symmetry implies the existence of several gauge equivalent but topologically different vacua as can be seen from Figure 1.4. The sphaleron process consists in a transition from one of these vacua to another. The exact variation of the total baryon number coming from this process can be computed by integrating (1.18) which has been done by 't Hooft [60] in 1976

$$\Delta B = \int_{t_i}^{t_f} \mathrm{d}t \int \mathrm{d}^3 x \; \partial_\mu J_B^\mu = 3n$$

where $n \in \mathbb{Z}$ corresponds to a winding number, usually called the Chern-Simons number. The factor 3 is linked to the presence of the three generations of quarks and leptons. This process is extremely rare at zero temperature as the rate is suppressed by the Boltzmann factor $\exp(-\frac{8\pi^2}{g^2}) \sim 10^{-180}$ since the only possibility to get such a process is by quantum tunneling. Indeed, as can be seen from Figure 1.4, the sphaleron process will bring the system from one minimum of the potential to another.

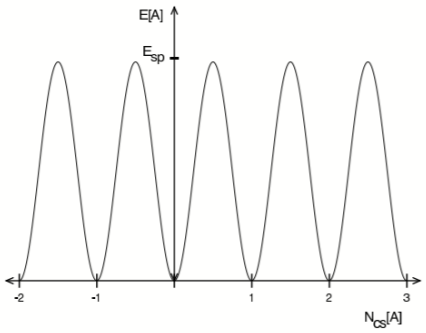

Figure 1.4: Energy dependence of a gauge configuration as a function of the winding number N_{cs}. Taken from [61].

However, as pointed out by Kuzmin, Rubakov and Shaposhnikov [15], thermal fluctuations reduce the potential barrier to overcome and increase the transition rate. The transition rate per unit volume then increases with the temperature as T^4. The process is therefore expected to be particularly abundant in the primordial universe. In fact, [35] computed that above approximately 131.7 GeV, those thermal fluctuations allow the sphaleron processes to be in

equilibrium[9]. We will later refer to this temperature as the sphaleron freeze-out temperature T_{sph}. This transition from sphaleron processes being in thermal equilibrium to being completely suppressed is in good approximation instantaneous. An example of a sphaleron process is the 12-fermions interaction ($\Delta n = +3$) [61]

$$\bar{u} + \bar{d} + \bar{c} \to d + 2s + 2b + t + \nu_e + \nu_\mu + \nu_\tau.$$

u, d, c, s, b, t are respectively the up, down, charm, strange, bottom and top quarks while the ν_a denotes the three flavours of neutrinos. Notice that, since the sphaleron is transitioning between different $SU(2)$-vacua, only the left-handed particles are concerned.

Finally, it is now known that the cooling of the universe also causes deviation from thermal equilibrium, allowing these C-, CP- and B-violating processes to actually generate baryon asymmetries. The particular temperature T_c at which a reaction ceases to be in thermal equilibrium can be estimated as the one where[10]

$$\Gamma(T_c) = H(T_c).$$

$\Gamma(T_c)$ is the rate at which the reaction happens and H is the Hubble constant, both of which depends on the temperature. At $T < T_c$, the expansion of the universe is so rapid that the particles cannot be kept in thermal equilibrium and one reaction becomes favoured compare to its inverse.

Despite being able to provide a mechanism explaining *qualitatively* the origin of the baryon asymmetry, more thorough studies have shown that the Standard Model was *quantitatively* not sufficient. [61,62] for instance show that the baryon asymmetry produced should be of the order of $Y_B \simeq 10^{-28}$ which is way below the experimental value (1.17). New mechanisms have to be found to generate additional CP-violation. Some among the most studied one are listed below.

- GUT baryogenesis. Developed for the first time in 1978 by Yoshimura [63], the asymmetry is generated in this type of model through the out-of-equilibrium decay of new heavy bosons. These new bosons find their origin in some Standard Model extensions: the Grand Unified Theories (GUT). These extensions increase the number of independent complex parameters and, therefore, the amount of CP-violation. Another convenient feature of these theories is the natural baryon number violation since baryons and leptons are unified into the same representation of the underlying gauge group.

- The Affleck-Dine mechanism [64]. It takes place in the context of a supersymmetric theory (SUSY). The asymmetry then arises from the decay of scalar superpartners into fermions due to interactions with the scalar inflaton field.

- Electroweak baryogenesis in which the departure from the thermal equilibrium arises during the electroweak phase transition. The Standard Model baryogenesis detailed earlier falls into this category. However, this one is not feasible as the Higgs is too heavy $m_H \gtrsim 70$ GeV meaning that the phase transition is of second order while it should be strongly first order for the electroweak baryogenesis to be successful. Moreover, CP-violation from the quark sector is also not sufficient. To overcome those two problems, some of the new approaches rely on extending the scalar sector [65].

[9] An upper bound $T \simeq 10^{12}$ GeV on the temperature for the sphaleron process to be in equilibrium has also been derived [19]

[10] In general, there exists more than one solution to this equation. The process is first brought to equilibrium at some high temperature T_e before freezing-out at T_c.

- Leptogenesis, in which the baryon asymmetry initially originated in a lepton asymmetry.

In the rest of this master thesis, we will solely focus on the latter, which we will detail in the next section.

1.4 An introduction to leptogenesis

In this section, we explain how the excess of matter may have been produced under the form of an initial lepton asymmetry which would have then been partially transformed into a baryon asymmetry by the sphaleron process. We mainly focus on the initial model of *thermal leptogenesis* developed in the 1980s by Yanagida and Fukugita [2].

Some of the most popular explanations for the baryon asymmetry such as GUT baryogenesis rely on the presence of new heavy particles which decay out of thermal equilibrium to produce an excess of baryons. However, as was first noted in 1986 by Yanagida and Fukugita [2], extending the gauge group of the Standard Model is not necessary to find new suitable heavy particles. Indeed, as mentioned earlier, the sphaleron process, which violates the baryon number, in fact conserves B-L. This opens us the possibility to get a baryon asymmetry from a lepton asymmetry as an initial lepton asymmetry will be redistributed by the sphaleron process into non-zero lepton and baryon asymmetries. Assuming the sphaleron and Standard Model processes are at equilibrium, it can in fact be shown that, within the type-I seesaw model and the symmetric phase of the Standard Model,

$$B = \frac{28}{79}(B - L). \tag{1.19}$$

A derivation of this relation is given in appendix A. This type of model is called *baryogenesis from leptogenesis* or more simply *leptogenesis*. The main asset of leptogenesis is that new heavy particles are already present in minimal extensions of the Standard Model as solutions to another fundamental problem: the origin of neutrino masses. Indeed, the three different types of seesaw mechanisms all make use of some heavy internal states to generate light neutrino masses. The same heavy particles can be used to generate the lepton asymmetry when they decay out of thermal equilibrium. In the rest of the present master thesis, we focus on the type-I seesaw-based leptogenesis which is by far the most studied of these three possible models.

The 1986-paper from Yanagida and Fukugita assumed minimal Lagrangian (1.5) and that heavy neutrinos reach thermal equilibrium way before the sphaleron freeze-out which effectively wash-out any prior asymmetry. This can be achieved if the mixing angle θ is sufficiently large that it can bring them to equilibrium very early in the universe history. Thereafter, when the temperature drops below their mass, their production rate can not keep up with the expansion of the universe anymore and they begin to decay out of equilibrium. Yanagida and Fukugita assumed the heavy neutrino masses lie way above the electroweak scale so that the Standard Model still was in its symmetric phase at that stage. As can be seen from Lagrangian (1.5) and the definition of mass eigenstates (1.12), the HNLs can decay following

$$N_i \to \ell_j + \phi \quad \text{and} \quad N_i \to \bar{\ell}_j + \phi^*.$$

The CP-violation coming from this decay first generates the lepton asymmetry and, as a consequence, a subsequent baryon asymmetry. One can notice that the amplitude $\mathcal{M}$ for the first decay is proportional at tree level to F_{ij} while the amplitude for the second decay is proportional

to F^*_{ij}. Therefore, if the Yukawa coupling F is complex, this process is CP-violating. However, since the decay rate is proportional to $|\mathcal{M}|^2$, this decay still remains CP-conserving at tree level. To actually generate CP-violation, one loop corrections have to be considered as the interference between the tree level and one loop diagrams is needed to generate the CP-asymmetry. The decay at one loop order contains the contribution of the following three diagrams.

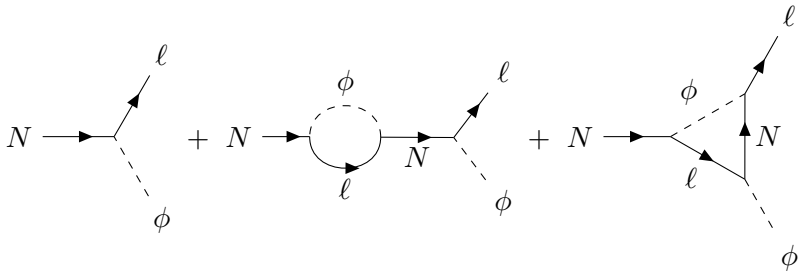

tree level *wave function* *vertex* (1.20)

The flavour indices were omitted as one can draw these diagrams for every combination of them. As shown above, the middle diagram in (1.20) is usually referred as the wave function diagram whereas the rightmost one is called the vertex diagram. One can also quantify the amount of asymmetry coming from this process and, therefore, get a rough approximation of the $B-L$ asymmetry generated. For instance, assuming hierarchical Majorana masses ($M_1 \ll M_2 \ll M_3$) and high temperature $T > 10^{12}$ GeV so that the Standard Model flavours are indistinguishable ("vanilla leptogenesis") and defining an asymmetry parameter ϵ_i, usually known as the *decay asymmetry*, for the right-handed neutrino flavour i as

$$\epsilon_i \equiv \frac{\Gamma_{N_i\to\ell+\phi} - \Gamma_{N_i\to\bar{\ell}+\phi^*}}{\Gamma_{N_i\to\ell+\phi} + \Gamma_{N_i\to\bar{\ell}+\phi^*}}, \tag{1.21}$$

one obtains [2]

$$\epsilon_i = -\frac{3}{16\pi}\frac{1}{(F^\dagger F)_{ii}}\sum_{j=2,3}\mathrm{Im}\Big[(FF^\dagger)^2_{ji}\Big] f(\frac{M_i^2}{M_j^2}) \tag{1.22}$$

where j is the flavour index and $f(\frac{M_1^2}{M_j^2})$ is a loop factor

$$f(x) = \sqrt{x}\,\big[1 + (1+x)\ln(\frac{x}{1+x})\big].$$

The contribution (1.22) neglects the contribution of the wave function diagram due to the large mass splittings between HNLs. To get a precise estimate for the baryon asymmetry and to be able to track the temperature dependence of these asymmetries, one can model the generation of asymmetries using the following system of Boltzmann equations[11]

$$\frac{\mathrm{d}}{\mathrm{d}z}n_1 = -\frac{\Gamma_D + \Gamma_S}{Hx}(n_1 - n_1^{eq}) \tag{1.23a}$$

$$\frac{\mathrm{d}}{\mathrm{d}z}n_{B-L} = \epsilon\frac{\Gamma_D}{Hz}(n_1 - n_1^{eq}) - \frac{\Gamma_W}{Hz}n_{B-L} \tag{1.23b}$$

[11] These equations were shown [21] to be a limiting case of the more general set of equations (2.14). Those allow for a comprehensive treatment when all neutrino flavours play a significant role.

n_1 (n_1^{eq}) and n_{B-L} being respectively the number density of HNLs N_1 (at equilibrium) and of $B-L$ asymmetries. $z = \frac{M_1}{T}$, M_1 being the mass of this heavy neutrino N_1. This particular set of equations relies on the "strong washout" assumption that the preexisting asymmetries and those created by $N_{2,3}$ are completely washed out, *i.e.* depleted, by N_1. Therefore, we can limit ourselves to only keep track of the asymmetries caused by N_1. When $n > 1$ heavy neutrinos do participate to leptogenesis, equation (1.23a) just have to be replaced by a set of n decoupled equations. Main processes contributing to the rates Γ_D, Γ_S and Γ_W include

- *1 ↔ 2 processes*: HNLs decays and inverse decays (1.20) $N \leftrightarrow \ell + \phi$. CP-violation from inverse decays have a contribution opposite to (1.22).
- *2 ↔ 2 scatterings*:
  - ⋆ $\Delta L = 1$ Higgs-mediated scatterings between quarks doublets Q, HNLs, lepton doublets and the right-handed top quarks ($\bar{Q} + \ell \leftrightarrow \bar{t}_R + N$, $\bar{Q} + t_R \leftrightarrow \bar{\ell} + N$, $L + t_R \leftrightarrow Q + N$).

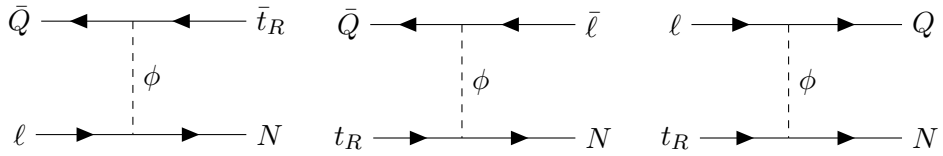

  The top quarks is the sole right-handed quarks to be considered as his Yukawa coupling is the only one to be of order one.
  - ⋆ $\Delta L = 1$ scatterings including gauge bosons. It includes scatterings between the Higgs fields, gauge boson G, HNLs and the leptons doublets ($G+\ell \to \phi^\dagger + N$, $\phi + \ell \to G + N$, $G + \phi \to \bar{\ell} + N$).

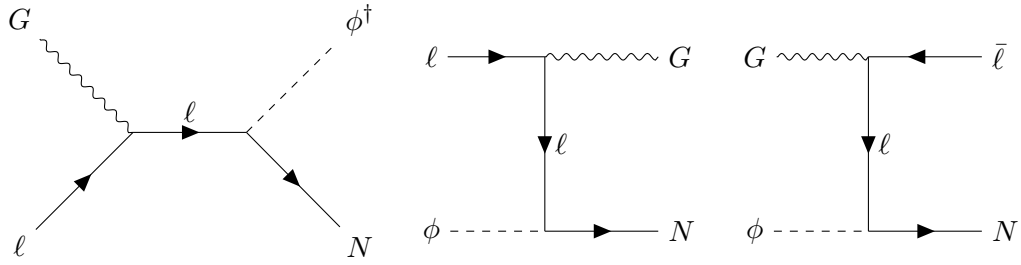

  - ⋆ $\Delta L = 2$ scatterings between lepton doublets and Higgs fields such as the HNL-mediated scattering $\ell + \phi \leftrightarrow \bar{\ell} + \phi^\dagger$

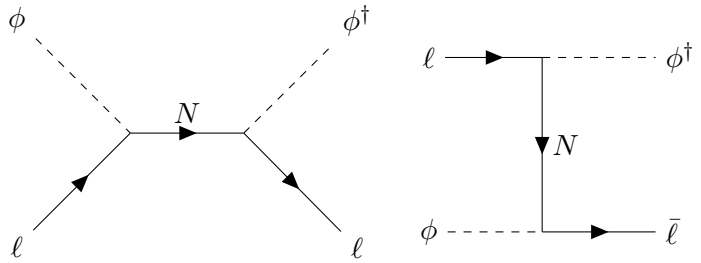

We limit ourselves to $2 \leftrightarrow 2$ processes for the scattering part as processes with three or more initial particles are much more rare[12]. Γ_D includes the contribution of decays and inverse decays, Γ_S only contains the contribution of $\Delta L = 1$ scatterings while Γ_W contains the contribution of inverse decays and $\Delta L = 1, 2$ scatterings. (1.23a) then just encodes the fact that only decays, inverse decays and $\Delta L = 1$ scatterings do modify the number of HNLs. Since $\Gamma_D, \Gamma_S > 0$, (1.23a) implies that the interaction of the HNLs with the thermal bath, *i.e.* the rest of the SM particles which are in thermal equilibrium, drives the HNL to equilibrium as is expected. The condition $\Gamma > H$ to be in equilibrium can easily be observed from this equation as $H \gg \Gamma_D + \Gamma_S$ makes $\frac{\mathrm{d}}{\mathrm{d}z} n_1$ small and effectively prevent the system to reach equilibrium.

(1.23b) presents two distinct contributions. The first one, proportional to ϵ the CP-asymmetry already computed in equation (1.22), enhances the asymmetry already present thanks to the CP-violating $N \to \ell + \phi$ decay mentioned earlier. The second term wash out any asymmetry present thanks to inverse decays and scattering processes. An example of numerical solutions to the set of equations (1.23) is given in Figure 1.5.

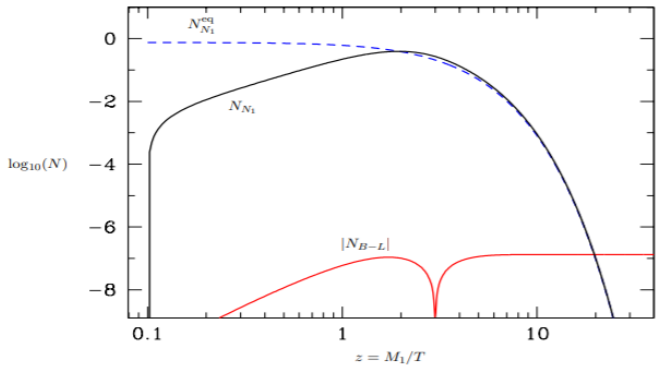

Figure 1.5: Evolution with the temperature of the N_1 number density (blue) and the asymmetry abundance (red). The dashed line represents the evolution of the N_1 abundance if HNLs reach thermal equilibrium very early in the universe history while the black line stands for the evolution of HNLs starting with vanishing number density. M_1 has been taken to be 10^{10} GeV. Taken from [68].

One can clearly observe the behaviour predicted by Yanagida and Fukugita. The heavy neutrino abundances, initially vanishing, reach thermal equilibrium after some time. At thermal equilibrium, the second equation of (1.23) rewrites

$$\frac{\mathrm{d}}{\mathrm{d}z} n_{B-L} = -\frac{\Gamma_W}{Hz} n_{B-L}.$$

The asymmetries are therefore washed out with no contribution of the CP-violating production of HNLs. The red curve goes back to zero. Finally, the HNLs fall out of equilibrium as the temperature continues to drop below M_1. The out-of-equilibrium N_1-decay will generate again

[12]For high energies and densities, multiple soft scatterings can happen and the interference between adjacent scattering sites will have a sizeable impact. This is known as the Landau-Pomeranchuk-Migdal effect [66, 67]. Realistic simulations for leptogenesis now takes this effect into account.

some asymmetries and the red curve grows up to some constant again. The asymmetry is therefore usually parameterised as

$$Y_{B-L} \equiv \frac{n_{B-L}}{s} \simeq \frac{\kappa\epsilon_1}{g_*}.$$

κ is the so-called *washout parameter* encoding the proportion of asymmetries that are not depleted by inverse decays and scatterings. $g_* = 106.75$ is the number of degrees of freedom within the Standard Model at temperatures higher than the electroweak scale. It is important to mention that the hierarchical structure of the HNL masses used as hypothesis for this model is not totally unconstrained. In absence of any cancellation in the seesaw formula (1.10a), one can [16] put an upper bound on the decay asymmetry

$$|\epsilon_1| \lesssim \frac{3}{8\pi}\frac{M_1}{v^2}\sqrt{\Delta m^2_{23}}.$$

The current experimental bounds on Δm^2_{23} combined with estimates for the washout parameter κ [69] yield a lower bound on the mass of the lightest HNL N_1

$$M_1 \gtrsim 2 \cdot 10^9 \text{ GeV}, \tag{1.24}$$

which is known as the *Davidson-Ibarra bound*. Taking flavour effects into account, it can be lowered by at least one order of magnitude [70]. Such large masses would prevent any direct detection of HNLs in the near future as these HNLs would never be produced on-shell. The experimentally accessible mass range only extends up to $\mathcal{O}(3)$ TeV masses as can be seen from Figure 1.6. However, there are several loopholes in the derivation of this lower bound and it was soon realised that other mechanisms would allow for lower HNLs masses. These are discussed in the next chapter.

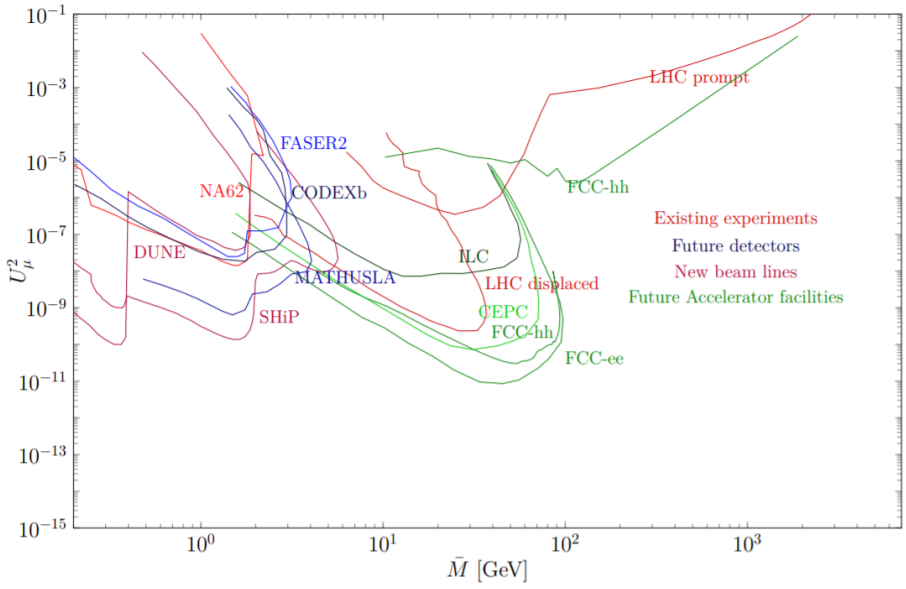

Figure 1.6: Expected sensitivity to the HNLs for several current or planned experiments: DUNE [13], NA62 [71], SHiP [72], FASER2 [73], CODEX-b [74], MATHUSLA [14], LHC main detectors [75–77] and future lepton [52] and proton colliders [78]. Only HNLs couplings to the muon flavour U^2_μ are represented here.

Chapter 2

Testable leptogenesis

In this chapter, we review low-scale leptogenesis. We start by a description of the two scenarios that we will consider in this thesis: resonant and ARS leptogenesis. We also quickly discuss how thermal effects can affect these regimes. We then make a brief aside to discuss an approximate symmetry that can be imposed on Lagrangian (1.5) to ensure large mixing angles while keeping the neutrino masses small. Next, we derive a set of density matrix equations governing the time evolution of the ARS and resonant regimes. We finish by a short review of previous studies of the parameter space of such models.

2.1 Low-scale models

As explained in the previous chapter, thermal leptogenesis implies a lower bound on the HNLs masses which would prevent any detection of these in the near future. However, the Davidson-Ibarra bound (1.24) relies on several assumptions that can be relaxed, including

1. A hierarchical HNL mass spectrum ($M_1 \ll M_2 \ll M_3$). Small mass splittings lead to *resonant leptogenesis*. This scenario is described in section 2.1.1.

2. CP-asymmetries produced by the decay of the heavy neutrinos. If the CP-asymmetries are produced during the approach of HNLs to equilibrium by their oscillations, we speak of *ARS leptogenesis*. This scenario is described in section 2.1.2.

In the rest of this master thesis, we will solely focus on these two leptogenesis scenario.

2.1.1 Resonant leptogenesis

In 1997, A. Pilaftsis showed [19] that a degeneracy in the HNL mass spectrum could enhance the asymmetry produced and therefore relax the condition[1] (1.24). In the case where the Majorana masses are not hierarchical but if on the contrary at least two of the heavy neutrinos $N_i,\ N_j$ are sufficiently degenerate, the contribution from the wave function diagrams, see (1.20), dominates over the vertex contribution. The contribution (1.22) can be neglected and the decay asymmetry ϵ_i related to the HNL N_i then takes the form [79]

$$\epsilon_i \simeq \frac{\mathrm{Im}(F^\dagger F)^2_{ij}}{(F^\dagger F)_{ii}(F^\dagger F)_{jj}} \frac{(M^2_{N_i} - M^2_{N_j}) \cdot M_{N_i}\Gamma_N}{(M^2_{N_i} - M^2_{N_j})^2 + M^2_{N_i}\Gamma^2_N}.$$

[1] Note that, from a historical perspective, the Davidson-Ibarra bound has only been derived after the development of resonant leptogenesis.

Γ_N is the finite width of the decay $N_j \to \ell_j + \phi$ and practically acts as a regulator for the asymmetry so that it does not diverge in the limit of small mass splittings. One clearly sees that ϵ_i is greatly enhanced in the limit where the mass splittings nearly vanish: Asymmetries are maximised for $M_{N_i} - M_{N_j} \simeq \frac{1}{2}\Gamma_N$.

$$\epsilon_i \simeq \frac{1}{2} \frac{\mathrm{Im}(F^\dagger F)^2_{ij}}{(F^\dagger F)_{ii}(F^\dagger F)_{jj}}$$

in this limit. ϵ_i is therefore not suppressed neither by the smallness of the mass splittings nor by the smallness of neutrino masses as it does not parametrically depend on F (only on $\frac{F^4}{F^4} \sim 1$) contrary to (1.22). Note that the asymmetry is still generated by the out-of-equilibrium decay of the heavy right-handed neutrinos as for standard thermal leptogenesis. This category of models are therefore called *freeze-out* leptogenesis models. Since HNLs decays would only happen when the temperature drops below its mass $T \lesssim M$, the sphaleron temperature T_{sph} is a natural lower bound on the HNLs masses. We will however show in chapter 3 that masses as low as $\mathcal{O}(2)$ GeV are actually sufficient for freeze-out leptogenesis with three heavy neutrinos.

2.1.2 Leptogenesis from neutrino oscillations

One could also think about the possibility of *freeze-in* leptogenesis models in which the asymmetry would be generated during the approach of right-handed neutrinos to equilibrium instead of during their decays. The *ARS mechanism*, also referred as leptogenesis from neutrino oscillations, originally proposed in 1998 by Akhmedov, Rubakov and Smirnov [3] precisely implements this idea. In this model, the asymmetry is mostly generated by the oscillations between the HNLs during their approach to equilibrium. Those are usually assumed to have masses at or below the GeV-scale. As can be seen from the seesaw relation (1.10a), M_ν is proportional to the ratio between Yukawa coupling matrix F and the Majorana mass M_M. A smaller Majorana mass must therefore be compensated by smaller Yukawa couplings to satisfy the light neutrino masses constraints. This makes the approach to equilibrium slower and allow for some of the HNLs to remain out of thermal equilibrium before the sphaleron freeze-out.

In their paper [3], Akhmedov, Rubakov and Smirnov neglected any total lepton number violating processes, *e.g.* Higgs decays as their rate are suppressed by a factor $(\frac{\bar{M}}{T})^2$. Even though these processes can dominate over the lepton number conserving processes for sufficiently heavy HNLs, we will make the same assumptions in order to keep the model simple at first. For more details on the effect of lepton number violating processes, see section 4 of [80]. We here present a schematic version of the ARS scenario where we distinguish four main steps. In realistic simulations, these steps are not as well separated. In this section, we work in the interaction basis, where the Yukawa coupling matrix F is diagonal but M_M *a priori* not.

1. Assuming Lagrangian (1.5), one can safely assume that, at temperature way above the sphaleron freeze-out, HNLs have vanishing number densities while the light neutrinos already are at thermal equilibrium [81]. HNLs are then produced as interaction eigenstates thanks to their Yukawa interactions with the SM neutrinos. This tree level process is CP-conserving and does not violate the lepton number, $\bar{L} = 0$, since the temperature is sufficiently high. $\bar{L}$ is here defined as the sum between the SM lepton number and the one associated to the heavy neutrinos $L + L_N$. More details on this matter along with an exact definition of L_N are provided in section 2.3.

2. In general, the Majorana mass M_M and the Yukawa coupling matrix F are not simultaneously diagonal. Therefore, HNLs begin to oscillate. If the off-diagonal matrix elements of M_M are complex, these oscillations are CP-violating and flavoured asymmetries in the sterile sector can be generated, *i.e.* $L_{N_i} \neq 0$. However, total lepton number is still conserved $\bar{L} = \sum_a L_a + \sum_i L_{N_i} = 0$ and, at that point, the active sector, *i.e.* the Standard Model, is still matter-antimatter symmetric $L_a = 0$.

3. Next, these asymmetries are partially communicated to ordinary neutrinos and charged leptons by scatterings and subsequently to the baryons by the electroweak sphalerons (relation (1.19)). One can show [82] that the total SM lepton number L is still conserved at that stage but not the flavoured asymmetries $L_a \neq 0$. The crucial step of this process lies in the rates at which these asymmetries in the active sector get washed out by inverse decays and scatterings. Since it happens at different rate for each flavour, the washing out can effectively produces some non-zero total SM lepton number if it is not completed by the time the sphaleron freezes out.

4. The sphaleron transfer the asymmetry produce in the lepton section to the baryon sector. Since the sphaleron is only sensitive to asymmetries produced within the left-handed sector, this is sufficient to generate a non-zero baryon asymmetry. At $T < T_{\text{sph}}$, the sphaleron process is no longer effective and the baryon number is afterwards conserved and non-zero.

Note that, initially, Akhmedov, Rubakov and Smirnov did not have this asymmetric washout of the SM asymmetries. Their mechanism needed two of the heavy neutrinos to reach equilibrium before the sphaleron freeze-out and the last one to equilibrate only after. However, as can be seen from Figure 2.1, sizeable baryon asymmetries can in reality be generated even when none of the HNLs reach equilibrium.

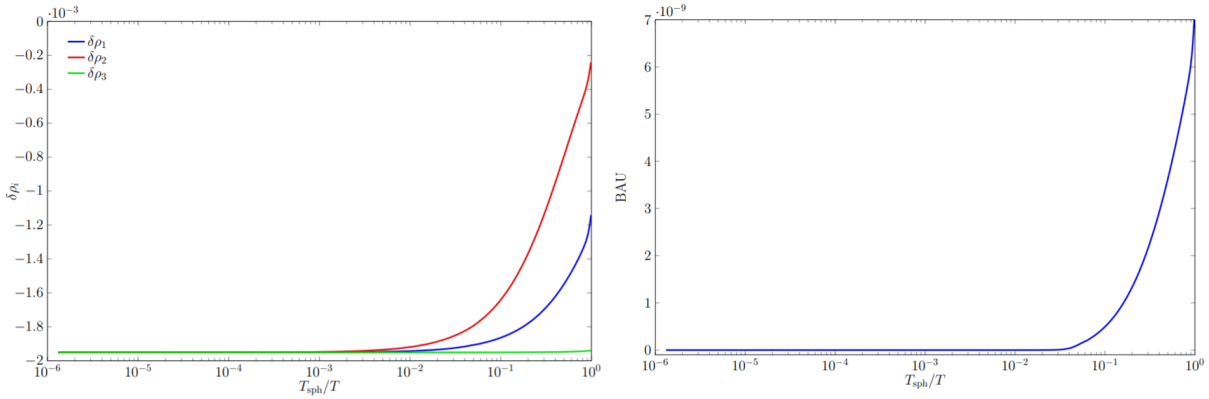

(a) (b)

Figure 2.1: Time evolution for the deviation from equilibrium $\delta\rho_i$ (left panel) and the baryon asymmetry (right panel) for a benchmark point with $\bar{M} = 20$ GeV.

As already mentioned, generic leptogenesis models crucially rely on the redistribution of the asymmetries between baryons and leptons by the sphaleron process and the ARS mechanism is no exception. Many more processes, called *spectator processes*, do not directly violate $B - L$ but do modify the density of left-handed leptons ℓ or Higgs doublets ϕ, thereby affecting the generation of asymmetries as the washout rates depend on their densities. They somehow "hide" part of the asymmetry from the washout. Examples of such processes include quarks Yukawa

interactions and the strong sphaleron process. The effect of such processes on the generation of the asymmetries is detailed in section 2.4.1 and even more in appendix A.

It was initially expected [83] that the ARS scenario would only be possible for HNLs masses under the W boson one as otherwise the decay channel $N \to \ell + W$ would open which will bring all the HNLs to equilibrium and effectively wash out all the produced lepton asymmetries. It has since been shown [21] that this mechanism is actually valid even beyond the TeV-scale. There is therefore significant overlap between ARS and resonant leptogenesis as will be illustrated in section 2.5. The smallness of the HNLs masses for which these low-scale models are feasible is particularly interesting from an experimental point of view as they should possibly be testable by current (NA62 [6], Atlas [7], CMS [8–10], T2K [11]) or near-future (SHiP [12], DUNE [13] or MATHUSLA [14]) experiments.

While resonant and ARS leptogenesis seem to be very different mechanisms, they really are two regimes of a unique mechanism [21] and a unique set of equations, developed in section 2.4.1, describes the time evolution of the HNLs in those two cases. What really distinguishes them is whether the main part of the asymmetries are produced during the approach to equilibrium (ARS) or during the HNLs freeze-out (resonant).

2.2 The importance of effective HNLs masses

Before continuing our study of the ARS and resonant scenario, one must mention an important side effect of the interactions of heavy neutrinos with the primordial plasma. We have shown earlier that neutrino oscillations and leptogenesis are strongly dependant on the mass splitting between the various neutrinos. Those mass splittings were considered as fixed in the previous sections. However, due to their interaction with the SM particles, heavy neutrinos[2] get a thermal contribution in addition to their vacuum mass at the one-loop order. In the case of heavy neutrinos, the diagram at the origin of their thermal mass is

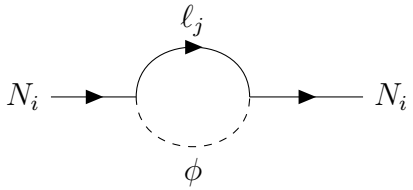

(2.1)

It will contribute with a factor

$$\frac{T^2}{8} F^\dagger F \tag{2.2}$$

to the Hamiltonian. The factor $F^\dagger F$ can easily be understood looking at Lagrangian (1.5). The factor $\frac{T^2}{8}$ is a little more tedious to derive and find its origin in the momentum integration of the Fermi-Dirac distribution $f_F(E,T) = (e^{E/T}+1)^{-1}$. An interested reader will find a pedagogical and comprehensive review of all these thermal effects and the formalism used to treat these problems in Le Bellac's book "Thermal field theory" [84].

[2] All particles interacting with the plasma in fact pick up a thermal mass.

The presence of a thermal mass opens up the possibility of having a dynamically generated resonant enhancement of the asymmetries or of the neutrino oscillations. Even though the mass splitting $\frac{\Delta M}{M}$ is of order one in the vacuum, we can expect it to be way smaller at some critical temperature where the production of asymmetries will be enhanced. This particular feature, called *avoided level crossing*, is illustrated in Figure 2.2 along with the resonant production of baryon asymmetries. The contribution (2.2) also highlights the fact that, at high temperature, the thermal mass always dominates the vacuum mass. Therefore, heavy neutrino oscillations are expected to be suppressed since they arise from the mismatch between the flavour basis, where F is diagonal, and the mass basis where $M_M^2 + \frac{T^2}{8} F^\dagger F$ is diagonal. At very high temperature, these two basis are aligned and no oscillations can take place which also limits the asymmetry production in this regime.

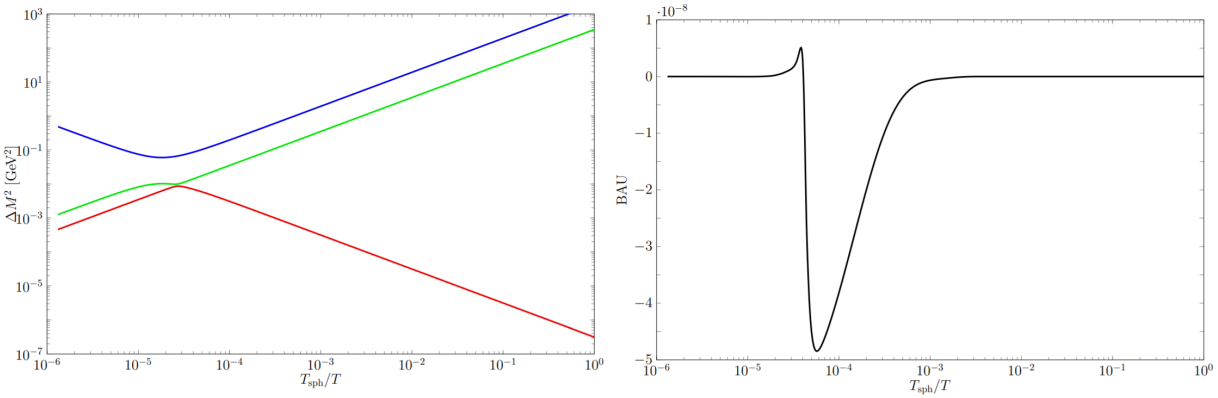

(a) (b)

Figure 2.2: Example of resonant enhancement for leptogenesis with three heavy neutrinos. The colored lines on the left panel represent the three different eigenvalues of the operator $\Delta M_M^2 + \frac{T^2}{8} F^\dagger F$ and represent the physical HNLs mass splittings. The vacuum mass splittings were taken to be $M_1 - M_2 = 10^{-1.5}$ and $M_1 - M_3 \simeq 10^{-1.59}$ while the average HNL mass $\bar{M} = 2$ TeV. The right panel clearly indicates the simultaneous enhancement of the baryon asymmetry with the avoided level crossing between the two smallest mass splittings.

2.3 Approximate $B - \bar{L}$ symmetry.

Within the framework of these low-scale models, two questions naturally arise.

1. Even though smaller heavy neutrino masses, compared to high-scale seesaw models, kinematically allow for an easier detection of HNLs, the light neutrino masses are proportional to the product of Yukawa couplings with the inverse Majorana mass matrix $v^2 F M_M^{-1} F^t$, one naively also expects smaller Yukawa couplings and therefore cross-sections.

2. Even though we have already defined the lepton number in section 1.3, a careful reader may have noticed that it was done previous to the extension of the Standard Model with right-handed neutrinos. One also has to define a lepton number for the

latter if we want to track the evolution of the lepton asymmetry generated by their decay and/or production.

Our answer to these two questions will make use of a new approximate symmetry that we will impose on Lagrangian (1.5). Let us first begin with the first problem.

As we know, right-handed neutrinos are in the simplest models only coupled to the left-handed one (in the broken phase). The strength of the coupling between ν_{La} and ν_{Ri}, as already mentioned in equation (1.15), can be parametrised in the seesaw limit through

$$U_{ai}^2 = |(\theta U_N^*)_{ai}|^2$$

using relations (1.8) and (1.9). If we forget about the matrix structure of all these relations, one can deduce from the constraint to reproduce light neutrino masses (1.10a) a gross upper bound on the coupling strength of these HNLs. Let us make for instance the simplifying hypothesis to be in the mass degenerate case $M_i = \bar{M}$ for every HNLs and that the Yukawa couplings are equal for every SM flavours and HNLs $F_{ai} \equiv F$. In this case, equation (1.10a) implies that

$$|F|^2 \sim \frac{\bar{M}}{v^2}\sqrt{\sum_a m_{\nu,a}^2}.$$

We neglected $\mathcal{O}(1)$ numerical factors in this expression. By definition of U_i^2, we get the upper bound

$$U_i^2 = \sum_a U_{ai}^2 \sim \frac{v^2}{\bar{M}^2}|F|^2 \sim \frac{\sqrt{\sum_a m_{\nu,a}^2}}{\bar{M}} < 10^{-10}\frac{\text{GeV}}{\bar{M}}. \tag{2.3}$$

This would be too tiny to be detected by experiments in the near future for HNLs masses around the electroweak scale. For instance, the expected sensitivity of the Future Circular Collider (FCC) is estimated to be at most $U^2 \sim 10^{-5}$ for HNLs masses[3] above 100 GeV [78]. However, condition (2.3) can be relaxed if some cancellations in the matrix product (1.10a) occur, and relatively high U_i^2 can be made consistent with the small values of SM neutrino masses. An elegant way, *i.e.* without requiring fine-tuning, to realise this is to impose an approximate lepton symmetry on the theory. This condition is actually necessary and sufficient under relatively weak assumptions as shown in [85]. Since the light neutrino masses are zero when the lepton number is exactly conserved, these are proportional to the symmetry breaking parameters and can therefore be made arbitrary small while keeping some of the F_{ai} relatively high, compared to the case where no symmetry is present. In this scenario, neutrino masses are said to be *technically natural*. This type of symmetry can also be motivated from theoretical considerations as such a symmetry can be realised in a various number of heavy neutrinos models like the linear [86] and inverse seesaw models [87] or the νMSM [88].

In general, there are several ways to impose this new symmetry. One could for instance ask the HNLs to have a vanishing Majorana masses. In this case, the HNL would be

[3]For lower masses, searches for displaced vertices at LHC still could theoretically probe the parameter space up to $U^2 \sim 10^{-11}$.

Dirac particles and no lepton violating processes would occur in this regime. But this solution have the problem mentioned in section 1.2 that the Yukawa couplings must be incredibly small to account for the light neutrino masses. Another solution, that allows for large Yukawa couplings this time, would be to arrange HNLs in pairs of different flavour to form a pseudo-Dirac spinor. It keeps the advantage of the previous solution while allowing for large Yukawas. When this approximate symmetry is realised, a possible form for the Majorana mass and the Yukawa coupling matrices, in the presence of three heavy neutrinos, is

$$M_M = \bar{M} \cdot \begin{pmatrix} 1-\mu & 0 & 0 \\ 0 & 1+\mu & 0 \\ 0 & 0 & \mu' \end{pmatrix} \text{ and } F = \frac{1}{\sqrt{2}} \begin{pmatrix} f_e(1+\epsilon_e) & if_e(1-\epsilon_e) & f_e\epsilon'_e \\ f_\mu(1+\epsilon_\mu) & if_\mu(1-\epsilon_\mu) & f_\mu\epsilon'_\mu \\ f_\tau(1+\epsilon_\tau) & if_\tau(1-\epsilon_\tau) & f_\tau\epsilon' \end{pmatrix}. \quad (2.4)$$

The symmetry breaking parameters are $\mu, \epsilon_i, \epsilon'_i \to 0$. In this case, μ' can significantly deviate from zero as the third heavy neutrino decouples anyway in the limit $\epsilon'_i \to 0$ and would therefore not contribute to the light neutrino masses. In the configuration of equation (2.4), ν_{R1} and ν_{R2} arrange themselves in a Dirac spinor, defined hereunder in (2.7), while the third heavy neutrino decouples.

As mentioned above, the $\mu, \epsilon_i, \epsilon'_i \to 0$ limit is equivalent to an exact conservation of the lepton number. To understand this statement, we need to define a lepton number for the HNLs, which is not as trivial as it may seem. Indeed, since, in our framework, neutrinos are Majorana particles, we cannot assign a $+1$ and -1 lepton number to the neutrino mass eigenstates and their antiparticles respectively as it is done for the rest of the SM particles. A first guess would be to assign a $\tilde{L} = +1$ lepton number to the spinor

$$\nu_{Rs} \equiv \frac{1}{\sqrt{2}}(\nu_{R1} + i\nu_{R2}) \quad (2.5)$$

while assigning a $\tilde{L} = -1$ lepton number to the spinor

$$\nu_{Rw} \equiv \frac{1}{\sqrt{2}}(\nu_{R1} - i\nu_{R2}) \quad (2.6)$$

and a zero lepton number to ν_{R3}. These two spinors can be combined together to form the pseudo-Dirac spinor mentioned earlier

$$\psi_N = \nu_{Rs} + \nu^c_{Rw}.$$

Lagrangian (1.5) would then read in the interaction basis

$$\begin{aligned} &\frac{1}{2}\bar{\psi}_N(i\partial\!\!\!/ - \bar{M})\psi_N + \frac{1}{2}\bar{\nu}_{R3}(i\partial\!\!\!/)\nu_{R3} - (\bar{\psi}_N\tilde{\phi}^\dagger)(f^*_a\ell_a) - (\bar{\psi}^c_N\tilde{\phi}^\dagger)(\epsilon^*_a f^*_a\ell_a) \\ &- (\bar{\nu}_{R3}\tilde{\phi}^\dagger)(\epsilon'^*_a f^*_a\ell_a) - \frac{1}{2}\mu\bar{M}\bar{\psi}^c_N\psi_N - \frac{1}{2}\mu'\bar{M}\bar{\nu}^c_{R3}\nu_{R3} + \text{ h.c.} \end{aligned} \quad (2.7)$$

Notice that the lepton number violating terms $\frac{1}{2}\mu\bar{M}\bar{\psi}^c_N\psi_N$, $(\bar{\psi}^c_N\tilde{\phi}^\dagger)(\epsilon^*_a f^*_a\ell_a)$ and $(\bar{\nu}_{R3}\tilde{\phi}^\dagger)(\epsilon'^*_a f^*_a\ell_a)$ are suppressed by the smallness of the symmetry breaking parameters. This quantum

number is therefore particularly suitable for strongly interacting HNLs (large U^2). Another possibility for the HNLs lepton number would be to use the concept of helicity. The helicity operator can be defined as the projection of the spin onto the momentum

$$\frac{\vec{S}\cdot\vec{p}}{s|\vec{p}|}. \tag{2.8}$$

Particles can have positive (+1) and negative (-1) helicities. The projector P_h, $h = \pm 1$, on each of these states is given by

$$P_h = \frac{1}{2}\Big(1 + h\gamma^0\gamma^j\gamma^5\frac{p_i}{|p|}\Big)$$

where p is the 3-momentum of the particle. One can then define a lepton number as

$$\bar{L} = L + L_N. \tag{2.9}$$

L_N is defined as being $+1$ for the positive helicity HNLs eigenstates and as being -1 for the negative helicity HNLs eigenstates N. In the high-energy limit, helicity and chirality are equivalent. This means that, in this limit, positive and negative helicity states can play the role of particles and antiparticles for all practical purposes. The main advantage of defining the lepton number in this way is that helicity flip processes are suppressed by a factor of $\frac{M^2}{T^2}$. The lepton number (2.9) is thus suitable for describing the relativistic regime where the HNLs masses are way smaller than the universe's temperature and, as a result, for a description of leptogenesis from neutrino oscillations.

2.4 Quantum kinetic equations

Up to here, our study of the resonant and ARS scenario was strictly qualitative. We still need to see how one can perform a quantitative study of those models. In order to get a reliable estimate of the lepton asymmetry generated by the previously mentioned low-scale models, we need to go beyond the classical Boltzmann equations (1.23) and take into account quantum effects. The Boltzmann equations indeed only consider one equation for each HNL flavour, all decoupled from each other, as explained in section 1.4. They neglect all correlations and oscillations between HNLs. While for large masses and a hierachical mass spectrum, oscillations are so fast they can be averaged out to get back these Boltzmann equations [89], this is not a valid approximation anymore for low-scale models. One can solve this problem by using an approach based on *matrices of densities* to account for all fields correlations. In this section, we begin, inspired by the approach of Sigl and Raffelt [90], by deriving evolution equations for these matrices of densities in absence of interactions and explaining what we would have to add to account for interactions using "standard" quantum field theory. We then explain why one should go beyond this approach and state the exact set of equations used in our work. We finish by mentioning two specific regimes for the solutions of these quantum kinetic equations.

Let us recall the definition of a matrix of density in quantum field theory. Let us write ψ the right-handed neutrino field of mass M. As usual in quantum field theory, we can

expand ψ into Fourier modes

$$\psi(x) = \int \frac{\mathrm{d}^3k}{(2\pi)^3} \frac{1}{\sqrt{2E_k}} \left(a(k,t)u_k + b^\dagger(-k,t)v_{-k}\right) e^{-ik\cdot x}$$

where u and v are respectively positive- and negative-helicity spinors and, therefore, $a(k), b(k), a(k)^\dagger, b(k)^\dagger$ are annihilation and creation operators for $\bar{L} = +1$ and $\bar{L} = -1$ HNLs with momentum k, verifying the standard anticommutation relations. In presence of n right-handed neutrinos generations, $a(k), b(k)$ ($a(k)^\dagger, b(k)^\dagger$) are[4] vectors containing n annihilation (creation) operators for each HNL. The energy $E_k = \sqrt{k^2 + M^2}$ in absence of interactions. The $n \times n$ matrix of density $\rho(k,t)$ is then defined by the relation

$$\langle a_j^\dagger(k) a_i(k') \rangle = (2\pi)^3 \delta^3(k - k') \rho_{ij}(k,t). \tag{2.10}$$

A similar definition can be done for the matrix of density $\bar{\rho}$ of negative helicity HNLs, replacing a's by b's. In the mass basis, the diagonal elements of the density matrix correspond to the number density of each of the HNLs as one can deduce from the interpretation of $a, b, a^\dagger, b^\dagger$ as creating and annihilation operators. In absence of interactions, the free Dirac equation

$$(i\partial\!\!\!/ - M)\psi = 0$$

implies that a, b evolves over time as

$$a(k,t) = a(0)e^{-iE_k t} \text{ and } b(k,t) = b(0)e^{-iE_k t}.$$

Applying these relations to the definition of the matrix of densities (2.10), one gets

$$i\frac{\mathrm{d}\rho}{\mathrm{d}t}(k,t) = \big[E_k, \rho(k,t)\big]. \tag{2.11}$$

A similar relation can be obtained for $\bar{\rho}$, replacing $\rho \to \bar{\rho}$ and $E_k \to -E_k$. Equation (2.11) is similar to the evolution equation for density matrices in quantum mechanics. Given that $\big[\mathbb{1}, \rho\big] = 0$, one can even replace E_k

$$E_k = \sqrt{k^2 + M^2} \simeq k \cdot \mathbb{1} + \frac{M^2}{2k} \to \frac{\Delta M^2}{2k}. \tag{2.12}$$

ΔM^2 represents the HNLs mass splittings in the mass basis (= diag$(0, M_2^2 - M_1^2, M_3^2 - M_1^2)$ for $n = 3$). Notice that M_i in general are the thermal masses, therefore including contributions like (2.2), and not the vacuum ones.

Equation (2.11) does not allow for production and destruction of particles as can be seen from

$$\frac{\mathrm{d}}{\mathrm{d}t}\mathrm{Tr}[\rho] = \mathrm{Tr}\Big(\big[E_k, \rho\big]\Big) = 0$$

and the observation that $\mathrm{Tr}[\rho]$ equals the sum of the number densities of all particles in the system. This is obviously expected from a non-interacting system. E_k is only responsible for oscillations between the various flavour eigenstates. Sigl and Raffelt generalised equation (2.11) for in presence of interactions to

$$i\frac{\mathrm{d}\rho}{\mathrm{d}t} = \big[E_k, \rho\big] - \frac{i}{2}\{\Gamma_{an}, \rho\} + \frac{i}{2}\{\Gamma_{cr}, \mathbb{1} - \rho\} \tag{2.13}$$

[4]The time dependence of these operators is here implicit.

where Γ_{an} and Γ_{cr} are the annihilation and creation rates respectively. The fact that the creation rate is proportional to $1-\rho$ can be seen as a manifestation of the Pauli principle. Notice that (2.13) is in principle true for each momenta k, on which depends ρ, $\hat{H}, \Gamma_{an}$ and Γ_{cr} as was already noticeable from equation (2.12). While the Sigl-Raffelt equation (2.13) is already relatively similar to what can be derived from more rigourous approach, see the next section, the computation of the correct rates Γ_{an} and Γ_{cr} can in practice be delicate. Therefore, we use in this work equation (2.14), derived from first principles, with the rates computed in [89].

2.4.1 QKEs for resonant and ARS leptogenesis

As mentioned, our work was based on equation (2.14) which is a variant of (2.13) where we included feedback effects and spectator processes. The set of quantum kinetic equations governing the time evolution of HNLs density matrices and SM chemical potentials is given below.

Quantum kinetic equations

$$i\frac{\mathrm{d}\rho}{\mathrm{d}t} = i\Big(\frac{\mathrm{d}\delta\rho}{\mathrm{d}t} + \frac{\mathrm{d}\rho_{eq}}{\mathrm{d}t}\Big) = [E_k, \delta\rho] - \frac{i}{2}\{\Gamma, \delta\rho\} - i\sum_{a\in\{e,\mu,\tau\}} \tilde{\Gamma}_a \frac{\mu_a}{T} f_F(1-f_F) \tag{2.14a}$$

$$i\Big(\frac{\mathrm{d}\delta\bar{\rho}}{\mathrm{d}t} + \frac{\mathrm{d}\rho_{eq}}{\mathrm{d}t}\Big) = -[E_k, \delta\bar{\rho}] - \frac{i}{2}\{\Gamma, \delta\bar{\rho}\} + i\sum_{a\in\{e,\mu,\tau\}} \tilde{\Gamma}_a \frac{\mu_a}{T} f_F(1-f_F) \tag{2.14b}$$

$$\frac{\mathrm{d}}{\mathrm{d}t} n_{\Delta_a} = -\frac{2i\mu_a}{T}\int \frac{\mathrm{d}^3\vec{k}}{(2\pi)^3}\mathrm{Tr}[\Gamma_a] f_F(1-f_F) + i\int \frac{\mathrm{d}^3\vec{k}}{(2\pi)^3}\mathrm{Tr}[\tilde{\Gamma}_a(\delta\bar{\rho}-\delta\rho)] \tag{2.14c}$$

at first order in the chemical potentials μ_a. The way it has been obtained is however slightly different. The derivation of (2.13) is based on standard quantum field theory and perturbation theory. However, one cannot use standard techniques from quantum field theory in the early universe due to high densities and temperature. In this formalism, the calculation of the rates Γ_{an}, Γ_{cr} are plagued with several problems including 1) The problem of the double counting of Feynman diagrams [91] entering in the decay and scatterings rates $\Gamma_{D,S,W}$ (see (1.23)) . Indeed, the $2 \to 2$ scattering $\ell + \phi \to \ell + \phi$ is for instance equivalent, when the internal propagator is on-shell, to the decay $\ell + \phi \to N$ following by the inverse decay $N \to \ell + \phi$. This can however be taken into account "by hand" following the "real intermediate state subtraction" (RIS) procedure. 2) The computation of the rates themselves cannot be done using the standard S-matrix approach as it relies on asymptotically free states (in-out states) while, in a high density plasma, particles are constantly interacting. The Closed Time Path formalism (CTP formalism) for non-equilibrium quantum field theories, developed in more details in appendix B, allows to solve these problems by only considering the time evolution of correlation functions, thereby avoiding references to asymptotic states and the splittings of the rates in different contributions for scatterings, decays,... A detailed derivation of (2.14) in the relativistic regime using this approach is presented in appendix B, closely following the approach of [92].

$\rho, \bar{\rho}$ are density matrices for positive and negative helicity heavy neutrinos respectively. These can be decomposed into an equilibrium component $\rho_{eq}, \bar{\rho}_{eq}$ ($\simeq f_F(k) \cdot \mathbb{1}$ at high temperatures, f_F being the Fermi-Dirac distribution) and a deviation from equilibrium $\delta\rho$. n_{Δ_a} is defined as the number density of asymmetries for the Standard Model flavour a. It can be related to the chemical potential μ at sufficiently low temperatures ($T \lesssim 10^5$ GeV) by a *susceptibility* matrix χ.

$$\mu = \chi \cdot n_\Delta = -\frac{2}{711}\begin{pmatrix} 257 & 20 & 20 \\ 20 & 257 & 20 \\ 20 & 20 & 257 \end{pmatrix} \cdot n_\Delta. \tag{2.15}$$

χ encodes the effect of the spectator processes mentioned in section 2.1.2. Since all SM particles are in thermal equilibrium and since HNLs are only coupled to the left-handed lepton doublet and the Higgs field, the knowledge of this chemical potential is sufficient and equation (2.14c) closes the system. This assertion is discussed in more details along with a derivation of relation (2.15) in appendix A. The corresponding evolution equation (2.14b) for $\bar{\rho}$ has been obtained from (2.14a) by making the replacement $F \to F^*$ and $\mu \to -\mu$ as can be seen from Lagrangian (1.5) and from the conservation law for chemical potentials[5].

One can now simply explain the different contributions to the quantum kinetic equations. As explained in section 2.2, E_k is the thermal Hamiltonian

$$E_k = \frac{\Delta M_M^2}{2k} + \frac{T^2}{16k} F^\dagger F$$

adding the thermal contribution (2.2) to the the vacuum mass splittings (2.12). It governs the oscillations between HNLs. The cooling of the universe induces a source term $\frac{\mathrm{d}}{\mathrm{d}t}\rho_{eq}$ for the deviation from equilibrium. Γ and $\tilde{\Gamma}$ are collision terms. The exact processes playing a role in the production and washout of the asymmetries have already been listed in section 1.4. Γ is a damping operator finding its origin in the interaction between the HNLs and the rest of the SM particles. It brings the HNLs to equilibrium. $\tilde{\Gamma}$ is a communication term between HNLs and SM particles, encoding how asymmetries in the active sector influence back the time evolution of the HNLs. The left-hand side of (2.14c) can be split into a washout term proportional to $\mathrm{Tr}[\Gamma_\alpha]$ and a source term proportional to $\tilde{\Gamma}_\alpha$, which is non-zero even when the asymmetries within the active sector are zero $\mu_a = 0$. While the rates $\Gamma, \tilde{\Gamma}$ are well-known in the relativistic regime $M_M \ll T$, see appendix B, a full computation of these in the intermediate regime $M_M \sim T$ is more difficult. In this work, we use the rates computed in [89] which are based on an extrapolation of $\Gamma, \tilde{\Gamma}$ between the relativistic regime and the non-relativistic one. More precisely, one extrapolates the rates from the relativistic regime, computed in [93], to the non-relativistic one and adds the contribution from heavy neutrino decays (into Higgs and W,Z bosons if in the broken phase of the SM). The full procedure followed for the rates extrapolations is to be found in section V of [89].

[5]The reaction $A + \bar{A} \to 2\gamma$ implies that $\mu_A + \mu_{\bar{A}} = 2\mu_\gamma = 0$ since the number of photons is not conserved.

Similarly to (2.13), equations (2.14) are in principle valid for each momentum separately. It is therefore needed to solve these equations for all momenta to get a completely reliable estimate. Moreover, couplings between different momenta $k \neq k'$ can appear through the backreaction term $\tilde{\Gamma}$. While precision calculations solving these equations for each momenta have already been performed [94] for benchmark points, the code is too slow to allow for an effective scan of the whole parameter space as is the goal of this work. Therefore, we integrate these equations with respect to the momentum — this has already been done for (2.14c). This procedure leads to some unphysical oscillations of the total lepton asymmetries but errors are still expected to be $\mathcal{O}(1)$ [95]. More details on this matter are given in appendix B-6.

2.4.2 Oscillatory and overdamped regimes

Equations (2.14) have no known general analytical solutions. How to implement and solve these equations numerically are discussed in the next chapter. One of the main problem when trying to solve these equations is the presence of multiple time scales. In presence of n HNLs generations, there exists n different time scales encoding how fast HNLs do equilibrate and $\frac{n(n-1)}{2}$ different time scales encoding when HNLs oscillations start when n HNLs do participate to leptogenesis. However, in the limit where those scales are well separated, one can still identify two main regimes, the oscillatory and overdamped regimes, where analytical approximates have been found [92]. The *oscillatory regime* takes place when HNLs oscillations start way earlier than their equilibration. The HNLs oscillations involving N_i and N_j start in general as soon as the temperature drops below

$$T_{\text{osc}} \simeq \left(a_R \cdot |M_i^2 - M_j^2|\right)^{\frac{1}{3}}, \tag{2.16}$$

where $M_{i,j}$ are the masses of $N_{i,j}$. a_R is a numerical factor, defined in appendix B, approximately equal to $7.1 \cdot 10^{17}$ GeV in the radiation era. On the other hand, the first HNLs equilibrate, in the relativistic limit, as soon as the temperature drops below

$$T_{\text{eq}} \simeq \gamma_{av} a_R ||F^\dagger F||, \tag{2.17}$$

where the norm $||F^\dagger F||$ is defined as the largest eigenvalue of $F^\dagger F$. γ_{av} is a momentum-average rate ($\simeq 0.012$ in the relativistic limit, see [96]). The oscillatory regime therefore happens when the slowest oscillation timescale is still faster than the fastest equilibration timescale. In this oscillatory scenario, HNLs have the time to complete many oscillations before they do equilibrate and the lepton asymmetry is generated during the first few oscillations. On the other hand, the *overdamped* regime happens when at least one HNLs species reaches thermal equilibrium before it has completed one oscillation. This scenario requires either mass degeneracies between the HNLs to reduce T_{osc} or large Yukawa couplings F to increase T_{eq}. In this regime, the washout is stronger which effectively limits the total HNLs coupling strength U^2 when only two heavy neutrinos participate to the generation of the baryon asymmetry. This observation is illustrated in the next section. We will show in section 3.2 that this constraint becomes weaker when three heavy neutrinos do participate. To distinguish the oscillatory from the overdamped regime, one could

use the simple criterion

$$\frac{T_{\rm osc}}{T_{\rm eq}} \simeq \frac{\gamma_{av} a_R^{\frac{2}{3}} ||F^\dagger F||}{\Delta M^{\frac{2}{3}}} \begin{cases} \ll 1 : \text{overdamped regime} \\ \gg 1 : \text{oscillatory regime.} \end{cases}$$

A comparison between the time evolution of various quantities between these two regimes is shown in Figure 2.3.

2.5 Scanning the low-scale leptogenesis parameter space: A short review of previous results.

From a phenomenological viewpoint, the most important quantities are the masses of the heavy neutrinos and their couplings to the Standard Model particles since they condition whether or not the HNLs of the model could be detected by said experiments. Many studies therefore focus on the range of mass and total mixing angle U^2 in which leptogenesis is feasible. From the $7n-3$ new parameters appearing in the type-I seesaw Lagrangian (1.5), only five are fixed by neutrino oscillations data. Leptogenesis is not viable for all choices of the experimentally unconstrained parameters and we are interested in the constraints on these parameters coming from leptogenesis itself. Comprehensive scans of this parameter space have already been performed in the minimal ($n=2$) scenario where only two heavy neutrinos participate to leptogenesis in several studies [21, 97, 98] for various mass ranges. An example of how one can perform such a scan is developed in the next chapter. The viable parameter space from [21], covering the regime where the resonant and ARS scenario are possible, is presented in Figure 2.4.

The white region delimits the allowed values for the mean HNLs mass $\bar{M}$ and the overall coupling strength U^2. One can make several observations from this figure. First, Figure 2.4 confirms what we mentioned in section 2.1.2 that freeze-in leptogenesis is even possible for masses above the TeV-scale. Second, resonant leptogenesis is viable for masses as low as 7 GeV. The total lepton asymmetry produced by decaying HNLs is proportional to 1) the decay asymmetry (1.21) 2) the deviation of the HNL from thermal equilibrium $\delta\rho$. While the latter is suppressed by a factor $(\frac{\bar{M}}{T})^2$ for GeV-scale HNLs, the resonance can overcome this suppression factor for HNLs masses down to 7 GeV. This implies that both the resonant and ARS regime do overlap.

The lower blue line mostly corresponds to the seesaw line. We do however observe some deviations from this straight line for small masses. This can be explained as the HNLs are far from reaching equilibrium for such small U^2. Indeed, from (2.17), we know that the equilibration temperature can be approximated by

$$T_{\rm eq} \sim \gamma_{av} a_R |F|^2.$$

Using the naive seesaw estimate (2.3) that defines the seesaw line, we get an order of magnitude estimate for the equilibration temperature

$$T_{\rm eq} \sim \frac{7.1 \cdot 10^{15}\text{GeV}}{v^2} \bar{M} \sqrt{\sum_a m_{\nu,a}^2} \sim 11.5 \cdot \bar{M}[\text{GeV}].$$

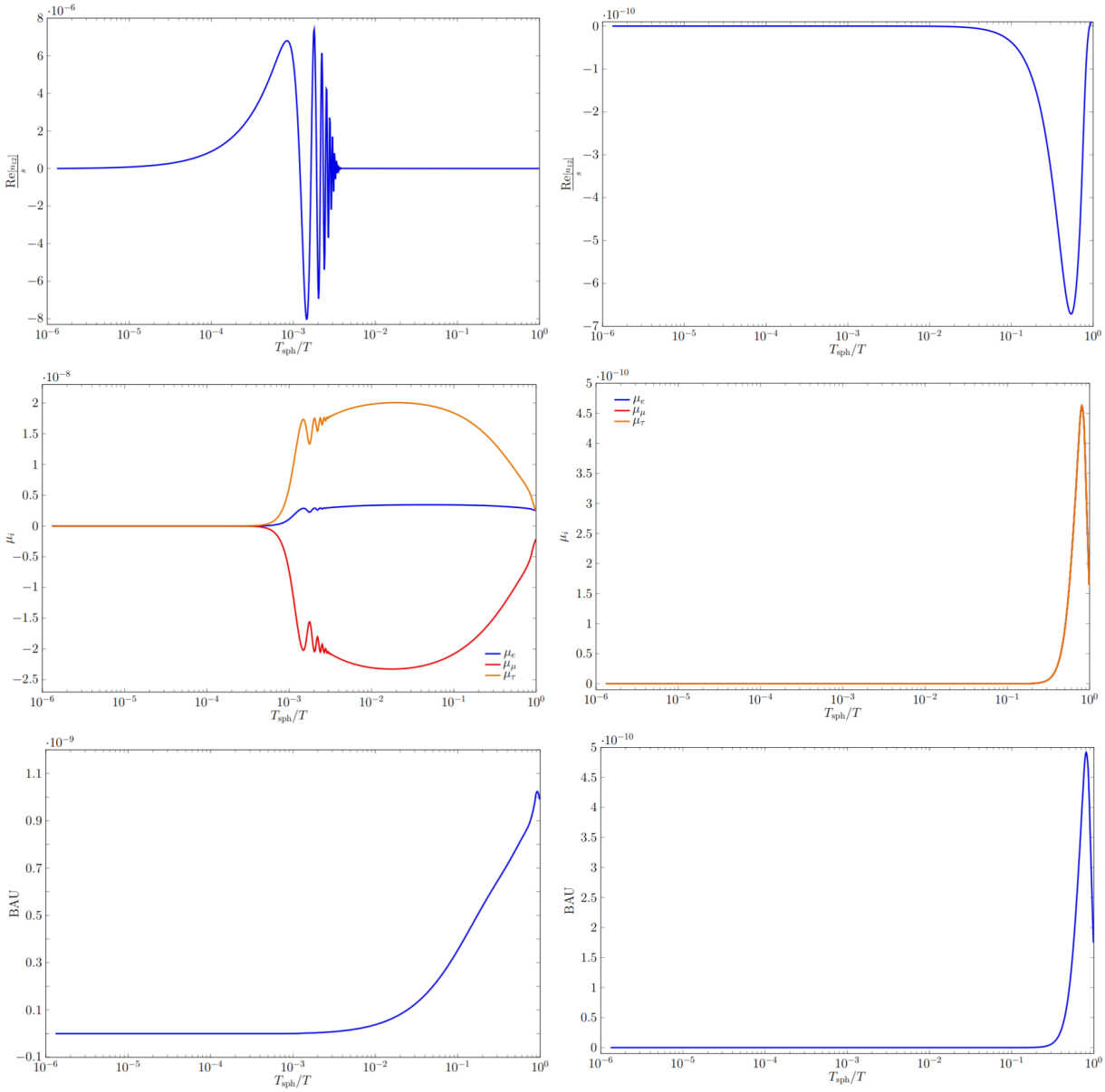

(a) (b)

Figure 2.3: Time evolution for various quantities for both oscillatory (left panel) and overdamped regime (right panel). Upper panel represents the evolution of the off-diagonal correlation between HNLs n_{12}. The middle panel shows the time evolution of all the chemical potentials while the lower panel represents the time evolution of the BAU. The stopping of oscillations for n_{12} is not physical and is a consequence of the replacement (3.2). These benchmark points have been simulated for a mass $\bar{M} = 100$ GeV. The ratios $\frac{T_{\mathrm{osc}}}{T_{\mathrm{eq}}} \simeq \{23.9, 5.7\} \gtrsim 1$ for the oscillatory regime and $\frac{T_{\mathrm{osc}}}{T_{\mathrm{eq}}} \simeq \{1.9 \cdot 10^{-10}, 9.9 \cdot 10^{-10}\} \ll 1$ for the overdamped one.

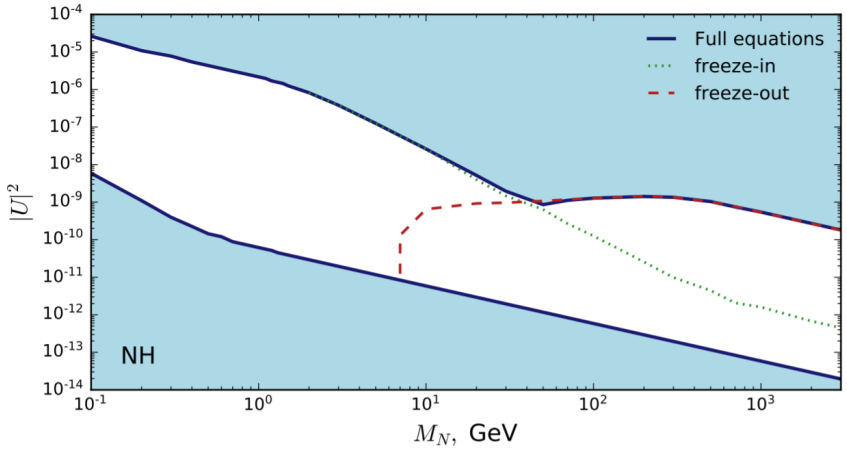

Figure 2.4: Allowed parameter space for $n = 2$ leptogenesis with normal ordering. Leptogenesis is possible within the white region. The green dotted (red dashed) curve delimits the allowed parameter space when only freeze-in (freeze-out) asymmetries are taken into account. Taken from [89].

For a mass $\bar{M} = 100$ MeV, this rough approximation leads to an equilibration temperature way below the sphaleron freeze-out. The asymmetric washout therefore cannot play a significant enough role to create a sufficient amount of baryon asymmetry.

Lastly, one can also notice that the allowed parameter space is relatively limited. Especially for masses above the W boson mass, the smallness of the permitted active-sterile mixings U^2 would not allow for detection of these HNLs in the near future, as can be noticed by comparing to the experimental sensitivities previously shown in Figure 1.6. This can be explained by the observation that, in the strong washout regime $U^2 \gg \frac{\sqrt{\sum_a m_{\nu,a}^2}}{\bar{M}}$, HNLs need a strong flavour hierarchy to hide part of the asymmetry from the washout in a specific flavour. This has been confirmed by explicit simulations in the $n = 2$ scenario [52] as illustrated in Figure 2.5. Edges and corners of the triangle, corresponding to more flavour asymmetric Yukawa couplings, are typically associated with larger mixing angles. This asymmetry can be parametrised by

$$\mathbb{f} \equiv \sum_i \frac{\min_a |F_{ai}|}{\max_a |F_{ai}|} \cdot \frac{\sum_b |F_{bi}|^2}{\sum_{c,j} |F_{cj}|^2}.$$

In presence of a strong flavour hierarchy, $\mathbb{f} \ll 1$. However, when only two HNLs do participate to leptogenesis, the constraint that these should also account for the light neutrino masses imposes [71] $\mathbb{f} \gtrsim 5 \cdot 10^{-3}$ and therefore limits the maximal coupling U^2.

Scanning the $n = 3$ parameter space is however more difficult due to the higher dimensionality of the parameter space and the multiple time scales that appears. Still, some scans have already been performed in the low mass range. Results from [80] are depicted hereunder in Figure 2.6.

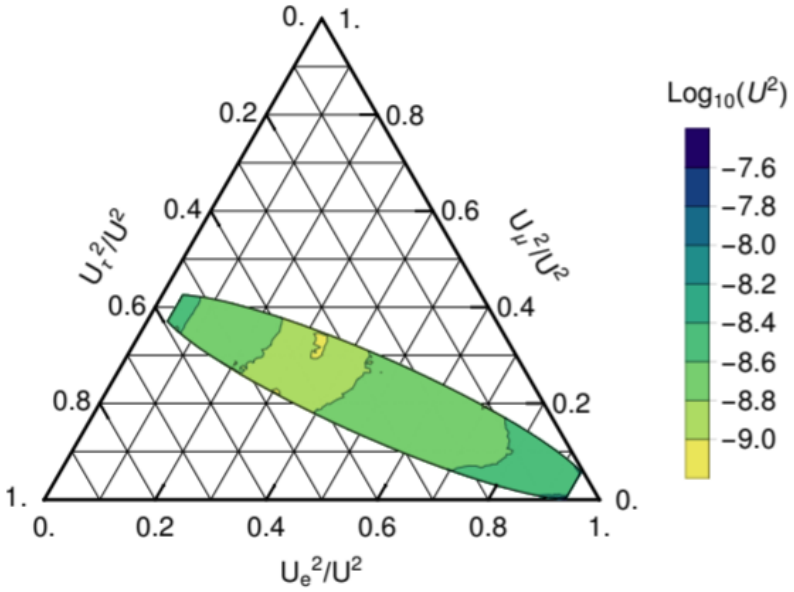

Figure 2.5: Triangle plot for the ratio $\frac{U_\alpha^2}{U^2}$ in the $n = 2$ scenario for inverted ordering and an average HNL mass $\bar{M} = 30$ GeV. Taken from [52].

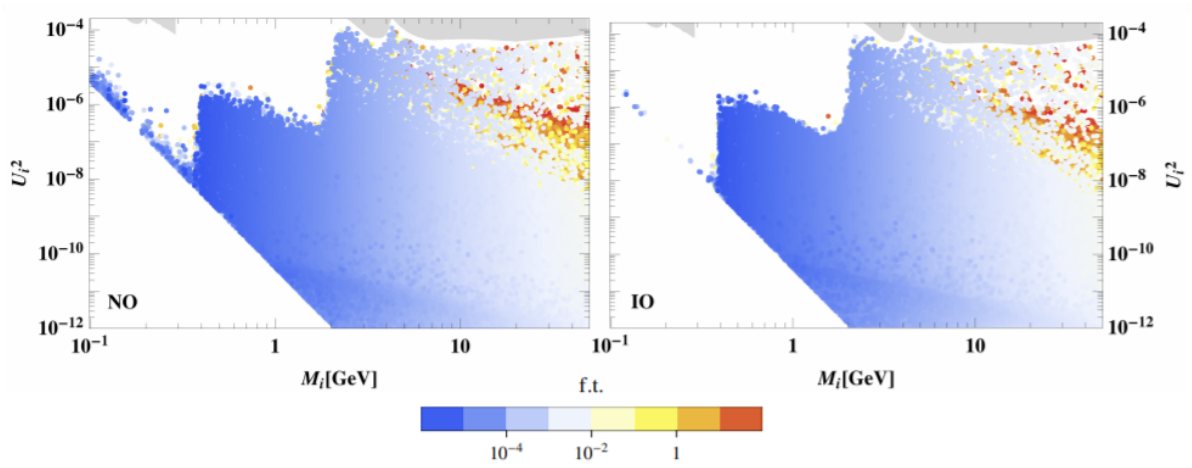

Figure 2.6: Allowed couplings U_i^2 in the low mass range in the $n = 3$ scenario for normal (left panel) and inverted ordering (right panel). Colours represent the level of fine-tuning as defined in (3.3). Taken from [80].

As one can see, much larger U^2 are permitted. Diverse reasons for this enlargement of the leptogenesis parameter space are given in section 3.2. Contrary to what we did in our work, this scan did impose constraints from direct searches, Big Bang nucleosynthesis (BBN), ... which explains the lack of points in the upper-left corner. It also used relativistic approximates for the rates in (2.14) which is sensible as the mass range lies way below the sphaleron freeze-out.

Chapter 3

Leptogenesis in presence of three heavy neutrinos

This last chapter is devoted to a description of our study of the $n = 3$ leptogenesis parameter space. We map the allowed range for the HNLs overall coupling strength U^2 in which type-I seesaw-based leptogenesis with three heavy neutrinos is possible for masses ranging from 50 MeV to 70 TeV, thereby covering the whole experimentally accessible mass range. We begin the chapter by a short description of how our numerical scan was performed. Afterwards, we describe the main outcomes of our analysis. We finish this section by mentioning limitations of the present work and possible improvements that could strengthen our analysis.

3.1 Numerical implementation of the scan

In this section, we briefly describe how we have implemented a code in Python to solve the differential equation (2.14) and what type of constraints we have imposed on the scan. The exact code used to solve these equations is an adaptation for three HNLs of the code used in [89].

The first step is to reduce the number of degrees of freedom introduced. Instead of the 39 variables introduced by equation (2.14) (18 for both density matrices $\delta\rho, \delta\bar{\rho}$ since we work with three heavy neutrinos and three for the chemical potential μ_α), one can use the property that density matrices are all hermitians to reduce the number of degrees of freedom to 21. Practically, we transform (2.14) in a vector equation by decomposing the density matrices into a basis of Gell-Mann-like 3×3 matrices $\delta\rho = c^i\tau^i$ and using their known (anti-)commutation relation to get a linear differential equation of the form

$$\frac{\mathrm{d}}{\mathrm{d}t}q_i = -A_{ij}q_j. \tag{3.1}$$

q_i is a 21-dimensional vector. Equations of the form of (3.1) can be solved using predefined numerical solver in Python. However, the solution can sometimes present a highly oscillatory behaviour, as described in section 2.4.2. This makes the problem numerically unstable unless the step size is chosen to be very small, a property called *stiffness*, and slows down the Python solver as the iteration number increases with the frequency. One way to overcome this problem would be to set an upper limit on the oscillation frequency and, equivalently, on the positive eigenvalues of A. To do this, one can introduce a

regulator Λ. We then make the replacement

$$A \to A \cdot (\frac{A}{\Lambda} + 1)^{-1} \tag{3.2}$$

inside (3.1). The rapid oscillations corresponds to eigenmodes of eigenvalues $A_{\text{fast}} \gg \Lambda$. In this limit, A is replaced by $\Lambda \cdot \mathbb{1}$ and the oscillations are effectively suppressed. An illustration of the effect of such a replacement can be seen in Figure 2.3a.

The scan is then performed as follows. As explained in section 1.2.1, the type-I seesaw model introduces $7n - 3$ beyond the Standard Model parameter. Five of them (two mass splittings and three PMNS angles) are now experimentally known. For leptogenesis with three heavy neutrinos, this means that our scan has to cover a 13-dimensional parameter space in order to fully explore the viability of leptogenesis. However, there are several constraints to impose on these parameters.

- First, we decided to limit ourselves to the case of approximately mass degenerate HNLs. The Majorana mass matrix can be parameterised through

$$M_M = \bar{M} \cdot \mathbb{1} + \frac{\Delta M_1}{2} \cdot \begin{pmatrix} 1 & 0 & 0 \\ 0 & -1 & 0 \\ 0 & 0 & 0 \end{pmatrix} + \frac{\Delta M_2}{3} \cdot \begin{pmatrix} 1 & 0 & 0 \\ 0 & 1 & 0 \\ 0 & 0 & -2 \end{pmatrix}.$$

  We decided to limit $\frac{\Delta M_1}{\bar{M}}, \frac{\Delta M_2}{\bar{M}} \in [10^{-10}, 10^{-1}]$. For $n = 2$ leptogenesis, mass splittings smaller than 10^{-10} were ruled out as radiative corrections to the HNLs masses from Higgs interactions are of this order of magnitude [99]. Motivations for this choice include the observation that large U^2 typically come with degeneracies in the heavy neutrino mass spectrum as seen in (2.4). Moreover, small mass splittings at zero temperature favour the possibility of having dynamically generated resonant enhancement, a phenomenon detailed in section 2.2. Mass degeneracies can also arise from additional symmetries [100]. Note however that the mass degenerate scenario is *a priori* not protected against loop corrections.

- As mentioned in the introduction, the aim of this work is to solve both the neutrino mass and baryogenesis problems. This means that the HNLs introduced have to generate the right neutrino masses and PMNS angles. Using the Casas-Ibarra parametrisation (1.13) of the Yukawa couplings F is sufficient for this purpose. Low-energy experiments impose a lower bound on the total HNLs coupling strength U^2 usually called the *seesaw line*. One can show [101] that the estimate (2.3) is actually a lower bound on U^2 by setting $\mathcal{R} = \mathbb{1}$. Only HNLs verifying $U^2 > \frac{\sqrt{\sum_a m_{\nu,a}^2}}{\bar{M}}$ are permitted.

We also have imposed three theoretical constraints.

- We imposed *perturbative unitarity*. If the particle has a decay width Γ and a mass M, this condition amounts to $\Gamma < \frac{M}{2}$. It is equivalent to asking the particle to be well-defined. If the decay is too quick, then one cannot consider the HNLs as "true"

particles. In the case of the minimal seesaw model considered and in the broken phase, the condition can be explicitly written at tree level by $U^2 < \frac{v^2(2\pi)^2}{M^2}$.

- The Casas-Ibarra parametrisation (1.13) can only be applied when the seesaw expansion $\theta \ll 1$ is valid[1]. For this reason, we limit $U^2 < 0.1$. Such high couplings are anyway already ruled out in the GeV-TeV range by collider experiments [103]. The combination of this constraint with perturbative unitarity automatically implies that Yukawa couplings stay in the perturbative regime $F \lesssim \mathcal{O}(1)$.

- We want to avoid significant modifications of the light neutrino masses by loop corrections. Parameter points that are unstable under these loop corrections are called *fine-tuned*. To avoid fine-tuning, we ask that the 1-loop corrections δm_{loop} are smaller than the tree level mass m_{tree} or, equivalently,

$$\left(1 - \|\frac{m_{\text{tree}} + \delta m_{\text{loop}}}{m_{\text{tree}}}\|\right)^2 < \frac{1}{4}. \tag{3.3}$$

  We have defined $\|\frac{A}{B}\| \equiv \max_{i,j} \frac{A_{ij}}{B_{ij}}$. These 1-loop corrections are given by the relation [104, 105]

$$\delta m_{\text{loop}} = \frac{1}{v^2} \theta M_M^2 f(M_M) M_M \theta^t$$

  at second order in the seesaw expansion. f is the loop coefficient

$$f(x) = \frac{1}{(4\pi)^2}\left[\frac{3\ln[(x/m_Z)^2]}{(x/m_Z)^2 - 1} + \frac{3\ln[(x/m_\phi)^2]}{(x/m_\phi)^2 - 1}\right]$$

  where m_Z and m_ϕ are the mass of the Z and Higgs boson respectively.

A visual representation of all these constraints is shown in Figure 3.1. The constraint on the loop corrections is not represented as it cannot be written as a universal constraint on U^2 only.

As we want to be the scan to be "agnostic", we do not impose any additional constraint from experimental direct or indirect HNLs searches (see *e.g.* [7, 10, 45, 106]). A summary of these constraints can be found in [103]. A table summarising the range and priors used for all the parameters not fixed by experiments is given in Table 3.1. To keep the computational time at a reasonable scale, only normal ordering and the two limiting cases $m_{\text{lightest}} \in \{0, 0.1\}$ eV were considered[2]. In addition to these, the five known parameters Δm^2_{ij}, Θ_{ij} were set at the best fit values, summarised in Table 1.1, from the ν-fit collaboration [30]. The mass $\bar{M}$ varies discretely from 50 MeV up to 70 TeV covering the whole experimentally accessible mass range. As mentioned in section 2.4.1, rates for each mass were computed in [89].

The scans can then be decomposed into three main steps.

1. First, we generate random parameter points verifying the five previous constraints.

[1] One can however adapt the Casas-Ibarra formula for the case where θ is not small anymore [102].

[2] While it is true that $m_{\text{lightest}} = 0.1$ eV slightly contradicts the upper bound (1.2), it was here only chosen as an "extreme" benchmark point.

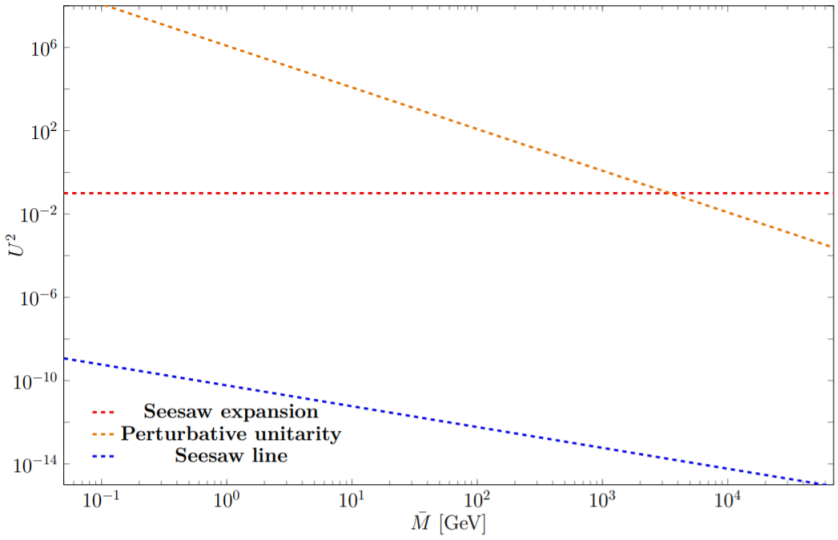

Figure 3.1: Representation of the main constraints imposed on our scan in the $\bar{M} - U^2$ plane. Only the region within these three curves is permitted for the scan.

Parameter	Physical interpretation	Range	Prior
$\frac{\Delta M_i}{\bar{M}}$	HNLs relative mass splittings	$[10^{-10}, 10^{-1}]$	Log_{10}
$\text{Im}(w_i)$	Imaginary part of $\mathcal{R}$ angles	[-10,10]	Uniform
$\text{Re}(w_i)$	Real part of $\mathcal{R}$ angles	[0,2π]	Uniform
δ	Dirac phase	[0,2π]	Uniform
α_i	Majorana phases	[0,4π]	Uniform
m_{lightest}	Mass of the lightest SM neutrino	$\{0, 0.1\}$ eV	Uniform
Ordering	Hierarchy of the light neutrino masses	Normal	Fixed

Table 3.1: Range, priors and physical interpretations of all used parameters.

2. We then compute the baryon asymmetry Y_B for each of these points by numerically solving the vector-form of equation (2.14). We typically start the simulations at $T = 10^8$ GeV. Two sets of initial conditions were considered. Either the HNLs started with vanishing initial density (minimal scenario) or they start at thermal equilibrium (presence of additional interactions at high energy). Starting from thermal initial conditions, only resonant contributions to the lepton asymmetry are considered since the asymmetries created during the approach to thermal equilibrium are considered as already washed out. On the contrary, assuming vanishing initial conditions means that both contribution from HNLs oscillations and HNLs decay are considered. Since we consider the scenario where there is no prior lepton asymmetry, we can assume the chemical potentials μ_α to be initially zero, see (2.15).

3. Lastly, we only keep parameter points whose baryon asymmetry is larger than the

observed one

$$Y_B \gtrsim 8.6 \cdot 10^{-11}.$$

3.2 Analysis of the numerical solutions

The results from our scan are presented in Figure 3.2. We first compare the maximal and minimal HNLs active-sterile mixings U^2 for vanishing and thermal initial conditions in the $n = 2$ case obtained in [21] with our results for the $n = 3$ case when the lightest active neutrino is massless $m_{\text{lightest}} = 0$ eV.

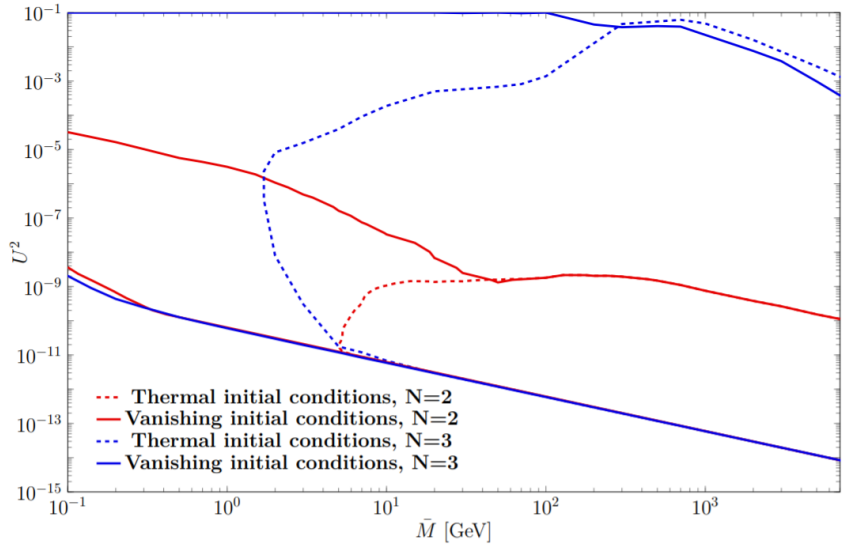

Figure 3.2: Comparison between the allowed parameter spaces for viable leptogenesis when two (red lines) and three (blue lines) HNLs do participate. The lightest neutrino is massless $m_{\text{lightest}} = 0$ eV.

We observe that the range of allowed mixing angle for the $n = 3$ scenario completely contains the one for the $n = 2$ scenario as is expected. We confirm the results from [80] that the range of permitted couplings is way larger than in the $n = 2$ scenario and extend this statement to the resonant regime. We even show that, for vanishing initial conditions, the upper bound imposed by leptogenesis is weaker than the theoretical upper bound $U^2 = 0.1$. Several effects can explain this observation. First, $\mathbb{f}$ is far less constrained in the $n = 3$ scenario [103] and stronger flavour hierarchies are thus allowed. As first hinted in [80], a second reason for these much larger couplings is the possibility of dynamically generated resonant enhancement. In the $n = 2$ scenario, the interaction basis must be maximally misaligned with the mass basis to explain the light neutrino masses which implies that the smallest mass splittings generated will typically be too large to trigger a resonant enhancement. The presence of a third HNL can solve this problem if it has a larger mass but smaller Yukawa couplings than the pseudo-Dirac pair so that, at high temperature, the thermal mass of the pseudo-Dirac pair becomes larger. This can be realised if $\mu' > 1$ and $\epsilon'_\alpha \ll 1$ in (2.4).

Throughout this master thesis, we have been guided by the potential testability of the

HNL hypothesis at high-energy experiments in the near future. Figure 3.3 compare the allowed range for the total mixing angle U^2 with the experimentally excluded regions and sensitivities of diverse current and planned experiments for both scenarios $m_{\text{lightest}} = 0$ eV and $m_{\text{lightest}} = 0.1$ eV. Experimental sensitivities are usually expressed in terms of U_a^2, U_μ^2 for Figure 3.3, instead of the overall coupling strength U^2. It is however a good approximation to assume that the upper limit on U_μ^2 is the same as the one on U^2 as is shown in Figure 3.4. Figure 3.4 is also consistent with the well-known fact [71] that, in the $n = 2$ case, the ratio $\frac{U_e^2}{U^2}$ is constrained to be smaller than ~ 0.12 (but the constraints are weaker for $n = 3$).

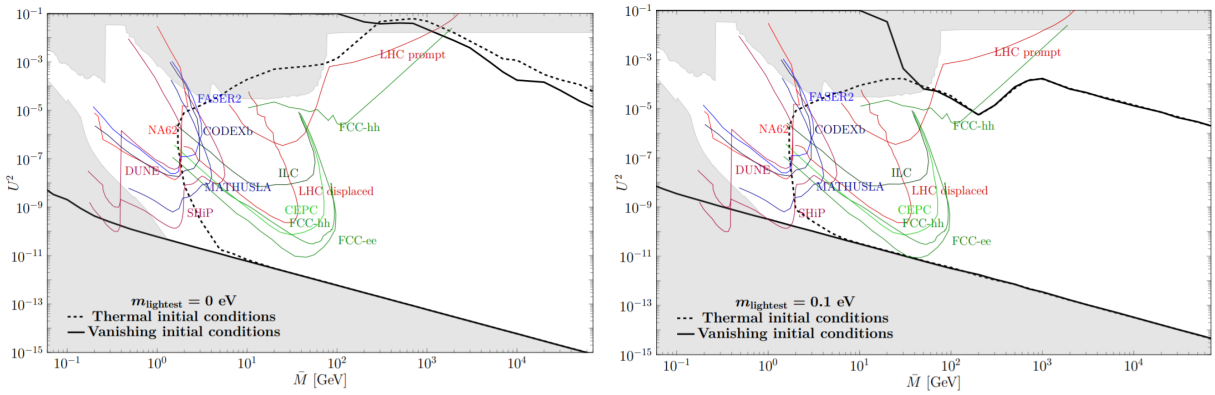

(a) (b)

Figure 3.3: Allowed parameter space for leptogenesis with three heavy neutrinos. Vanishing (continuous black line) and thermal (dashed black line) initial conditions are represented. The grey area represents the already excluded region from the global GAMBIT scan [103] and the combined BBN bounds [107, 108]. The continuous coloured lines stands for the expected sensitivity for current and planned experiments, detailed in Figure 1.6.

Given its increased size, planned experiments will cut deep into the viable parameter space. If the overall couplings of the HNLs lie at the current experimental limits, one could expect to detect thousands of displaced vertices at HL-LHC for instance [22]. This will allow us to perform consistency checks on the HNL hypothesis, *e.g.* constrain the ratio $\frac{U_a^2}{U^2}$ to a percent level or assess the proportion of lepton number violating processes, see *e.g.* [52].

One can also notice from Figure 3.3 that the parameter space is larger when the lightest neutrino is massless. This can be explaining by looking at the structure of the Yukawa coupling matrix (2.4). We notice that the third heavy neutrino decouples in the $B - \bar{L}$ symmetric limit. This is also crucial for the generation of the asymmetries. In the ARS regime, the fact that the third HNL decouples allows to hide part of the baryon asymmetry from the washout. In the resonant regime, the deviation from a neutrino to equilibrium during decays is proportional the lifetime of the HNL

$$\delta\rho \approx -\frac{\dot{\rho}_{\text{eq}}}{\Gamma}$$

where Γ is the decay rate of the HNL. One can obtain this relation from (2.14a) neglecting the backreaction term and assuming that $\delta\rho$ changes slowly. Having long lived HNLs leads

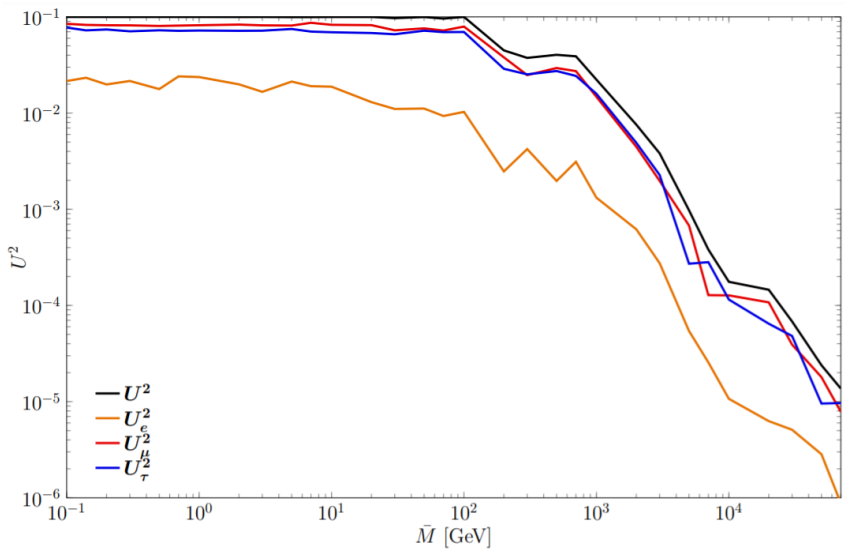

Figure 3.4: Hierarchy between the maximal couplings U_a^2 of each flavour for leptogenesis with three heavy neutrino, vanishing initial conditions and $m_{\text{lightest}} = 0$ eV. These upper limits converge less rapidly which is responsible for the noisy behaviour of the curves. Note however that the upper limit for all U_a^2 are always strictly smaller than the upper limit for U^2 as, for $m_{\text{lightest}} = 0$, the corner of the triangle plot are never reached, see *e.g.* Figure 2.5.

to large deviation from equilibrium. It can be noticed from Figure 3.5 that lower couplings U_3^2 to the third heavy neutrino can be achieved when the lightest neutrino is massless. This comes from the Casas-Ibarra parametrisation (1.13) where the Yukawa couplings are proportional to the square root of the light neutrino mass matrix. For $m_{\text{lightest}} = 0$ eV, one of the eigenvalues of F must therefore be small and the lifetime of this heavy neutrino can be considerable. Similarly, the approach to equilibrium of this heavy neutrino is slower. This explains the dip at $T \simeq 200$ GeV visible in Figure 3.3b as strongly coupled HNLs will reach thermal equilibrium too soon in this mass range and washout be too strong.

Lastly, we wanted to compare the form of the parameter space when HNLs start with thermal initial conditions with the form of the parameter space when HNLs start with vanishing initial conditions. As one can see, leptogenesis with thermal initial conditions is possible for HNLs masses as low as 1.7 GeV, slightly lower than in the minimal $n = 2$ scenario. This has the interesting consequence that thermal initial conditions could be tested by a few present-day experiments such as NA62. One can also observe that the upper limit for thermal initial conditions is nearly equal but still slightly superior to the one for vanishing initial conditions for large masses. For large masses, strongly coupled heavy neutrinos indeed reach thermal equilibrium quite early and the main part of the asymmetries will be produced during their decay. However, the sign of the CP-asymmetries created during freeze-in is opposite to the one of the CP-asymmetries created during HNLs decays. This behaviour is illustrated in the following Figure 3.6. The lepton asymmetries are first negative during the approach to equilibrium before being compensated by positive baryon asymmetries coming from HNLs decays. This explains why the baryon asymmetry is usually smaller for vanishing initial conditions in this mass range.

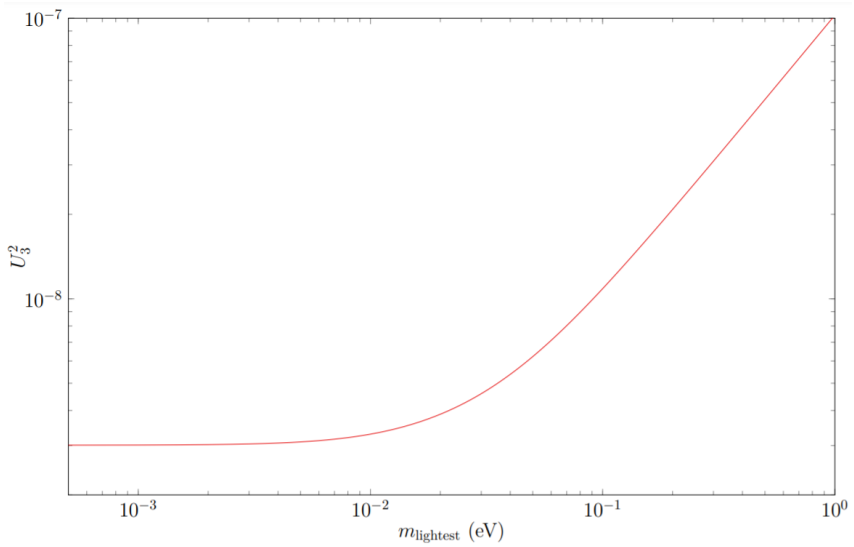

Figure 3.5: Evolution of the coupling to the third HNL U_3^2 for different m_{lightest} for a benchmark point with $\bar{M} = 2$ TeV. One clearly observe the increase of U_3^2 along with m_{lightest}.

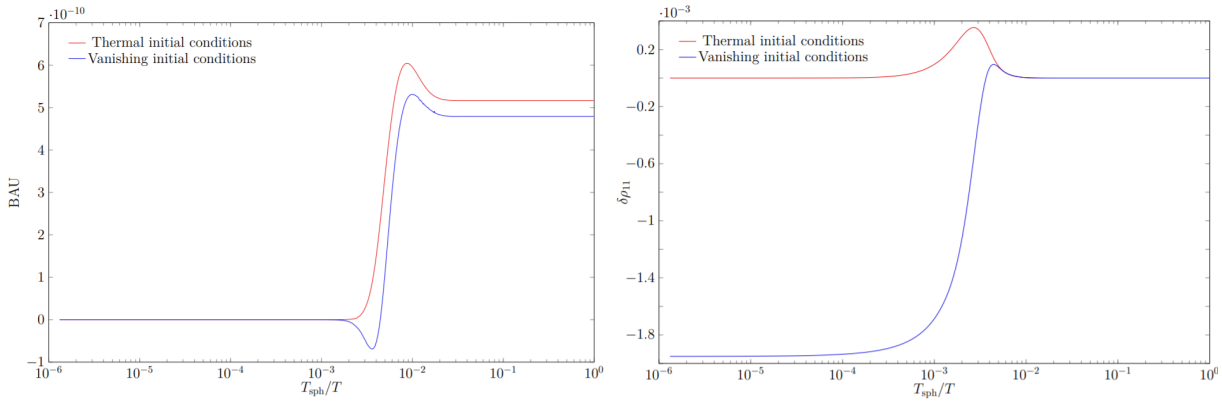

(a) (b)

Figure 3.6: Time evolution for the baryon asymmetry (left panel) and approach to equilibrium of the most weakly coupled HNL (right panel) for thermal (red curve) and vanishing (blue curve) initial conditions. The average heavy neutrino mass $\bar{M}$ is taken to be 70 TeV.

3.3 Limitations of our model and future improvements

This work is not the final word regarding the numerical evaluations of the baryon asymmetry in low-scale leptogenesis models and some aspects that have been neglected in this work need to be taken into account.

1. The sphaleron freeze-out does not happen instantaneously. If we consider the sphaleron freeze-out as a slow process, one has to extend (2.14) with an additional equation describing the time evolution of the baryon asymmetry, see [109]. One has also to account for the temperature dependence of the susceptibility matrix, defined in (2.15).

2. Plasma effects such as multiple soft scatterings, *e.g.* the Landau-Pomeranchuk-Migdal (LPM) effect ($1 + n \leftrightarrow 2 + n$ processes) [66, 67], can have a sizeable impact and have to be taken into account. As already mentioned, the rates $\Gamma, \tilde{\Gamma}$ used for this thesis are extrapolations [89] from the relativistic regime to the non-relativistic regime and do account for the LPM effect. The impact of this change however is expected to be relatively limited as illustrated in Fig. 5 of [89]. The helicity-averaged rates without taking into account this LPM effect only slightly deviates from the full calculation.

3. The momentum dependence of the quantum kinetic equations (2.14) has to be taken into account. This last replacement is expected to be the more challenging but also the more relevant. Tracking all momenta would not be numerically realistic but one could potentially still use moments of the distribution function, solve the QKEs only for the most important momenta modes or search for conserved charges that could simplify the problem.

Conclusion

In this work, we for the first time mapped the range of active-sterile mixings U^2 in which type-I seesaw-based leptogenesis with three heavy neutrinos is possible, in the limit of approximately degenerate heavy neutrino mass spectrum and for HNLs masses ranging from 50 MeV to 70 TeV, thereby covering the whole experimentally accessible range. For this purpose, we used the quantum kinetic equations (2.14) which were averaged on the momentum. The knowledge of momentum-averaged damping and backreaction rates from [89] then enabled us to compute the baryon asymmetry for the considered mass range.

We extended the observation from [80] that the parameter space is much larger in the $n = 3$ scenario compared to the $n = 2$ scenario to masses above the electroweak scale. It is actually so much bigger that the upper limit from leptogenesis itself for masses below[1] 100 GeV is weaker than the combined theoretical constraints. This is very promising from an experimental point of view as many experiments will be able to explore large part of the parameter space consistent with both leptogenesis and neutrino masses. Under ideal assumption, *e.g.* large coupling U^2 and low masses, one could not only detect those heavy neutrinos, but also produce a sufficient number of these to constrain the relative coupling to SM flavours $\frac{U_\alpha^2}{U^2}$ to a percent level or estimate the proportion of $B-\bar{L}$ violating processes.

We also lowered the lower bound on the HNL mass in which leptogenesis with thermal initial conditions, very well-motivated in presence of additional gauge interactions, is feasible from $\mathcal{O}(7)$ GeV, in the $n = 2$ scenario, to $\mathcal{O}(1.7)$ GeV in the $n = 3$ scenario. This last observation is quite interesting from an experimental viewpoint as the leptogenesis parameter space could already be probed at current experiments, some (*e.g.* NA62, CMS) in which UCLouvain is involved.

This work has to be pursued as several effects, detailed in section 3.3, have not been taken into account. In particular, it is crucial to have a better control on the momentum averaging procedure as it leads *e.g.* to unphysical oscillations and soft modes ($k \lesssim T$) have a more important contribution to the final baryon asymmetry compared to the kinetic equilibrium scenario [95]. However, the focus should be placed on a balance between precision and numerical efficiency for successful scans of the whole parameter space. For this, ideas could be to sample the momentum space in a clever way, search for conserved charges or perform en series expansion of the QKEs using moments of the distributions functions. Outside of its direct continuity, one could extend our work to related models. One could *e.g.* generalise the QKEs in presence of additional gauge interactions (Left-Right Symmetric Model, $U(1)_{B-L}$ extensions) and perform a similar scan.

[1]The exact statement depends on the value of m_{lightest}. For $m_{\text{lightest}} = 0.1$ eV, this is only valid up to $\simeq 10$ GeV.

Appendices

A Chemical potential and asymmetry

In this section, we aim to give a proof of relation (2.15) and study its range of validity. Our proof is mostly based on the one given in [92]. The main idea behind the proof is to use the property that, at chemical equilibrium, the sum of the chemical potentials is conserved, *i.e.*

$$\sum_i \mu_{A_i} = \sum_i \mu_{B_i}$$

for a reaction of the form

$$A_1 + A_2 + \cdots \longleftrightarrow B_1 + B_2 + \ldots$$

It is therefore important to search which processes are at equilibrium at the temperature of interest for leptogenesis to impose a maximum number of conditions on the chemical potentials. Fortunately, the exact temperature at which Standard Model Yukawa interactions and sphaleron processes equilibrate have already been computed in previous work [110]. Equilibration temperatures for most SM Yukawa interactions and both sphalerons processes are listed in the next figure.

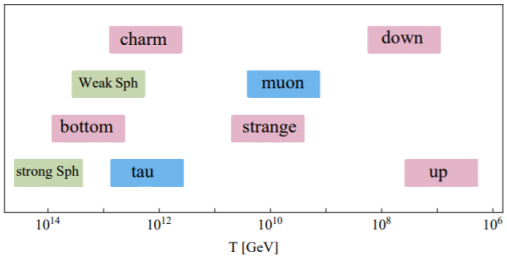

T_{ss}	2.4×10^{13} GeV	strong sphaleron
T_{ws}	1.8×10^{12} GeV	weak sphaleron
T_b	4.2×10^{12} GeV	bottom-quark Yukawa
T_c	3.8×10^{11} GeV	charm-quark Yukawa
T_s	2.5×10^{9} GeV	strange-quark Yukawa
T_u	1.9×10^{6} GeV	up-quark Yukawa
T_d	8.8×10^{6} GeV	down-quark Yukawa
T_τ	3.7×10^{11} GeV	τ-lepton Yukawa
T_μ	1.3×10^{9} GeV	μ-lepton Yukawa
T_e	3.1×10^{4} GeV	electron Yukawa

Figure 7: Equilibration temperatures of the SM Yukawa interactions and spahleron processes. Taken from [110].

The strong sphaleron process is the analogue of the weak sphaleron process for the strong interaction as QCD also has various topologically different vacua. From Figure 7, one can conclude that under $T \simeq 100$ TeV, all the SM Yukawa interactions are at equilibrium. Moreover, we also know from section 1.3 that the sphaleron process is at equilibrium for $T \gtrsim 131.7$ GeV. Inside this temperature range, in which most of the asymmetries are produced for resonant and ARS leptogenesis, we can consider all the spectator processes to be at equilibrium. Outside this range however, relation (2.15) is

slightly modified, see *e.g.* [111]. Moreover, as mentioned in section 3.3, the fact that the sphaleron freeze-out does not happen instantaneously also implies a temperature dependence for the susceptibility matrix. We do not consider these corrections in the present section. The following relations

$$\mu_{Q_i} = \mu_{u_i} - \mu_\phi, \tag{A.4a}$$

$$\mu_{Q_i} = \mu_{d_i} + \mu_\phi, \tag{A.4b}$$

$$\mu_{\ell_i} = \mu_{l_i} + \mu_\phi \tag{A.4c}$$

hold due to the equilibrium of the Yukawa interactions

$$Q_i \to u_i + \phi^*, \quad Q_i \to d_i + \phi \text{ and } \ell_i \to l_i + \phi.$$

Q_i and ℓ_i are quark and lepton doublets, ϕ is the Higgs field whereas l_i, u_i and d_i are right-handed charged leptons, up-type and down-type quarks respectively. The index $i \in \{1, 2, 3\}$ labels the flavour of the concerned particle. In addition, the equilibrium of both sphaleron processes imply that

$$3\sum_i \mu_{Q_i} + \sum_i \mu_{\ell_i} = 0, \tag{A.5a}$$

$$2\sum_i \mu_{Q_i} - \sum_i \mu_{u_i} - \sum_i \mu_{d_i} = 0. \tag{A.5b}$$

The factors 3 and 2 respectively accounts for the three different colours of each quark and the two different isospin eigenstates in each weak doublet. Note that equation (A.5b) does not bring new constraints as it is trivially verified from relations (A.4a) and (A.4b). Let us now denote the number density of a particle A as n_A. The last relation that will be useful for this proof is the condition that the density of weak hypercharges Y must vanish. We can rewrite this as

$$\begin{aligned} 2Y_\phi n_\phi + \sum_i \Big[6Y_{Q_i} n_{Q_i} + 2Y_{\ell_i} n_{\ell_i} + 3Y_{u_i} n_{u_i} + 3Y_{d_i} n_{d_i} + Y_{l_i} n_{l_i}\Big] = 0 \\ \implies 2n_\phi + \sum_i \Big[2n_{Q_i} - 2n_{\ell_i} + 4n_{u_i} - 2n_{d_i} - 2n_{l_i}\Big] = 0 \end{aligned} \tag{A.6}$$

using the exact value of the weak hypercharge of each of these particles. Again, the factors 2, 3 and 6 comes from the multiplicity (flavour and weak isospin) of each state. We can reexpress this last expression in function of the chemical potential using the observation that, for small chemical potentials ($\frac{\mu_i}{T} \ll 1$),

$$n_\phi - n_{\phi^*} \simeq g_\phi \frac{T^3}{3} \mu_\phi \tag{A.7}$$

for the Higgs field and

$$n_f - n_{\bar{f}} \simeq g_f \frac{T^3}{6} \mu_f \tag{A.8}$$

for a fermion.g is the field's intrinsic number of degrees of freedom. Combining now equations (A.4), (A.5) and (A.6), we get after some algebra

$$n_\ell = \frac{1}{711} \begin{pmatrix} -221 & 16 & 16 \\ 16 & -221 & 16 \\ 16 & 16 & -221 \end{pmatrix} \cdot n_\Delta \text{ and } n_\phi = -\frac{8}{79} \begin{pmatrix} 1 & 1 & 1 \end{pmatrix} \cdot n_\Delta. \tag{A.9}$$

As mentioned in section 2.4.1, $n_\Delta = (n_{\Delta_e}, n_{\Delta_\mu}, n_{\Delta_\tau})$ denotes the number density for the asymmetries within each SM flavour $a \in \{e, \mu, \tau\}$. Relation (A.9) implies that

$$2n_\ell + n_\phi = -\frac{2}{711}\begin{pmatrix} 257 & 20 & 20 \\ 20 & 257 & 20 \\ 20 & 20 & 257 \end{pmatrix} \cdot n_\Delta$$

which is equivalent to relation (2.15). Note that equation (A.9) also implies that

$$2n_\ell + n_l = 3n_\ell - \frac{n_\phi}{2} = \frac{1}{711}\begin{pmatrix} -627 & 84 & 84 \\ 84 & -627 & 84 \\ 84 & 84 & -627 \end{pmatrix} \cdot \Delta$$

which in turn implies that

$$L = \sum_j (2n_\ell + n_l)_j = -\frac{51}{79}\sum_j \Delta_j \implies B = \frac{28}{79}(B - L)$$

as mentioned in section 1.4.

B Quantum kinetic equations from first principles

In this appendix, we aim to provide a brief derivation of relation (2.14a) from the first principles of non-equilibrium quantum field theory. Our proof closely follows the one given in [92] and [112]. As will be noticed, we first restrict ourselves to the case where the space-time is equipped with a Minkowski metric before slightly modifying our equations in section B-5 to take into account the observation that the universe is in fact expanding. The proof given here is limited to the relativistic regime, suitable for the ARS scenario, but equations (2.14) are also consistent with what have been derived in the literature for larger masses [113]. The rates $\Gamma, \tilde{\Gamma}$ are however different in this scenario as discussed in section 2.4.1.

As in the Sigl-Raffelt formalism, the derivation of relation (2.14a) through first principles will involve the computation of correlation functions. In standard quantum field theory, the computations of S-matrix elements are strongly facilitated by the so-called *Gell-Mann and Low theorem* [114] which allow to reexpress correlation functions evaluated at the vacuum of the interacting theory into correlation functions evaluated at the vacuum of the free theory. However, this theorem assumes in particular that the particles are free "far" from the interaction point. This is the *in-out formalism*. In a primordial plasma, such as the one in which the heavy neutrinos evolve, this cannot be true as the particle density is so high that particles are constantly interacting. In- and out-states are ill defined in such an environment. A new formalism is therefore needed. The *CTP formalism*, independently developed by Schwinger and Keldysh [115,116], precisely allows us

to overcome this difficulty. In this approach, we study the time evolution of these correlation functions without any reference to the asymptotic states in themselves. One can then extract observables like the HNLs number densities from these correlations functions as is shown in section B-6. Besides, as discussed in section 2.4.1, the CTP approach naturally avoids the double counting problem faced by the early computations of rates entering the Boltzmann equations (1.23) and can account for thermodynamical and statistical effects such as the LPM effect, see section 3.3, or Bose enhancement and Pauli blocking. In this appendix, we only introduce the tools necessary for the derivation of (2.14a). However, an interested reader will find a good introduction to the CTP formalism presented here in [117] or in chapter 1 of [118]. [119] also provides a exhaustive review of non-equilibrium quantum field theory on which the CTP formalism is based.

We can split our derivation of (2.14a) into three main steps which are shown in the following figure. We first state the Kadanoff-Baym equations, a set of integro-differential equations governing the time evolution of the two-point correlation functions, and approximate these in the limit where macroscopic and microscopic time scales are well separated. We then apply these to the specific case of heavy neutrinos interacting with SM fields in thermal equilibrium. This will make naturally appear HNLs distribution functions. Finally, we will integrate these equation with respect to the momentum to get rate equations, *i.e.* independent of the momentum $\vec{k}$, constraining the particle number densities δn. This procedure allows us to get a better control on the approximations we are making to get these quantum kinetic equations.

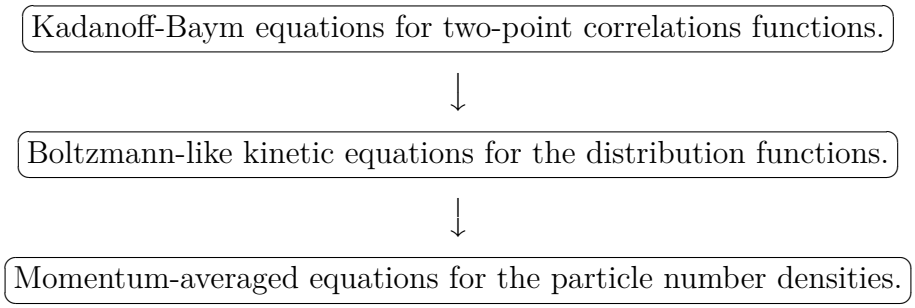

B-1 Correlation functions in the CTP formalism

The CTP approach initially originated from the real time formalism in thermal field theory. In the presence of a non-negligible thermal background of inverse temperature β, we are usually interested in the thermal Green functions

$$G_{\mathcal{C}}(x_1, \dots, x_n) = \langle T_{\mathcal{C}}\big(\phi(x_1) \dots \phi(x_n)\big)\rangle_{\beta}$$

where ϕ is the field of interest and C a contour in the complex plane. Giving the parametric expression of the path $\mathcal{C} = q(\lambda),\ \lambda \in [0, 1]$, the contour must verify the boundary condition

$$\mathrm{Re}(q(0)) = \mathrm{Re}(q(1)) \text{ and } \mathrm{Im}(q(0)) - \beta = \mathrm{Im}(q(1))$$

using the property that the Hamiltonian is the generator of time translations. A practically very useful example of such a contour is given in Figure 8. $T_{\mathcal{C}}$ is the time ordering

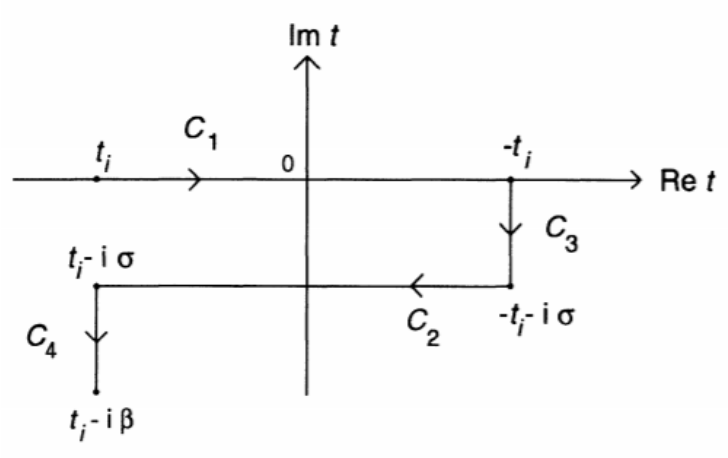

Figure 8: Time path in the complex plane. Taken from [84].

operator along the path $\mathcal{C}$. A more comprehensive overview on this matter is given in chapter 2 and 3 of [84].

In the context of leptogenesis from neutrino oscillations, it is useful to consider a peculiar form of the latter contour. The closed time path or Schwinger-Keldysh contour used in non-equilibrium field theory is given by the contour of Figure 8 in the limit where $t_i \to -\infty$ and $\sigma \to 0$. As will be seen in the next section, this will prove to be very practical when performing a Wigner transformation on the variables x, y. Even though sending $t_i \to -\infty$ seems to modify the initial conditions of our fields, the latter can still be imposed by adding an external singular source term. Another advantage of this limit is that the contour $\mathcal{C}_3$ will not contribute when integrating along the contour and $\mathcal{C}_4$ will only contribute with an overall normalisation factor [84] so that we can only consider $\mathcal{C}_1$ and $\mathcal{C}_2$. An illustration of this new contour is shown in Figure 9.

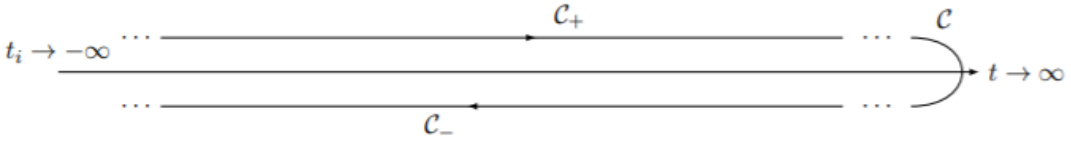

Figure 9: Closed time path in the limit $t_i \to -\infty$. Taken from [118].

One can then define on this contour the following two-point correlation functions for a fermionic field ψ

$$
\begin{aligned}
iS^{++}_{\alpha\beta}(x,y) &\equiv \langle T\big[\psi_\alpha(x)\bar{\psi}_\beta(y)\big]\rangle\,, \\
iS^{--}_{\alpha\beta}(x,y) &\equiv \langle \bar{T}\big[\psi_\alpha(x)\bar{\psi}_\beta(y)\big]\rangle\,, \\
iS^{+-}_{\alpha\beta}(x,y) &\equiv iS^{<}_{\alpha\beta}(x,y) = -\langle \bar{\psi}_\beta(y)\psi_\alpha(x)\rangle\,, \\
iS^{-+}_{\alpha\beta}(x,y) &\equiv iS^{>}_{\alpha\beta}(x,y) = \langle \psi_\alpha(x)\bar{\psi}_\beta(y)\rangle
\end{aligned}
$$

where the indices $\pm$ refers to which branch $\mathcal{C}_\pm$ of the contour the point is located at. T is the standard time ordering operator and $\bar{T}$ is the anti-time ordering as time flows backwards on the $\mathcal{C}_-$ contour. The last two correlation functions $S^>$ and $S^<$ are usually

known as the *Wightman functions*. Bear in mind that the expectation values are computed as

$$\langle \dots \rangle = \mathrm{Tr}[\rho \dots]$$

as usual for quantum statistical systems. ρ is the density matrix at the initial time. For the ARS scenario, ρ is given by

$$\rho = \rho_{SM}^{eq} \otimes \rho_N^{vac}$$

since the SM fields are expected to be in equilibrium in the range of temperature of interest. ρ_N^{vac} is the vacuum density matrix of the heavy neutrinos. This is suitable within the ARS mechanism as we expect the SM fields to equilibrate much sooner than the production of HNLs. From these functions, we can define the spectral and statistical functions

$$\begin{aligned} S^{\mathcal{A}}(x,y) &= \frac{i}{2}(S^{>}(x,y) - S^{<}(x,y)), \\ S^{+}(x,y) &= \frac{1}{2}(S^{>}(x,y) + S^{<}(x,y)) \end{aligned}$$

respectively. These have a more physical interpretation. The spectral function indeed encodes the spectrum of the (quasi)particle while the statistical function contains the information about the particles number densities. These two functions can be obtained by solving the so-called *Kadanoff-Baym* equations

$$\begin{aligned} (i\not{\partial}_x - M)S^{\mathcal{A}}(x,y) &= 2i \int \mathrm{d}^3 w \int_{x_0}^{y_0} \mathrm{d}w_0 \; \not{\Sigma}^{\mathcal{A}}(x,w) S^{\mathcal{A}}(w,y), \\ (i\not{\partial}_x - M)S^{+}(x,y) &= 2i\Big(\int \mathrm{d}^3 w \int_{-\infty}^{y_0} \mathrm{d}w_0 \; \not{\Sigma}^{+}(x,w) S^{\mathcal{A}}(w,y) - \int \mathrm{d}^3 w \int_{-\infty}^{x_0} \mathrm{d}w_0 \; \not{\Sigma}^{\mathcal{A}}(x,w) S^{+}(w,y) \Big). \end{aligned} \tag{B.10}$$

This particular form of the more well-known Schwinger-Dyson equation can be derived using the framework of the two particles irreducible actions [120]. The self-energy Σ of the particle is the correction to the free propagator coming from the interacting Lagrangian and is therefore defined through the relation

$$(S)^{-1}(k_1,k_2) = (S_0)^{-1}(k_1,k_2) + \Sigma(k_1,k_2)$$

in the momentum space. We did not precise a specific index for S as we can define a self-energy for each choice of S ($S^{\mathcal{A}}, S^{+}, ...$). Strictly speaking, equations (B.10) are only valid for Gaussian initial conditions which makes it not suitable to describe the time evolution of the SM fields since they initially start in thermal equilibrium[1]. [120] gives an example of how one can treat non-Gaussian initial conditions. Fortunately, we are only interested in this work in the time evolution of the heavy neutrinos. In absence of additional gauge interactions, the latter can be assumed to have vanishing initial density and Gaussian quantum fluctuations. Equations (B.10) are therefore applicable. To simplify (B.10),

[1] Working in the canonical ensemble, the density matrix of fields in thermal equilibrium is indeed given by $\rho^{eq} \propto e^{-\beta \mathcal{H}}$.

one can get rid of the x_0, y_0 in the integral bounds by using the retarded, advanced and Hermitian propagators

$$\begin{aligned} iS^R(x,y) &= 2\theta(x_0-y_0)S^{\mathcal{A}}(x,y),\\ iS^A(x,y) &= -2\theta(y_0-x_0)S^{\mathcal{A}}(x,y),\\ S^H(x,y) &= \frac{1}{2}\big(S^R(x,y)+S^A(x,y)\big). \end{aligned}$$

The Kadanoff-Baym equations can then be rewritten

$$\begin{aligned} (i\not{\partial}_x - M)S^{\mathcal{A}}(x,y) &= \int \mathrm{d}^4w\Big(\not{\Sigma}^H(x,w)S^{\mathcal{A}}(w,y)+\not{\Sigma}^{\mathcal{A}}(x,w)S^H(w,y)\Big),\\ (i\not{\partial}_x - M)S^{+}(x,y) &= \int \mathrm{d}^4w\ \Big(\not{\Sigma}^{+}(x,w)S^H(w,y)+\not{\Sigma}^H(x,w)S^{+}(w,y)\Big)\\ &\quad+\frac{1}{2}\int \mathrm{d}^4w\Big(\not{\Sigma}^{>}(x,w)S^{<}(w,y)-\not{\Sigma}^{<}(x,w)S^{>}(w,y)\Big). \end{aligned} \tag{B.11}$$

The Heaviside functions θ allowed us to integrate on the whole real axis for the time component.

B-2 Approximation scheme: The gradient expansion

We now want to simplify the latter equations when applying these to our case of interest. We can first transform these relations to the Wigner space by making the change of variables

$$\begin{pmatrix} x\\ y\end{pmatrix} \to \begin{pmatrix} z\\ r\end{pmatrix} = \begin{pmatrix} \frac{x+y}{2}\\ x-y\end{pmatrix}$$

and Fourier transforming every function (G in our following example) with respect to the variable r

$$G(z,k) = \int \mathrm{d}^4r\ e^{ikr}G(z+\frac{r}{2}, z-\frac{r}{2}).$$

Combining the properties

$$\partial_x = \partial_z + 2\partial_r$$

and

$$\int \mathrm{d}^4r e^{ikr}\int \mathrm{d}^4w\ G_1(x,w)G_2(w,y) = e^{-i\Xi}\big(G_1(z,k),G_2(z,k)\big), \tag{B.12}$$

where Ξ is an operator[2] generalising the Poisson brackets and defined by

$$\Xi\big(G_1(z,k),G_2(z,k)\big) = \frac{1}{2}\big(\partial_zG_1\cdot\partial_kG_2-\partial_kG_1\cdot\partial_zG_2\big), \tag{B.13}$$

we can simplify the Kadanoff-Baym equations (B.11) as

$$\begin{aligned} \big(\not{k}+\frac{i}{2}\not{\partial}_z - M\big)S^{\mathcal{A}}(z,k) &= e^{-i\Xi}\Big(\not{\Sigma}^HS^{\mathcal{A}}+\not{\Sigma}^{\mathcal{A}}S^H\Big),\\ \big(\not{k}+\frac{i}{2}\not{\partial}_z - M\big)S^{+}(z,k) &= e^{-i\Xi}\Big(\not{\Sigma}^HS^{+}+\not{\Sigma}^{+}S^H\Big)+\frac{1}{2}e^{-i\Xi}\Big(\not{\Sigma}^{>}S^{<}-\not{\Sigma}^{<}S^{>}\Big). \end{aligned} \tag{B.14}$$

[2] Ξ is a particular example of a Moyal product. For a proof of relation (B.12) and a more rigorous definition the operator Ξ, see *e.g.* [121].

Up to now, we have remained fairly general in our derivation. We need to particularise these equations to our system in order to simplify them. First, we are working in an isotropic and homogeneous universe. We can therefore neglect all spatial derivatives $\partial_z \to \partial_{z^0} \equiv \partial_t$. Second, we can use an approximation scheme known as the *gradient expansion* on the operator $e^{-i\Xi}$ using the clear separation of time scales between microscopic and macroscopic processes. Microscopical processes, *e.g.* scatterings, have a typical timescale of the order of $\frac{1}{T}$ while macroscopical processes take place at a much slower rate. During the radiation era, the Hubble constant $H = \frac{\dot{T}}{T} \sim \sqrt{\frac{8\pi^3}{90} g_*} \frac{T^2}{M_P} \ll T$ in the range of temperature of interest, M_P being here defined as the Planck mass. We can therefore assume that the temperature changes slowly with respect to the microscopic processes. In addition, the rates associated to 1) HNLs oscillations ($\sim \frac{\Delta M^2}{T}$, see (2.12)) 2) equilibration processes and modifications of the chemical potentials ($\sim |F|^2 T$) are all way smaller than the energy scale T within the ARS scenario. One can therefore assume that the scale of microscopic variation ∂_z is way smaller than the energy scale $(\partial_k)^{-1}$, implying that $\partial_z G_1 \cdot \partial_k G_2 \ll 1$. Given the definition (B.13) of Ξ, we can expand to first order $e^{-i\Xi}$

$$e^{-i\Xi}(G_1, G_2) = G_1 \cdot G_2 + \mathcal{O}\big(\partial_z G_1 \cdot \partial_k G_2\big).$$

Equation (B.14) then becomes

$$\big(\not{k} + \frac{i\gamma^0}{2}\partial_t - M\big) S^{\mathcal{A}}(z,k) = \not{\Sigma}^H S^{\mathcal{A}} + \not{\Sigma}^{\mathcal{A}} S^H, \tag{B.15a}$$

$$\big(\not{k} + \frac{i\gamma^0}{2}\partial_t - M\big) S^{+}(z,k) = \not{\Sigma}^H S^{+} + \not{\Sigma}^{+} S^H + \frac{1}{2}\Big(\not{\Sigma}^{>} S^{<} - \not{\Sigma}^{>} S^{<}\Big). \tag{B.15b}$$

One then gets the system of four equations

$$\{\mathcal{H}, \mathcal{S}^{\mathcal{A}}\} = \{\mathcal{G}, \mathcal{S}^H\}, \tag{B.16a}$$

$$i\partial_t \mathcal{S}^{\mathcal{A}} + \big[\mathcal{H}, \mathcal{S}^{\mathcal{A}}\big] = \big[\mathcal{G}, \mathcal{S}^H\big], \tag{B.16b}$$

$$\{\mathcal{H}, \mathcal{S}^{+}\} = \{\mathcal{N}, \mathcal{S}^H\} + \frac{1}{2}\Big(\big[\mathcal{G}^{>}, \mathcal{S}^{<}\big] - \big[\mathcal{G}^{<}, \mathcal{S}^{>}\big]\Big), \tag{B.16c}$$

$$i\partial_t \mathcal{S}^{+} + \big[\mathcal{H}, \mathcal{S}^{+}\big] = \big[\mathcal{N}, \mathcal{S}^H\big] + \frac{1}{2}\Big(\{\mathcal{G}^{>}, \mathcal{S}^{<}\} - \{\mathcal{G}^{<}, \mathcal{S}^{>}\}\Big) \tag{B.16d}$$

if one adds and subtracts equations (B.15a),(B.15b) with their respective hermitian conjugate. We have used the notation shortcuts

$$\mathcal{S}^{+/H} \equiv i\gamma^0 S^{+/H}, \quad \mathcal{H} \equiv (\not{k} - \not{\Sigma}^H - M)\gamma^0, \quad \mathcal{G}^{\gtrless} \equiv i\not{\Sigma}^{\gtrless}\gamma^0, \quad \mathcal{G} \equiv \frac{i}{2}(\mathcal{G}^{>} - \mathcal{G}^{<}), \quad \mathcal{N} \equiv \not{\Sigma}^{+}\gamma^0.$$

Equation (B.16d) highlights the physical meaning of these terms. We mentioned in the previous section that S^+ encodes the information about particle number densities. Moreover, equation (B.16d) is relatively similar to the quantum kinetic equations derived in the Sigl-Raffelt formalism (2.13). The commutator $\big[\mathcal{H}, \mathcal{S}^{+}\big]$ therefore induces oscillations between the HNLs and $\mathcal{H}$ represents the Hermitian part of an effective Hamiltonian. Similarly, we recognise $\mathcal{G}^{\gtrless}$ as damping terms.

One can then split these equations (B.16) into an equilibrium and a non-equilibrium part. Let us write $\bar{\mathcal{H}}$ and $\bar{\mathcal{G}}$ for $\mathcal{H}$ and $\mathcal{G}$ computed at thermal equilibrium and for vanishing

chemical potentials. By definition, these do not depend on time. One can now define the equilibrium two-point correlation functions $\bar{\mathcal{S}}^{+}$ and $\bar{\mathcal{S}}^{\mathcal{A}}$ as solutions of the system

$$\big[\bar{\mathcal{H}},\bar{\mathcal{S}}^{+}\big]=\big[\bar{\mathcal{N}},\bar{\mathcal{S}}^{H}\big]+\frac{1}{2}\Big(\{\bar{\mathcal{G}}^{>},\bar{\mathcal{S}}^{<}\}-\{\bar{\mathcal{G}}^{<},\bar{\mathcal{S}}^{>}\}\Big),\quad \{\bar{\mathcal{H}},\bar{\mathcal{S}}^{\mathcal{A}}\}=\{\bar{\mathcal{G}},\bar{\mathcal{S}}^{H}\} \tag{B.17}$$

setting $\partial_t\bar{\mathcal{S}}^{+}=0$. One can then expand around these static solutions

$$\mathcal{H}=\bar{\mathcal{H}}+\delta\mathcal{H} \text{ and } \mathcal{G}=\bar{\mathcal{G}}+\delta\mathcal{G}.$$

In addition, as already mentioned, the HNLs mostly interact with SM fields that are in thermal equilibrium. We can therefore assume that

$$\mathcal{S}^{\gtrless}=\bar{\mathcal{S}}^{\gtrless}+\delta\mathcal{S}\implies \mathcal{S}^{\mathcal{A}}=\frac{i}{2}(\mathcal{S}^{>}-\mathcal{S}^{<})=\bar{\mathcal{S}}^{\mathcal{A}},\quad \mathcal{S}^{H}=\bar{\mathcal{S}}^{H} \text{ and } \mathcal{S}^{+}=\bar{\mathcal{S}}^{+}+\delta\mathcal{S}.$$

Putting together all these expansions inside equations (B.16d) and keeping only first order terms, we get

$$\partial_t\delta\mathcal{S}=-\partial_t\bar{\mathcal{S}}^{+}+i[\mathcal{H},\delta\mathcal{S}]+i[\delta\mathcal{H},\bar{\mathcal{S}}^{+}]-i[\delta\mathcal{N},\bar{\mathcal{S}}^{H}]-\{\bar{\mathcal{G}},\delta\mathcal{S}\}-\frac{i}{2}(\{\delta\mathcal{G}^{>},\bar{\mathcal{S}}^{<}\}-\{\delta\mathcal{G}^{<},\bar{\mathcal{S}}^{>}\}). \tag{B.18}$$

Contrary to equation (B.17), we keep the term $\partial_t\bar{\mathcal{S}}^{+}$ as it cannot be neglected at first order in the non-equilibrium expansion due to the expansion of the universe.

B-3 Heavy neutrinos self-energy

We now continue the simplification of equation (B.18) by studying the form taken by the HNLs self-energy. One can indeed split the self-energy into a component evaluated at thermal equilibrium and null chemical potential and a deviation originating from the non-zero chemical potential of the SM fields

$$\not{\Sigma}=\bar{\not{\Sigma}}+\delta\not{\Sigma}. \tag{B.19}$$

From now on, the quantities without any lower indices are attached to HNLs, *i.e.* $\not{\Sigma}\equiv\not{\Sigma}_N$. The absence of an index $+,>,...$ associated to Σ just means that this equation is valid for all types of self-energy. One can also observe from Lagrangian (1.5) that HNLs only interact with SM fields through their mixing with the light neutrinos. Two terms indeed contribute to their self-energy

$$F_{ij}\big(\bar{\ell}_i\tilde{\phi}\big)(\nu_R)_j \text{ and } F^{*}_{ij}(\bar{\nu}_R)_j\big(\tilde{\phi}^{\dagger}\ell_i\big).$$

Σ may then be computed using Feynman diagram (2.1). Recalling that the antiparticle of a left-handed particle is right-handed, the self-energy of the HNLs can therefore be split, see *e.g.* appendix E of [112], into two contributions of different chiralities

$$\bar{\not{\Sigma}}_{\mu}=g_w\hat{\not{\Sigma}}\Big(F^{\dagger}FP_R+F^{t}F^{*}P_L\Big). \tag{B.20}$$

$g_w=2$ is the gauge factor coming from the fact that each field running in the loop (2.1) is a SU(2) doublet. $P_{R/L}$ is defined as the projector operator on the right/left-handed part

of the spinor. In the case where chemical potential are non-zero, this relation needs to be modified to

$$\left(\not{\Sigma}_\mu\right)_{ij} = g_w \sum_{a\in\{e,\mu,\tau\}} \left(\hat{\not{\Sigma}}_{Ra} F^\dagger_{ia} F_{aj} P_R + \hat{\not{\Sigma}}_{La} F^t_{ia} F^*_{aj} P_L\right). \tag{B.21}$$

As already mentioned, the HNLs only interact with fields which are in thermal equilibrium. This implies that $\hat{\not{\Sigma}}$ must verify the well-known Kubo-Martin-Schwinger (KMS) relation [84]

$$\hat{\not{\Sigma}}^{>}_{R/La} = -e^{(k_0 \pm \mu_{La} \pm \mu_\phi)/T} \hat{\not{\Sigma}}^{<}_{R/La}. \tag{B.22}$$

Combining equations (B.19),(B.20), (B.21) and (B.22) together and limiting ourselves to first order, we get the relations

$$\bar{\not{\Sigma}}^{>}_\mu = -e^{k_0/T} \cdot \bar{\not{\Sigma}}^{<}_\mu, \tag{B.23a}$$

$$\delta\hat{\not{\Sigma}}^{>}_{R/La} = -e^{k_0/T}\left[\delta\hat{\not{\Sigma}}^{<}_{R/La} \mp \frac{\mu_{La}+\mu_\phi}{T} \cdot \bar{\not{\Sigma}}^{<} P_{R/La}\right]. \tag{B.23b}$$

This last relation comes from the observation that we have two expansion parameters $\delta\hat{\not{\Sigma}}$ and $\frac{\mu}{T}$. This means that the term $\delta\hat{\not{\Sigma}}^{<}_{R/La} \cdot \frac{\mu_{La}+\mu_\phi}{T}$ can safely be neglected. These equations have as direct consequence that we can neglect $\delta\mathcal{N}$ as it is at least quadratic in the chemical potentials due to the sign difference between the right- and left-handed self-energies in (B.22). The second approximation we will make is to neglect the term proportional to $\delta\mathcal{H}$. It is by itself a first order term. However, we know that, in the ARS scenario, the abundance of the heavy neutrinos is initially vanishing which implies that $\delta\mathcal{S} = -\bar{\mathcal{S}}^+$. Since $\delta\mathcal{S}$ only slightly deviates from being an identity matrix at high temperature[3] and for small Yukawa couplings, $[\delta\mathcal{H}, \bar{\mathcal{S}}^+] \propto [\delta\mathcal{H}, \mathbb{1}] = 0$ can be neglected. Combining all our previous results, we can write a new equation

$$\partial_t \delta\mathcal{S} = \frac{2\partial_t f_F}{1-2f_F}\bar{\mathcal{S}}^+ + i[\mathcal{H}, \delta\mathcal{S}] - \{\bar{\mathcal{G}}, \delta\mathcal{S}\} - \frac{2}{1-2f_F}\sum_{a\in\{e,\mu,\tau\}} \frac{\mu_{La}+\mu_\phi}{T}\{\tilde{\mathcal{G}}^a, \bar{\mathcal{S}}^+\}. \tag{B.24}$$

where $\tilde{\mathcal{G}}^a$ is the term representing the backreaction of the SM lepton asymmetries on the heavy neutrinos

$$\tilde{\mathcal{G}}^a = -g_w f_F(1-f_F)\not{\Sigma}^{\mathcal{A}}\left(F^\dagger_{ia}F_{aj}P_R + F^t_{ia}F^*_{aj}P_L\right)\gamma^0.$$

The Fermi-Dirac factors $f_F(k) = (e^{k/T}+1)^{-1}$ originate from the KMS relation (B.22). The derivation of (B.24) relies on the observation that $\bar{\mathcal{S}}^+$ and the static self-energy $\bar{\mathcal{S}}^{\mathcal{A}}$ are related through

$$\bar{\mathcal{S}}^+ = -i\frac{e^{k/T}-1}{e^{k/T}+1}\bar{\mathcal{S}}^{\mathcal{A}} = -i(1-2f_F)\cdot\bar{\mathcal{S}}^{\mathcal{A}} \tag{B.25}$$

which implies

$$\partial_t\bar{\mathcal{S}}^+ = -i\bar{\mathcal{S}}^{\mathcal{A}}\partial_t(1-2f_F) = (-2\partial_t f_F)\frac{\bar{\mathcal{S}}^+}{1-2f_F}.$$

This is also the reason why $\tilde{\mathcal{G}}^a$ is proportional to $\not{\Sigma}^{\mathcal{A}}$ and not $\not{\Sigma}^+$.

[3] $\delta S \simeq -f_F(k)\cdot\mathbb{1}$ at high temperatures as the energy does not depend on the mass of the HNLs in this limit and all HNLs have therefore the same equilibrium distribution $f_F(k)$.

B-4 Lorentz decomposition of the HNL propagator

It will reveal useful to decompose the deviation from equilibrium $\delta\mathcal{S}$ into different helicity and Lorentz components as such

$$\delta\mathcal{S} = -\frac{1}{2}\sum_{h=\pm1} P_h\big(g_{0h} + g_{1h}\gamma^0 - ig_{2h}\gamma^0\gamma^5 - g_{3h}\gamma^5\big) \tag{B.26}$$

where P_h is the usual helicity projector for a 4-momentum k

$$P_h(k) = \frac{1}{2}\big(1 + h\gamma^0(\vec{\gamma}\cdot\hat{k})\gamma^5\big).$$

$\hat{k}$ is the normalised spatial component of k. The various g_{ih} are all functions depending on the momentum k. In the regime where the Majorana mass and the Yukawa couplings are small $M \ll T, |F| \ll 1$, which sounds reasonable for the ARS scenario, these functions are related between each other through the following set of equations

$$\begin{aligned} g_{1h} &= \frac{1}{2k^0}\Big(\{\mathrm{Re}(M), g_{0h}\} + [i\mathrm{Im}(M), g_{3h}]\Big), \\ g_{2h} &= \frac{1}{2ik^0}\Big([\mathrm{Re}(M), g_{3h}] + \{i\mathrm{Im}(M), g_{0h}\}\Big), \\ g_{3h} &= h\mathrm{sign}(k^0)g_{0h}. \end{aligned} \tag{B.27}$$

These equations are derived by taking the trace over the product of equation (B.16c) with P_h or one of the matrices $\{\mathbb{1}, \gamma^i\gamma^5, \gamma^5, \gamma^i\}$ respectively and by limiting ourselves to first order in $\frac{M}{T}$ and Yukawa couplings. More details on this decomposition and how to get the previous equations can be found in [113]. Analogously to what has been done in the previous section B-3, one can develop g_{ih} into an equilibrium and out-of-equilibrium component

$$g_{ih} = \bar{g}_{ih} + \delta g_{ih}.$$

$\bar{g}$ is formally defined through a similar relation (B.26) where we replace $\delta\mathcal{S}$ by $\bar{\mathcal{S}}^+$. Replacing (B.26) and (B.27) into (B.24), one finally gets

$$\partial_t\delta g_{0h} = \frac{2\partial_t f_F}{1-2f_F}\bar{g}_{0h} - \frac{i}{2}[H, \delta g_{0h}] - \frac{1}{2}\{\Gamma, \delta g_{0h}\} - \frac{1}{1-2f_F}\sum_{a\in\{e,\mu,\tau\}}\frac{\mu_{La}+\mu_\phi}{T}\{\tilde{\Gamma}^a, \bar{g}_{0h}\}f_F(1-f_F) \tag{B.28}$$

where

$$\begin{aligned} H &= 2g_w\Big(\mathrm{Re}[F^\dagger F]\frac{k\cdot\hat{\Sigma}^H}{k^0} - ih\mathrm{sign}(k^0)\mathrm{Im}[F^\dagger F]\frac{k\cdot\hat{\Sigma}^H}{k^0}\Big) \\ &\quad + \frac{\mathrm{Re}[M_M^\dagger M_M] + ih\mathrm{sign}(k^0)\mathrm{Im}[M_M^\dagger M_M]}{k^0}, \\ \Gamma &= 2g_w\Big(\mathrm{Re}[F^\dagger F]\frac{k\cdot\hat{\Sigma}^{\mathcal{A}}}{k^0} - ih\mathrm{sign}(k^0)\mathrm{Im}[F^\dagger F]\frac{k\cdot\hat{\Sigma}^{\mathcal{A}}}{k^0}\Big) \end{aligned} \tag{B.29}$$

and

$$\tilde{\Gamma}^a_{ij} = 2g_w h\Big(\mathrm{sign}(k^0)\mathrm{Re}[F^\dagger_{ia}F_{aj}]\frac{k\cdot\hat{\Sigma}^{\mathcal{A}}}{k^0} - ih\mathrm{Im}[F^\dagger_{ia}F_{aj}]\frac{k\cdot\hat{\Sigma}^{\mathcal{A}}}{k^0}\Big).$$

One can clearly observe the splitting of the effective Hamiltonian H into a vacuum part proportional to the Majorana matrix M_M and a thermal part proportional to the Yukawa coupling matrix F.

B-5 Kinetic equations in an expanding universe

We now have an equation for two-point correlation functions which already has a form similar to (2.14a). However, what we really want is an equation for the particle number densities. For that purpose, we will have to factorise the quasiparticle distributions f from g_{0h}. It is long known [84] that an harmonic oscillator of frequency w has the spectral function

$$\bar{S}^{\mathcal{A}}(k^0) = \frac{1}{2} 2\pi \text{sign}(k^0) \delta\big((k^0)^2 - w^2\big). \tag{B.30}$$

The *narrow-width approximation* consists in assuming that the spectral function of feebly coupled particles is the same as the one of a free particle but with the slight replacement $w \to \Omega$, where Ω is the quasiparticle pole. Ω corresponds to a mass term as in the free case but includes thermal corrections from the interaction with the plasma in addition to the vacuum mass. In general, a feebly interacting particle has a well defined mass and the spectral function will present a pole at this value. Practically, all phase-space integrals are dominated by the value of the integrand at this pole. In this limit, one can approximate $\bar{g}_{0h}$ as

$$\bar{g}_{0h}(k)_{ij} \simeq -\frac{1 - 2f_F}{2} 2\pi \delta\big((k^0)^2 - \Omega_i^2\big) 2k^0 \text{sign}(k^0) \delta_{ij} \tag{B.31}$$

combining (B.25), (B.26) (adapted for $\bar{\mathcal{S}}^+$) and the equivalent of (B.30) for free fermions, hence the additional k^0 in the numerator of (B.31). Deriving (B.25) also leads to a condition on the deviation $\delta f_F \equiv \delta f$ from the Fermi-Dirac distribution $\delta\mathcal{S} = -2\bar{\mathcal{S}}^{\mathcal{A}} \delta f$. This in turn implies

$$g_{ih} = -\frac{2\bar{g}_{ih}}{1 - 2f_F} \delta f_{ih}. \tag{B.32}$$

The Fermi-Dirac distribution represents in general the distribution for the energies of a fermion at temperature T. One can therefore define $f(\vec{k}, \Omega_i) = f_F(\Omega_i) + \delta f(\vec{k}, \Omega_i)$ and[4] $1 - f_F(-\Omega_i) + \delta f(\vec{k}, -\Omega_i)$ as the momentum distribution of particles and antiparticles respectively. However, we will only have to track the evolution of the particle number densities and can therefore restrict to the case where $\text{sign}(k^0) = 1$. Indeed, HNLs are Majorana particles which implies that the relation

$$S^{\gtrless} = C(S^{\gtrless})^t C^\dagger$$

is fulfilled. C is the usual charge conjugation operator. The latter equation directly implies that

$$\delta f_{0h}(-k^0) = \delta f_{0h}^*(k^0).$$

With all this in mind and combining relations (B.31) and (B.32) to get

$$\int \frac{\mathrm{d}k^0}{2\pi} g_{ih} = \delta f_{ih},$$

[4]The definition of the antiparticle number density can be obtained from the constraint that the trace of the density matrix must be exactly one at thermal equilibrium.

one obtains a kinetic equation for δf instead of δg by integrating (B.28) with respect to k^0

$$\partial_t \delta f_{0h} = -\partial_t f_F - \frac{i}{2}[H, \delta f_{0h}] - \frac{1}{2}\{\Gamma, \delta f_{0h}\} - \sum_{a\in\{e,\mu,\tau\}} \tilde{\Gamma}^a \cdot \frac{\mu_{La} + \mu_\phi}{T} f_F(1 - f_F). \quad \text{(B.33)}$$

The last anti-commutator disappeared as f_F is just a number and not a matrix. In the above equation, $H, \Gamma, \tilde{\Gamma}^a$ were all evaluated in the ultra-relativistic limit $k^0 = |\vec{k}|$. Indeed, while it is important to include these in the definition of H to reproduce the HNLs oscillations, thermal corrections can be neglected for all other practical purposes $\delta\big((k^0)^2 - \Omega_i^2\big) \simeq \delta\big((k^0)^2\big)$ within the ARS scenario. This equation is exactly (2.14) (apart that it has not yet been momentum averaged) and gives us an explicit formula for the different rates (B.29).

As mentioned in the introduction of this appendix, we begun our reasoning in a flat Minkowski universe. It is nonetheless fairly easy to generalise equation (B.33) to a radiation dominated and flat Friedman-Lemaitre-Robertson-Walker (FLRW) universe as is the primordial universe. The metric g is indeed only rescaled $g_{\mu\nu} = a^2(t)\eta_{\mu\nu}$ compared to the Minkowski metric $\eta_{\mu\nu}$. The factor a^2 can be reabsorbed in Lagrangian (1.5) by using the conformal time η, defined though the relation $\mathrm{d}t = a\mathrm{d}\eta$, and rescale the fields so that the kinetic terms are correctly normalised. We also have to make the replacement[5] $M_M \to \frac{M_M}{a}$ in the Lagrangian 1.5 to preserve the mass and interaction terms. In summary, (B.33) remains valid if we replace t by η and use the comoving momenta, temperature, distribution function and mass ($A_{\text{comoving}} = a \cdot A_{\text{physical}}$ for all these variables) in the rates. During the radiation era, we have that

$$\eta = \frac{a}{a_{\mathrm{R}}} = \frac{1}{T}$$

where $a_{\mathrm{R}} = \frac{T^2}{H} \simeq 7.1 \cdot 10^{17}$ GeV. (B.33) then becomes

$$\big(\delta f_{0h}\big)' = -\frac{i}{2}[H, \delta f_{0h}] - \frac{1}{2}\{\Gamma, \delta f_{0h}\} - \sum_{a\in\{e,\mu,\tau\}} \tilde{\Gamma}^a \cdot \frac{\mu_{La} + \mu_\phi}{T}. \quad \text{(B.34)}$$

A $'$ denotes a derivative with respect to the conformal time. Note that, while f_F depends on the time through the temperature, it does not depends on the conformal time

$$f_F(\vec{k}) = \frac{1}{e^{|\vec{k}|/a_{\mathrm{R}}} + 1}.$$

In conformal time, the momentum indeed compensates for the conformal time dependence of the temperature. In the non-relativistic regime, this conclusion does not hold as $\sqrt{k^2 + M^2}$ will depend on the conformal time through the mass M. The derivative of the equilibrium distribution f_F then acts as a source for the asymmetries. This effect was included in our code.

[5]The Yukawa interaction is automatically well rescaled if the kinetic terms are.

B-6 Momentum-averaged equations for particle number densities

In this section, we integrate equation (B.34) with respect to $\vec{k}$ to get momentum independent equations for the particle number densities. As already explained in section 2.4.1, one has to solve equation (B.34) for each momentum $\vec{k}$, which is not numerically realistic for large parameter scan. Moreover, couplings between different modes could in principle arise through the backreaction term $\tilde{\Gamma}$. This particularly complicates the problem and the search for efficient codes or analytical solutions. It seems therefore wise to average the equations over the momentum in a first approximation.

In this context, we can introduce the equilibrium density number

$$n_F = \int \frac{\mathrm{d}^3\vec{k}}{(2\pi)^3} f_F(\vec{k}) = \frac{3a_{\mathrm{R}}^3}{4\pi^2}\zeta(3)$$

and the averaged deviations to equilibrium

$$\big(\delta n_h\big)_{ij} = \int \frac{\mathrm{d}^3\vec{k}}{(2\pi)^3}\big(\delta_{0h} f(\vec{k})\big)_{ij}.$$

$\zeta(s)$ denotes the usual Riemann zeta function. The interaction terms $H, \Gamma, \tilde{\Gamma}^a$ have also to be averaged. From (B.29), we can see that these terms depends on $\vec{k}$ through a term $\hat{k}\cdot\hat{\Sigma}$ and a term $\frac{1}{k^0} = \frac{1}{|\vec{k}|}$ in the relativistic approximation. The term $\frac{1}{|\vec{k}|}$ is usually replaced by its averaged value

$$\langle\frac{1}{|\vec{k}|}\rangle \equiv \frac{1}{n_F}\int \frac{\mathrm{d}^3\vec{k}}{(2\pi)^3}\frac{1}{|\vec{k}|} f_F(\vec{k}) = \frac{\pi^2}{18 a_{\mathrm{R}}\zeta(3)}. \tag{B.35}$$

Regarding the numerator, we will follow what has been done in [122] and replace the spectral self-energy through

$$\frac{\hat{k}\cdot\hat{\Sigma}^{\mathcal{A}}}{|\vec{k}|} \to \frac{\Gamma_{av}}{T}\frac{a_{\mathrm{R}}}{2g_w} \equiv \frac{a_{\mathrm{R}}}{2g_w}\gamma_{av}.$$

The coefficient γ_{av} has already been computed [96], in the ultrarelativistic limit where the top loop dominates, and can be estimated to $\gamma_{av} \simeq 0.012$. One can make a similar replacement for the Hermitian part of the self-energy

$$\frac{\hat{k}\cdot\hat{\Sigma}^{H}}{|\vec{k}|} \to \frac{a_{\mathrm{R}}}{2g_w}\gamma_{th}$$

where $\gamma_{th} \simeq 0.23$. This computation [123] has been done using the Hard Thermal Loop (HTL) approximation, *i.e.* assuming the momenta running in the loop are $\sim T$, which allows us to replace

$$\hat{k}\cdot\hat{\Sigma}^{H} \to \frac{T^2}{8}. \tag{B.36}$$

The factor g_w arise from the fact that SU(2) doublets are running in the loops. Finally, it is practically useful to replace the chemical potentials with the associated number densities n_ℓ, n_ϕ as has been done in appendix A, see (A.7) and (A.8). With all this in mind, we can replace equation (B.34) with

$$\frac{\mathrm{d}}{\mathrm{d}z}\delta n_h = -\frac{i}{2}\big[H^{th} + z^2 H^{vac}, \delta n_h\big] - \frac{1}{2}\{\Gamma, \delta n_h\} + \sum_{a\in\{e,\mu,\tau\}} \tilde{\Gamma}^a\big(n_{La} + \frac{1}{2}n_\phi\big). \tag{B.37}$$

$z \equiv \frac{T_{\mathrm{ref}}}{T}$, T_{ref} is an arbitrary reference temperature, is a new variable allowing us to get rid of the temperature coming from relations of the form (B.36) since $\partial_z = \frac{1}{Hz}\partial_t$. As explained in section B-4, we decomposed the Hermitian Hamiltonian into a vacuum and thermal part. Definitions (B.29) become after momentum averaging

$$\begin{aligned}
H^{th} &= \frac{a_{\mathrm{R}}}{T_{\mathrm{ref}}}\gamma_{th}\Big(\mathrm{Re}[F^\dagger F] - ih\mathrm{Im}[F^\dagger F]\Big)\\
H^{vac} &= \frac{\pi^2}{18\zeta(3)}\frac{a_{\mathrm{R}}}{T_{\mathrm{ref}}^3}\Big(\mathrm{Re}[M_M^\dagger M_M] + ih\mathrm{Im}[M_M^\dagger M_M]\Big),\\
\Gamma &= \frac{a_{\mathrm{R}}}{T_{\mathrm{ref}}}\gamma_{av}\Big(\mathrm{Re}[F^\dagger F] - ih\mathrm{Im}[F^\dagger F]\Big)\\
&\text{and}\\
\tilde{\Gamma}^a_{ij} &= \frac{h}{2}\frac{a_{\mathrm{R}}}{T_{\mathrm{ref}}}\gamma_{av}\Big(\mathrm{Re}[F^\dagger_{ia}F_{aj}] - ih\mathrm{Im}[F^\dagger_{ia}F_{aj}]\Big).
\end{aligned} \tag{B.38}$$

One can see from (B.35) that we average $\frac{1}{|\vec{k}|}$ by integrating its product with the Fermi-Dirac distribution, in the relativistic limit. This would only lead to small errors if we assume kinetic equilibrium, *i.e.* if δf had the form of a Fermi-Dirac distribution. Unfortunately, we cannot assume in general that interactions do not modify the momentum distribution. Large deviations from the equilibrium distribution are expected, see [94]. However, this assumption is valid for very high momenta $|\vec{k}| \gg a_{\mathrm{R}}$ so that errors generated by this procedure are still only of order one. As a final word, we remind the reader that results (B.38) are only valid in the ultra-relativistic regime. To find a more comprehensive computation of these rates, see [89]. These were the rates used in this work for numerical simulations.

Bibliography

[1] P. Minkowski, "$\mu \to e\gamma$ at a Rate of One Out of 10^9 Muon Decays?," *Phys. Lett. B*, vol. 67, pp. 421–428, 1977. DOI: 10.1016/0370-2693(77)90435-X.

[2] M. Fukugita and T. Yanagida, "Baryogenesis Without Grand Unification," *Phys. Lett. B*, vol. 174, pp. 45–47, 1986. DOI: 10.1016/0370-2693(86)91126-3.

[3] E. K. Akhmedov, V. A. Rubakov, and A. Y. Smirnov, "Baryogenesis via neutrino oscillations," *Phys. Rev. Lett.*, vol. 81, pp. 1359–1362, 1998. DOI: 10.1103/PhysRevLett.81.1359.

[4] S. Dodelson and L. M. Widrow, "Sterile-neutrinos as dark matter," *Phys. Rev. Lett.*, vol. 72, pp. 17–20, 1994. DOI: 10.1103/PhysRevLett.72.17.

[5] T. Asaka, S. Blanchet, and M. Shaposhnikov, "The nuMSM, dark matter and neutrino masses," *Phys. Lett. B*, vol. 631, pp. 151–156, 2005. DOI: 10.1016/j.physletb.2005.09.070.

[6] E. Cortina Gil *et al.*, "Search for heavy neutral lepton production in K^+ decays," *Phys. Lett. B*, vol. 778, pp. 137–145, 2018. DOI: 10.1016/j.physletb.2018.01.031.

[7] G. Aad *et al.*, "Search for heavy neutral leptons in decays of W bosons produced in 13 TeV pp collisions using prompt and displaced signatures with the ATLAS detector," *JHEP*, vol. 10, p. 265, 2019. DOI: 10.1007/JHEP10(2019)265.

[8] V. Khachatryan *et al.*, "Search for Heavy Neutrinos and W Bosons with Right-Handed Couplings in Proton-Proton Collisions at $\sqrt{s} = 8\,\text{TeV}$," *Eur. Phys. J. C*, vol. 74, no. 11, p. 3149, 2014. DOI: 10.1140/epjc/s10052-014-3149-z.

[9] V. Khachatryan *et al.*, "Search for heavy Majorana neutrinos in ee+ jets and e μ+ jets events in proton-proton collisions at $\sqrt{s} = 8$ TeV," *JHEP*, vol. 04, p. 169, 2016. DOI: 10.1007/JHEP04(2016)169.

[10] A. M. Sirunyan *et al.*, "Search for heavy Majorana neutrinos in same-sign dilepton channels in proton-proton collisions at $\sqrt{s} = 13$ TeV," *JHEP*, vol. 01, p. 122, 2019. DOI: 10.1007/JHEP01(2019)122.

[11] K. Abe *et al.*, "Search for heavy neutrinos with the T2K near detector ND280," *Phys. Rev. D*, vol. 100, no. 5, p. 052006, 2019. DOI: 10.1103/PhysRevD.100.052006.

[12] S. Alekhin *et al.*, "A facility to Search for Hidden Particles at the CERN SPS: the SHiP physics case," *Rept. Prog. Phys.*, vol. 79, no. 12, p. 124201, 2016. DOI: 10.1088/0034-4885/79/12/124201.

[13] P. Ballett, T. Boschi, and S. Pascoli, "Heavy Neutral Leptons from low-scale seesaws at the DUNE Near Detector," *JHEP*, vol. 03, p. 111, 2020. DOI: 10.1007/JHEP03(2020)111.

[14] D. Curtin *et al.*, "Long-Lived Particles at the Energy Frontier: The MATHUSLA Physics Case," *Rept. Prog. Phys.*, vol. 82, no. 11, p. 116201, 2019. DOI: 10.1088/1361-6633/AB28D6.

[15] V. A. Kuzmin, V. A. Rubakov, and M. E. Shaposhnikov, "On the Anomalous Electroweak Baryon Number Nonconservation in the Early Universe," *Phys. Lett. B*, vol. 155, p. 36, 1985. DOI: 10.1016/0370-2693(85)91028-7.

[16] S. Davidson and A. Ibarra, "A Lower bound on the right-handed neutrino mass from leptogenesis," *Phys. Lett. B*, vol. 535, pp. 25–32, 2002. DOI: 10.1016/S0370-2693(02)01735-5.

[17] H. Fritzsch and P. Minkowski, "Unified Interactions of Leptons and Hadrons," *Annals Phys.*, vol. 93, pp. 193–266, 1975. DOI: 10.1016/0003-4916(75)90211-0.

[18] J. C. Pati and A. Salam, "Lepton Number as the Fourth Color," *Phys. Rev. D*, vol. 10, pp. 275–289, 1974. [Erratum: Phys.Rev.D 11, 703–703 (1975)] DOI: 10.1103/PhysRevD.10.275.

[19] A. Pilaftsis, "CP violation and baryogenesis due to heavy Majorana neutrinos," *Phys. Rev. D*, vol. 56, pp. 5431–5451, 1997. DOI: 10.1103/PhysRevD.56.5431.

[20] B. Garbrecht, "Why is there more matter than antimatter? Calculational methods for leptogenesis and electroweak baryogenesis," *Prog. Part. Nucl. Phys.*, vol. 110, p. 103727, 2020. DOI: 10.1016/J.PPNP.2019.103727.

[21] J. Klarić, M. Shaposhnikov, and I. Timiryasov, "Uniting low-scale leptogeneses," 8 2020. ARXIV:2008.13771.

[22] M. Drewes, Y. Georis, and J. Klarić, "Mapping the viable parameter space for testable leptogenesis," 6 2021. ARXIV:2106.16226.

[23] T. collaboration, "*A Brief History Of Neutrinos*." `http://t2k-experiment.org/neutrinos/a-brief-history/betaspec/`, (last consulted on August 11, 2021).

[24] W. Pauli, "Dear radioactive ladies and gentlemen," *Phys. Today*, vol. 31N9, p. 27, 1978.

[25] C. L. Cowan, F. Reines, F. B. Harrison, H. W. Kruse, and A. D. McGuire, "Detection of the free neutrino: A Confirmation," *Science*, vol. 124, pp. 103–104, 1956. DOI: 10.1126/SCIENCE.124.3212.103.

[26] G. Danby, J. M. Gaillard, K. A. Goulianos, L. M. Lederman, N. B. Mistry, M. Schwartz, and J. Steinberger, "Observation of High-Energy Neutrino Reactions and the Existence of Two Kinds of Neutrinos," *Phys. Rev. Lett.*, vol. 9, pp. 36–44, 1962. DOI: 10.1103/PhysRevLett.9.36.

[27] K. Kodama *et al.*, "Observation of tau neutrino interactions," *Phys. Lett. B*, vol. 504, pp. 218–224, 2001. DOI: 10.1016/S0370-2693(01)00307-0.

[28] R. Davis, Jr., J. C. Evans, and B. T. Cleveland, "The solar neutrino problem," *AIP Conf. Proc.*, vol. 52, pp. 17–27, 1979. DOI: 10.1063/1.31802.

[29] Q. R. Ahmad *et al.*, "Measurement of the rate of $\nu_e + d \to p + p + e^-$ interactions produced by ^{8}B solar neutrinos at the Sudbury Neutrino Observatory," *Phys. Rev. Lett.*, vol. 87, p. 071301, 2001. DOI: 10.1103/PhysRevLett.87.071301.

[30] I. Esteban, M. C. Gonzalez-Garcia, M. Maltoni, T. Schwetz, and A. Zhou, "The fate of hints: updated global analysis of three-flavor neutrino oscillations," *JHEP*, vol. 09, p. 178, 2020. DOI: 10.1007/JHEP09(2020)178.

[31] B. Abi *et al.*, "Measurement of the Positive Muon Anomalous Magnetic Moment to 0.46 ppm," *Phys. Rev. Lett.*, vol. 126, no. 14, p. 141801, 2021. DOI: 10.1103/PhysRevLett.126.141801.

[32] G. Caria *et al.*, "Measurement of $\mathcal{R}(D)$ and $\mathcal{R}(D^*)$ with a semileptonic tagging method," *Phys. Rev. Lett.*, vol. 124, no. 16, p. 161803, 2020. DOI: 10.1103/PhysRevLett.124.161803.

[33] P. Stöcker *et al.*, "Strengthening the bound on the mass of the lightest neutrino with terrestrial and cosmological experiments," 9 2020. ARXIV:2009.03287.

[34] P. Mermod, "Right-handed neutrinos: the hunt is on!," in *Prospects in Neutrino Physics*, 4 2017. ARXIV:1704.08635.

[35] M. D'Onofrio, K. Rummukainen, and A. Tranberg, "Sphaleron Rate in the Minimal Standard Model," *Phys. Rev. Lett.*, vol. 113, no. 14, p. 141602, 2014. DOI: 10.1103/PhysRevLett.113.141602.

[36] F. Englert and R. Brout, "Broken Symmetry and the Mass of Gauge Vector Mesons," *Phys. Rev. Lett.*, vol. 13, pp. 321–323, 1964. DOI: 10.1103/PhysRevLett.13.321.

[37] P. W. Higgs, "Broken Symmetries and the Masses of Gauge Bosons," *Phys. Rev. Lett.*, vol. 13, pp. 508–509, 1964. DOI: 10.1103/PhysRevLett.13.508.

[38] J. Schechter and J. W. F. Valle, "Neutrino Masses in SU(2) x U(1) Theories," *Phys. Rev. D*, vol. 22, p. 2227, 1980. DOI: 10.1103/PhysRevD.22.2227.

[39] R. Foot, H. Lew, X. G. He, and G. C. Joshi, "Seesaw Neutrino Masses Induced by a Triplet of Leptons," *Z. Phys. C*, vol. 44, p. 441, 1989. DOI: 10.1007/BF01415558.

[40] K. S. Babu, S. Nandi, and Z. Tavartkiladze, "New Mechanism for Neutrino Mass Generation and Triply Charged Higgs Bosons at the LHC," *Phys. Rev. D*, vol. 80, p. 071702, 2009. DOI: 10.1103/PhysRevD.80.071702.

[41] E. Ma, "Verifiable radiative seesaw mechanism of neutrino mass and dark matter," *Phys. Rev. D*, vol. 73, p. 077301, 2006. DOI: 10.1103/PhysRevD.73.077301.

[42] P. A. Zyla *et al.*, "Review of Particle Physics," *PTEP*, vol. 2020, no. 8, p. 083C01, 2020. DOI: 10.1093/ptep/ptaa104.

[43] M. Agostini *et al.*, "Improved Limit on Neutrinoless Double-β Decay of ^{76}Ge from GERDA Phase II," *Phys. Rev. Lett.*, vol. 120, no. 13, p. 132503, 2018. DOI: 10.1103/PhysRevLett.120.132503.

[44] G. Anton *et al.*, "Search for Neutrinoless Double-β Decay with the Complete EXO-200 Dataset," *Phys. Rev. Lett.*, vol. 123, no. 16, p. 161802, 2019. DOI: 10.1103/PhysRevLett.123.161802.

[45] A. Gando *et al.*, "Search for Majorana Neutrinos near the Inverted Mass Hierarchy Region with KamLAND-Zen," *Phys. Rev. Lett.*, vol. 117, no. 8, p. 082503, 2016. [Addendum: Phys.Rev.Lett. 117, 109903 (2016)], DOI: 10.1103/PhysRevLett.117.082503.

[46] M. Drewes, "The Phenomenology of Right Handed Neutrinos," *Int. J. Mod. Phys. E*, vol. 22, p. 1330019, 2013. DOI: 10.1142/S0218301313300191.

[47] F. Maltoni, J. M. Niczyporuk, and S. Willenbrock, "Upper bound on the scale of Majorana neutrino mass generation," *Phys. Rev. Lett.*, vol. 86, pp. 212–215, 2001. DOI: 10.1103/PhysRevLett.86.212.

[48] R. N. Mohapatra and A. Y. Smirnov, "Neutrino Mass and New Physics," *Ann. Rev. Nucl. Part. Sci.*, vol. 56, pp. 569–628, 2006. DOI: 10.1146/annurev.nucl.56.080805.140534.

[49] R. N. Mohapatra and G. Senjanovic, "Neutrino Mass and Spontaneous Parity Nonconservation," *Phys. Rev. Lett.*, vol. 44, p. 912, 1980. DOI: 10.1103/PhysRevLett.44.912.

[50] H. Georgi and S. L. Glashow, "Unity of All Elementary Particle Forces," *Phys. Rev. Lett.*, vol. 32, pp. 438–441, 1974. DOI: 10.1103/PhysRevLett.32.438.

[51] J. A. Casas and A. Ibarra, "Oscillating neutrinos and $\mu \to e, \gamma$," *Nucl. Phys. B*, vol. 618, pp. 171–204, 2001. DOI: 10.1016/S0550-3213(01)00475-8.

[52] S. Antusch, E. Cazzato, M. Drewes, O. Fischer, B. Garbrecht, D. Gueter, and J. Klarić, "Probing Leptogenesis at Future Colliders," *JHEP*, vol. 09, p. 124, 2018. DOI: 10.1007/JHEP09(2018)124.

[53] C. Giunti and C. W. Kim, *Fundamentals of neutrino physics and astrophysics*. Oxford university press, 2007.

[54] C. L. Bennett *et al.*, "Nine-Year Wilkinson Microwave Anisotropy Probe (WMAP) Observations: Final Maps and Results," *Astrophys. J. Suppl.*, vol. 208, p. 20, 2013. DOI: 10.1088/0067-0049/208/2/20.

[55] W. Pauli, "Exclusion principle, lorentz group, and reversal of space-time and charge," *Niels Bohr and the Development of Physics, W. Pauli (ed.) New York: Pergamon*, 1955.

[56] G. Luders, "Proof of the TCP theorem," *Annals Phys.*, vol. 2, pp. 1–15, 1957. DOI: 10.1016/0003-4916(57)90032-5.

[57] J. H. Christenson, J. W. Cronin, V. L. Fitch, and R. Turlay, "Evidence for the 2π Decay of the K_2^0 Meson," *Phys. Rev. Lett.*, vol. 13, pp. 138–140, 1964. DOI: 10.1103/PhysRevLett.13.138.

[58] A. D. Sakharov, "Violation of CP Invariance, C asymmetry, and baryon asymmetry of the universe," *Pisma Zh. Eksp. Teor. Fiz.*, vol. 5, pp. 32–35, 1967. DOI: 10.1070/PU1991v034n05ABEH002497.

[59] R. L. Garwin, L. M. Lederman, and M. Weinrich, "Observations of the Failure of Conservation of Parity and Charge Conjugation in Meson Decays: The Magnetic Moment of the Free Muon," *Phys. Rev.*, vol. 105, pp. 1415–1417, 1957. DOI: 10.1103/PhysRev.105.1415.

[60] G. 't Hooft, "Symmetry Breaking Through Bell-Jackiw Anomalies," *Phys. Rev. Lett.*, vol. 37, pp. 8–11, 1976. DOI: 10.1103/PhysRevLett.37.8.

[61] M.-C. Chen, "TASI 2006 Lectures on Leptogenesis," in *Theoretical Advanced Study Institute in Elementary Particle Physics: Exploring New Frontiers Using Colliders and Neutrinos*, pp. 123–176, 3 2007. ARXIV:HEP-PH/0703087.

[62] M. E. Shaposhnikov, "Possible Appearance of the Baryon Asymmetry of the Universe in an Electroweak Theory," *JETP Lett.*, vol. 44, pp. 465–468, 1986.

[63] M. Yoshimura, "Unified Gauge Theories and the Baryon Number of the Universe," *Phys. Rev. Lett.*, vol. 41, pp. 281–284, 1978. [Erratum: Phys.Rev.Lett. 42, 746 (1979)] DOI: 10.1103/PhysRevLett.41.281.

[64] I. Affleck and M. Dine, "A New Mechanism for Baryogenesis," *Nucl. Phys. B*, vol. 249, pp. 361–380, 1985. DOI: 10.1016/0550-3213(85)90021-5.

[65] D. E. Morrissey and M. J. Ramsey-Musolf, "Electroweak baryogenesis," *New J. Phys.*, vol. 14, p. 125003, 2012. DOI: 10.1088/1367-2630/14/12/125003.

[66] L. D. Landau and I. Pomeranchuk, "Limits of applicability of the theory of bremsstrahlung electrons and pair production at high-energies," *Dokl. Akad. Nauk Ser. Fiz.*, vol. 92, pp. 535–536, 1953.

[67] A. B. Migdal, "Bremsstrahlung and pair production in condensed media at high energies," *Physical Review*, vol. 103, no. 6, p. 1811, 1956. DOI: 10.1103/PhysRev.103.1811.

[68] W. Buchmuller, R. D. Peccei, and T. Yanagida, "Leptogenesis as the origin of matter," *Ann. Rev. Nucl. Part. Sci.*, vol. 55, pp. 311–355, 2005. DOI: 10.1146/annurev.nucl.55.090704.151558.

[69] W. Buchmuller and M. Plumacher, "Matter antimatter asymmetry and neutrino properties," *Phys. Rept.*, vol. 320, pp. 329–339, 1999. DOI: 10.1016/S0370-1573(99)00057-5.

[70] P. S. B. Dev, P. Di Bari, B. Garbrecht, S. Lavignac, P. Millington, and D. Teresi, "Flavor effects in leptogenesis," *Int. J. Mod. Phys. A*, vol. 33, p. 1842001, 2018. DOI: 10.1142/S0217751X18420010.

[71] M. Drewes, J. Hajer, J. Klarić, and G. Lanfranchi, "NA62 sensitivity to heavy neutral leptons in the low scale seesaw model," *JHEP*, vol. 07, p. 105, 2018. DOI: 10.1007/JHEP07(2018)105.

[72] C. Ahdida *et al.*, "Sensitivity of the SHiP experiment to Heavy Neutral Leptons," *JHEP*, vol. 04, p. 077, 2019. DOI: 10.1007/JHEP04(2019)077.

[73] A. Ariga *et al.*, "FASER's physics reach for long-lived particles," *Phys. Rev. D*, vol. 99, no. 9, p. 095011, 2019. DOI: 10.1103/PhysRevD.99.095011.

[74] G. Aielli *et al.*, "Expression of interest for the CODEX-b detector," *Eur. Phys. J. C*, vol. 80, no. 12, p. 1177, 2020. DOI: 10.1140/epjc/s10052-020-08711-3.

[75] E. Izaguirre and B. Shuve, "Multilepton and Lepton Jet Probes of Sub-Weak-Scale Right-Handed Neutrinos," *Phys. Rev. D*, vol. 91, no. 9, p. 093010, 2015. DOI: 10.1103/PhysRevD.91.093010.

[76] M. Drewes and J. Hajer, "Heavy Neutrinos in displaced vertex searches at the LHC and HL-LHC," *JHEP*, vol. 02, p. 070, 2020. DOI: 10.1007/JHEP02(2020)070.

[77] S. Pascoli, R. Ruiz, and C. Weiland, "Heavy neutrinos with dynamic jet vetoes: multilepton searches at $\sqrt{s} = 14$, 27, and 100 TeV," *JHEP*, vol. 06, p. 049, 2019. DOI: 10.1007/JHEP06(2019)049.

[78] S. Antusch, E. Cazzato, and O. Fischer, "Sterile neutrino searches at future e^-e^+, pp, and e^-p colliders," *Int. J. Mod. Phys. A*, vol. 32, no. 14, p. 1750078, 2017. DOI: 10.1142/S0217751X17500786.

[79] A. Pilaftsis and T. E. J. Underwood, "Resonant leptogenesis," *Nucl. Phys. B*, vol. 692, pp. 303–345, 2004. DOI: 10.1016/j.nuclphysb.2004.05.029.

[80] A. Abada, G. Arcadi, V. Domcke, M. Drewes, J. Klarić, and M. Lucente, "Low-scale leptogenesis with three heavy neutrinos," *JHEP*, vol. 01, p. 164, 2019. DOI: 10.1007/JHEP01(2019)164.

[81] F. Bezrukov, D. Gorbunov, and M. Shaposhnikov, "On initial conditions for the Hot Big Bang," *JCAP*, vol. 06, p. 029, 2009. DOI: 10.1088/1475-7516/2009/06/029.

[82] B. Shuve and I. Yavin, "Baryogenesis through Neutrino Oscillations: A Unified Perspective," *Phys. Rev. D*, vol. 89, no. 7, p. 075014, 2014. DOI: 10.1103/PhysRevD.89.075014.

[83] A. Blondel, E. Graverini, N. Serra, and M. Shaposhnikov, "Search for Heavy Right Handed Neutrinos at the FCC-ee," *Nucl. Part. Phys. Proc.*, vol. 273-275, pp. 1883–1890, 2016. DOI: 10.1016/j.nuclphysbps.2015.09.304.

[84] M. L. Bellac, *Thermal Field Theory*. Cambridge Monographs on Mathematical Physics, Cambridge University Press, 3 2011. DOI: 10.1017/CBO9780511721700.

[85] K. Moffat, S. Pascoli, and C. Weiland, "Equivalence between massless neutrinos and lepton number conservation in fermionic singlet extensions of the Standard Model," 12 2017. arXiv:1712.07611.

[86] M. Malinsky, J. C. Romao, and J. W. F. Valle, "Novel supersymmetric SO(10) see-saw mechanism," *Phys. Rev. Lett.*, vol. 95, p. 161801, 2005. DOI: 10.1103/PhysRevLett.95.161801.

[87] R. N. Mohapatra, "Mechanism for Understanding Small Neutrino Mass in Superstring Theories," *Phys. Rev. Lett.*, vol. 56, pp. 561–563, 1986. DOI: 10.1103/PhysRevLett.56.561.

[88] M. Shaposhnikov, "A Possible symmetry of the nuMSM," *Nucl. Phys. B*, vol. 763, pp. 49–59, 2007. DOI: 10.1016/j.nuclphysb.2006.11.003.

[89] J. Klarić, M. Shaposhnikov, and I. Timiryasov, "Reconciling resonant leptogenesis and baryogenesis via neutrino oscillations," 3 2021. arXiv:2103.16545.

[90] G. Sigl and G. Raffelt, "General kinetic description of relativistic mixed neutrinos," *Nucl. Phys. B*, vol. 406, pp. 423–451, 1993. DOI: 10.1016/0550-3213(93)90175-O.

[91] E. W. Kolb and S. Wolfram, "Baryon Number Generation in the Early Universe," *Nucl. Phys. B*, vol. 172, p. 224, 1980. [Erratum: Nucl.Phys.B 195, 542 (1982)] DOI: 10.1016/0550-3213(82)90012-8.

[92] M. Drewes, B. Garbrecht, D. Gueter, and J. Klarić, "Leptogenesis from Oscillations of Heavy Neutrinos with Large Mixing Angles," *JHEP*, vol. 12, p. 150, 2016. DOI: 10.1007/JHEP12(2016)150.

[93] J. Ghiglieri and M. Laine, "GeV-scale hot sterile neutrino oscillations: a derivation of evolution equations," *JHEP*, vol. 05, p. 132, 2017. DOI: 10.1007/JHEP05(2017)132.

[94] T. Asaka, S. Eijima, and H. Ishida, "Kinetic Equations for Baryogenesis via Sterile Neutrino Oscillation," *JCAP*, vol. 02, p. 021, 2012. DOI: 10.1088/1475-7516/2012/02/021.

[95] J. Ghiglieri and M. Laine, "GeV-scale hot sterile neutrino oscillations: a numerical solution," *JHEP*, vol. 02, p. 078, 2018. DOI: 10.1007/JHEP02(2018)078.

[96] B. Garbrecht, "More Viable Parameter Space for Leptogenesis," *Phys. Rev. D*, vol. 90, no. 6, p. 063522, 2014. DOI: 10.1103/PhysRevD.90.063522.

[97] M. Drewes, B. Garbrecht, D. Gueter, and J. Klarić, "Testing the low scale seesaw and leptogenesis," *JHEP*, vol. 08, p. 018, 2017. DOI: 10.1007/JHEP08(2017)018.

[98] S. Eijima, M. Shaposhnikov, and I. Timiryasov, "Parameter space of baryogenesis in the νMSM," *JHEP*, vol. 07, p. 077, 2019. DOI: 10.1007/JHEP07(2019)077.

[99] A. Roy and M. Shaposhnikov, "Resonant production of the sterile neutrino dark matter and fine-tunings in the [nu]MSM," *Phys. Rev. D*, vol. 82, p. 056014, 2010. DOI: 10.1103/PhysRevD.82.056014.

[100] G. C. Branco, R. Gonzalez Felipe, M. N. Rebelo, and H. Serodio, "Resonant leptogenesis and tribimaximal leptonic mixing with A(4) symmetry," *Phys. Rev. D*, vol. 79, p. 093008, 2009. DOI: 10.1103/PhysRevD.79.093008.

[101] M. Drewes, "On the Minimal Mixing of Heavy Neutrinos," 4 2019. arXiv:1904.11959.

[102] A. Donini, P. Hernandez, J. Lopez-Pavon, M. Maltoni, and T. Schwetz, "The minimal 3+2 neutrino model versus oscillation anomalies," *JHEP*, vol. 07, p. 161, 2012. DOI: 10.1007/JHEP07(2012)161.

[103] M. Chrząszcz, M. Drewes, T. E. Gonzalo, J. Harz, S. Krishnamurthy, and C. Weniger, "A frequentist analysis of three right-handed neutrinos with GAMBIT," *Eur. Phys. J. C*, vol. 80, no. 6, p. 569, 2020. DOI: 10.1140/EPJC/S10052-020-8073-9.

[104] A. Pilaftsis, "Radiatively induced neutrino masses and large Higgs neutrino couplings in the standard model with Majorana fields," *Z. Phys. C*, vol. 55, pp. 275–282, 1992. DOI: 10.1007/BF01482590.

[105] J. Lopez-Pavon, S. Pascoli, and C.-f. Wong, "Can heavy neutrinos dominate neutrinoless double beta decay?," *Phys. Rev. D*, vol. 87, no. 9, p. 093007, 2013. DOI: 10.1103/PHYSREVD.87.093007.

[106] M. Aoki *et al.*, "Search for Massive Neutrinos in the Decay $\pi \to e\nu$," *Phys. Rev. D*, vol. 84, p. 052002, 2011. DOI: 10.1103/PHYSREVD.84.052002.

[107] N. Sabti, A. Magalich, and A. Filimonova, "An Extended Analysis of Heavy Neutral Leptons during Big Bang Nucleosynthesis," *JCAP*, vol. 11, p. 056, 2020. DOI: 10.1088/1475-7516/2020/11/056.

[108] A. Boyarsky, M. Ovchynnikov, O. Ruchayskiy, and V. Syvolap, "Improved BBN constraints on Heavy Neutral Leptons," 8 2020. ARXIV:2008.00749.

[109] S. Eijima, M. Shaposhnikov, and I. Timiryasov, "Freeze-out of baryon number in low-scale leptogenesis," *JCAP*, vol. 11, p. 030, 2017. DOI: 10.1088/1475-7516/2017/11/030.

[110] B. Garbrecht and P. Schwaller, "Spectator Effects during Leptogenesis in the Strong Washout Regime," *JCAP*, vol. 10, p. 012, 2014. DOI: 10.1088/1475-7516/2014/10/012.

[111] R. Barbieri, P. Creminelli, A. Strumia, and N. Tetradis, "Baryogenesis through leptogenesis," *Nucl. Phys. B*, vol. 575, pp. 61–77, 2000. DOI: 10.1016/S0550-3213(00)00011-0.

[112] J. Klarić, *Right-handed Neutrinos: From the Early Universe to Experiments*. PhD thesis, Munich, Tech U., 2019.

[113] B. Garbrecht and M. Herranen, "Effective Theory of Resonant Leptogenesis in the Closed-Time-Path Approach," *Nucl. Phys. B*, vol. 861, pp. 17–52, 2012. DOI: 10.1016/J.NUCLPHYSB.2012.03.009.

[114] M. E. Peskin and D. V. Schroeder, *An Introduction to quantum field theory*. Reading, USA: Addison-Wesley, 1995. DOI: 10.1201/9780429503559.

[115] J. S. Schwinger, "Brownian motion of a quantum oscillator," *J. Math. Phys.*, vol. 2, pp. 407–432, 1961. DOI: 10.1063/1.1703727.

[116] L. V. Keldysh, "Diagram technique for nonequilibrium processes," *Zh. Eksp. Teor. Fiz.*, vol. 47, pp. 1515–1527, 1964.

[117] J. Rammer, *Quantum field theory of non-equilibrium states*, vol. 22. Cambridge University Press Cambridge, 2007. DOI: 10.1017/CBO9780511618956.006.

[118] G. Buldgen, *Quantum and thermal effects on inflation and neutrino dynamics in the early Universe*. PhD thesis, Louvain U., 2020.

[119] J. Berges, "Introduction to nonequilibrium quantum field theory," *AIP Conf. Proc.*, vol. 739, no. 1, pp. 3–62, 2004. DOI: 10.1063/1.1843591.

[120] M. Garny and M. M. Muller, "Kadanoff-Baym Equations with Non-Gaussian Initial Conditions: The Equilibrium Limit," *Phys. Rev. D*, vol. 80, p. 085011, 2009. DOI: 10.1103/PhysRevD.80.085011.

[121] R. Wezeman, *Weyl quantization and Wigner distributions on phase space*. PhD thesis, Faculty of Science and Engineering, 2014.

[122] M. Drewes and B. Garbrecht, "Leptogenesis from a GeV Seesaw without Mass Degeneracy," *JHEP*, vol. 03, p. 096, 2013. DOI: 10.1007/JHEP03(2013)096.

[123] H. A. Weldon, "Effective Fermion Masses of Order gT in High Temperature Gauge Theories with Exact Chiral Invariance," *Phys. Rev. D*, vol. 26, p. 2789, 1982. DOI: 10.1103/PhysRevD.26.2789.

UNIVERSITÉ CATHOLIQUE DE LOUVAIN

Faculté des sciences

Place des sciences, 2 bte L6.06.01, 1348 Louvain-la-Neuve, Belgique | www.uclouvain.be/sc